

MICROCOPY RESOLUTION TEST CHART  
NATIONAL BUREAU OF STANDARDS-1963-A

AD-A174 803

AFOSR-TR- 86-2037

2

Final Report

Approved for public release;  
distribution unlimited.

June 1986

**THE ANALYSIS PHASE OF MITHRAS**

By: VINCENT B. WICKWAR ODILE DE LA BEAUJARDIERE CAROL A. LEGER

Prepared for:

DEPARTMENT OF THE AIR FORCE  
AIR FORCE OFFICE OF SCIENTIFIC RESEARCH  
BOLLING AIR FORCE BASE  
WASHINGTON, D.C. 20332

Attention: DR. DONALD L. BALL

DTIC  
SELECTE  
DEC 4 1986  
B

CONTRACT F49620-83-K-0005

DTIC FILE COPY

AIR FORCE OFFICE OF SCIENTIFIC RESEARCH (AFSC)  
NOTICE OF TRANSMISSION TO DTIC  
This technical report has been reviewed and is  
approved for public release under FAR 190-12.  
Distribution is unlimited.  
MATTHEW J. KEYSER  
Chief, Technical Information Division

\*Original copies on microfiche  
plates: All DTIC reproductions  
will be in black and  
white\*

333 Ravenswood Avenue  
Menlo Park, California 94025 U.S.A.  
(415) 326-6200  
Cable: SRI INTL MPK  
TWX: 910-373-2046



410281 SH

86 12 04 032

# SRI International



*Final Report*  
*Covering the Period 1 October 1982 to 30 September 1985*

*June 1986*

## **THE ANALYSIS PHASE OF MITHRAS**

*By:* VINCENT B. WICKWAR      ODILE DE LA BEAUJARDIERE      CAROL A. LEGER

*Prepared for:*

DEPARTMENT OF THE AIR FORCE  
AIR FORCE OFFICE OF SCIENTIFIC RESEARCH  
BOLLING AIR FORCE BASE  
WASHINGTON, D.C. 20332

Attention: DR. DONALD L. BALL

CONTRACT F49620-83-K-0005

SRI Project 4995

*Approved by:*

ROBERT S. LEONARD, *Acting Vice President*  
*Research and Analysis Division*

333 Ravenswood Avenue • Menlo Park, California 94025 • U.S.A.  
(415) 326-6200 • Cable: SRI INTL MPK • TWX: 910-373-2046

## REPORT DOCUMENTATION PAGE

1a. REPORT SECURITY CLASSIFICATION Unclassified		1b. RESTRICTIVE MARKINGS	
2a. SECURITY CLASSIFICATION AUTHORITY		3. DISTRIBUTION/AVAILABILITY OF REPORT  Approved for public release, distribution unlimited	
2b. DECLASSIFICATION/DOWNGRADING SCHEDULE		4. PERFORMING ORGANIZATION REPORT NUMBER(S)	
4. PERFORMING ORGANIZATION REPORT NUMBER(S)		5. MONITORING ORGANIZATION REPORT NUMBER(S) <b>AFOSR-TR- 86 - 2037</b>	
6a. NAME OF PERFORMING ORGANIZATION SRI International	6b. OFFICE SYMBOL (if applicable)	7a. NAME OF MONITORING ORGANIZATION Department of the Air Force	
6c. ADDRESS (City, State, and ZIP Code) 333 Ravenswood Avenue Menlo Park, California 94025		7b. ADDRESS (City, State, and ZIP Code) Air Force Office of Scientific Research Bolling AFB, Washington, DC 90332	
8a. NAME OF FUNDING/SPONSORING ORGANIZATION AFOSR	8b. OFFICE SYMBOL (if applicable) NC	9. PROCUREMENT INSTRUMENT IDENTIFICATION NUMBER F49620-83-K-0005	
8c. ADDRESS (City, State, and ZIP Code) AFOSR/HQ Bldg 41J Bolling AFB DC 20332-6448		10. SOURCE OF FUNDING NUMBERS	
		PROGRAM ELEMENT NO. 61102F	PROJECT NO. 2310
		TASK NO. A2	WORK UNIT ACCESSION NO.
11. TITLE (Include Security Classification) The Analysis Phase of MITHRAS			
12. PERSONAL AUTHOR(S) Vincent B. Wickwar, Odile de la Beaujardiere, and Carol A. Leger			
13a. TYPE OF REPORT Final Scientific	13b. TIME COVERED FROM 10/1/82 TO 9/30/85	14. DATE OF REPORT (Year, Month, Day) 1986 June 23	15. PAGE COUNT 127
16. SUPPLEMENTARY NOTATION			
17. COSATI CODES		18. SUBJECT TERMS (Continue on reverse if necessary and identify by block number)	
FIELD	GROUP	SUB-GROUP	Incoherent-scatter radar, high latitudes, magnetosphere, ionosphere, thermosphere, aurora, particle precipitation,
19. ABSTRACT (Continue on reverse if necessary and identify by block number)			
<p>MITHRAS is a coordinated multiradar program to study the upper atmosphere. Its purpose is to examine the interactions among the magnetosphere, ionosphere, and thermosphere, as well as the phenomena that result from these interactions. It is based around a data set acquired by the Chatanika, Millstone Hill, and EISCAT incoherent-scatter radars between May 1981 and June 1982. A large portion of this period was unique because it was the only time that three radars, well separated in local and magnetic time, operated together to probe the high-latitude region. The period was also unique because it coincided closely with solar maximum and the DE-2 spacecraft was available for correlative observations.</p> <p>To learn as much as possible from the observations, several tools were developed to improve the handling and analysis: a data-exchange tape format</p>			
20. DISTRIBUTION/AVAILABILITY OF ABSTRACT <input type="checkbox"/> UNCLASSIFIED/UNLIMITED <input type="checkbox"/> SAME AS RPT. <input type="checkbox"/> DTIC USERS		21. ABSTRACT SECURITY CLASSIFICATION Unclassified	
22a. NAME OF RESPONSIBLE INDIVIDUAL Lt Col Koermer		22b. TELEPHONE (Include Area Code) 7167-4963	22c. OFFICE SYMBOL NC

was developed, new display methods using color were implemented to present the data, F-region analysis procedures were extended, and binning procedures were developed to facilitate statistical analysis of the data. In addition, workshops were held so that the observations could be discussed and interpreted by the MITHRAS participants. As the studies developed, the results have been presented at meetings and a large number of publications have resulted. Because it was such a valuable data set and as a result of the above activities, the number of MITHRAS participants grew considerably from those actually supported by AFOSR. Although many studies have been completed, others begun later or based on earlier results are under way. MITHRAS has become the model for other global studies involving the full network of six radars.

The project has led to the following scientific accomplishments: The best view, to date, has been obtained of the instantaneous shape of the convection pattern in the auroral region and polar cap by combining Millstone Hill, Chatanika, and DE-2 electric-field measurements. A series of case studies established that the convection intensifies simultaneously in the morning and afternoon convection cells. During a substorm, another case study showed that the large-scale convection pattern could remain stable for a prolonged period, even though the period was one of sustained magnetic activity. Average patterns of plasma convection were calculated for two different orientations of the IMF By component. The patterns obtained showed that the effect of the By component is stronger and different than previously thought. At or near the convection reversal in the afternoon cell, i.e., at the polar cap boundary, there can be large energy inputs to the electron gas by soft particles and a large downward heat flux. The winter nighttime F-region density strongly depends on longitude; this dependency was attributed to cross-polar cap transport of ionization and to the fact that, because of the offset of the geographic and geomagnetic poles, the solar illumination of the large-scale convection pattern varies with UT. Using more inputs and being subject to more constraints than ever before, a theoretical model of the high-latitude ionosphere was able to successfully reproduce auroral-zone observations made from two widely spaced longitudes. Theoretical calculations of the 6300-A intensity from atomic oxygen, showed that the hot electrons found near the afternoon convection reversal are responsible for a much larger proportion of the emission than previously considered. Although convection has the dominant role in determining the large-scale nighttime meridional neutral wind at F-region altitudes, local effects such as particle and Joule heating can create significant perturbations. At midnight in the polar cap a new phenomenon was observed, an abatement or sometimes even a reversal of the southward meridional wind. The importance of ion drag was further demonstrated in statistical analyses that showed the meridional component of the neutral wind to be significantly correlated with the By component of the IMF. These analyses also showed that the neutral wind varies significantly with season. Several phenomena observed in the early morning at Chatanika--such as elevated ion and neutral temperatures, significantly perturbed meridional neutral winds, and reduced plasma densities--could be the result of very large Joule heating just poleward of the radar or in the polar cap. Finally, new methods were devised to determine the neutral exospheric temperature from high-latitude radar data; the daily and solar-cycle variations were studied.

CONTENTS

LIST OF ILLUSTRATIONS . . . . .	v
LIST OF ACRONYMS . . . . .	vii
I INTRODUCTION. . . . .	1
A. The Magnetospheric-Ionospheric-Thermospheric System . . . . .	1
B. MITHRAS . . . . .	9
II DATA CONSIDERATIONS . . . . .	15
A. Data Exchange . . . . .	15
B. Data Display. . . . .	16
C. Data Analysis . . . . .	33
III RESEARCH. . . . .	37
A. Magnetosphere . . . . .	37
1. Convection. . . . .	37
a. Global Convection Pattern . . . . .	38
b. Effect of the IMF B <sub>y</sub> Component. . . . .	44
c. Data/Theory Comparison with Utah State University Group . . . . .	47
d. Determination of the Electrostatic Potential Distribution from Magnetometers . . . . .	48
e. Electric Fields at Subauroral Latitude. . . . .	50
f. Substorm Studies. . . . .	52
2. Precipitation . . . . .	58
a. Relation of Precipitation and Convection. . . . .	59
b. Very Energetic Particles. . . . .	60
B. Ionosphere. . . . .	60
1. Electron Density. . . . .	60
a. Daytime Density Depletion . . . . .	62
b. Longitudinal or UT Density Variations . . . . .	64
c. Trough and Other Large-Scale Structures . . . . .	66
d. Comparison with Theory. . . . .	67
2. Electron Temperature. . . . .	69

CONTENTS (Concluded)

a.	Elevated Electron Temperatures. . . . .	70
b.	Large Temperature Increases at the Afternoon Convection Reversal . . . . .	71
c.	Excitation of the Red Line of Atomic Oxygen . . . . .	74
3.	Ion Temperatures. . . . .	77
a.	Elevated Ion Temperature in the Morning Sector. . . . .	77
b.	Comparison with Theory. . . . .	79
C.	Neutral Atmosphere. . . . .	79
1.	Neutral Wind. . . . .	80
a.	Meridional Wind at Chatanika. . . . .	80
b.	Nighttime Behavior. . . . .	81
c.	The Role of Particle and Joule Heating. . . . .	84
d.	B <sub>y</sub> Dependence of the Neutral Wind . . . . .	84
e.	Seasonal Dependence of the Neutral Wind . . . . .	86
f.	Altitude Gradients. . . . .	86
g.	Comparison with Theory. . . . .	89
2.	Neutral Temperature . . . . .	89
a.	Morning Increase. . . . .	89
b.	Behavior during Decreasing Phase of Solar Cycle . . . . .	91
IV	DEVELOPMENT . . . . .	93
V	CONCLUSIONS . . . . .	95
VI	REFERENCES. . . . .	98
APPENDICES		
A	MITHRAS RADAR OBSERVATIONS. . . . .	109
B	PARTICIPANTS IN MITHRAS . . . . .	112
C	MITHRAS PUBLICATIONS, REPORTS, AND PRESENTATIONS. . . . .	115



Accession For	
NRIS	<input checked="" type="checkbox"/>
DEPT	
Dist	
A-1	

## ILLUSTRATIONS

I-1	Schematic Representation of the Magnetosphere . . . . .	2
I-2	Empirical Model of the Ionospheric Convection Cells in the Northern Hemisphere. . . . .	3
I-3	Schematic Representation of the Auroral Oval Showing Several Type of Aurora. . . . .	5
I-4	Schematic Representation of the Large-Scale Birkeland Currents. . . . .	6
I-5	Auroral Diagram . . . . .	7
I-6	Relative Locations of the Incoherent-Scatter Radar Facilities. . . . .	11
II-1	Prismatic Representation of the Region in Space and Time Probed by a Radar. . . . .	19
II-2	Cut in Magnetic Meridian Plane at Chatanika Between 1558 and 1612 UT (0558 and 0612 AST) on 27 January 1982 . . .	20
II-3	Cut Along Magnetic Field at Chatanika on 27 January 1982 . . . . .	23
II-4	Cut at Fixed Altitude for Electron Density at Chatanika on 27 January 1982. . . . .	25
II-5	Cut at 350 km at Chatanika on 27 January 1982 . . . . .	27
II-6	Ion-Convection Velocities at Chatanika on 27 January 1982 . . . . .	29
II-7	Solar Zenith Angles at Chatanika on 27 January 1982 . . . . .	30
II-8	Electron Densities at Three Radars on 18 November 1981. . . .	31
III-1	Recently Proposed Convection Patterns . . . . .	39
III-2	Convection Pattern at 1050 UT on 25 October 1981 Based on Observations by DE-2, Chatanika, and Millstone Hill. . . .	43
III-3	IMF $B_y$ Influence on Convection. . . . .	45
III-4	Average Ion Drifts Measured by Sondrestrom Radar for $B_y > 0$ and $< 0$ . . . . .	46
III-5	Selected Plasma Stream Lines Predicted for 27 and 28 June 1981 as a Result of Fitting Convection Velocities at Chatanika, Millstone Hill, and STARE. . . . .	49

ILLUSTRATIONS (Continued)

III-6	Stack Plot of the Magnetometer Perturbations in the Geomagnetic North Direction from Approximately 60 High-Latitude Stations on 11 November 1981 . . . . .	51
III-7	Detailed Chatanika and DE-2 Observations in the Evening Sector Auroral Zone on 11 November 1981 . . . . .	53
III-8	A Summary of the Substorm Sequence Showing the Roles of the Magnetotail and the Ionosphere and also Showing the Aspects of Substorms that are regarded as Driven and Unloading Processes . . . . .	55
III-9	Sequence of Events Following IMF Change at 2100 UT on 23 April 1983. . . . .	57
III-10	Penetration of Energetic Particles to D-Region Altitudes at Chatanika. . . . .	61
III-11	Daytime Density Depletion and Recovery at Chatanika During 48 Hours on 25 and 26 October 1981 . . . . .	63
III-12	Magnetic-Local-Time Dependence of the F-Region Electron Density at Millstone Hill, Chatanika, and EISCAT on 18 and 19 November 1981 and 15 and 16 December 1981. . . . .	65
III-13	Main Electron Density Trough at Chatanika on 11 November 1981. . . . .	68
III-14	Comparison of F-Region Electron Temperature and E-Region Electron Density on 18 November 1981 . . . . .	72
III-15	Elevated Electron Temperatures and Large Downward Heat Fluxes in the Afternoon Sector . . . . .	73
III-16	Observed and Calculated 630.0-nm Intensity Along the Magnetic Field at Chatanika on 5 March 1981 . . . . .	76
III-17	Preferential Ion Heating in the Early Morning at Chatanika and Millstone Hill. . . . .	78
III-18	Second Maximum in the Meridional Wind Near Midnight Under Disturbed Conditions at Chatanika . . . . .	82
III-19	Abatement in the Meridional Wind Near Midnight and Large Day-to-Day Variation at Sondrestrom . . . . .	83
III-20	$B_y$ Dependence of the Meridional Wind. . . . .	85
III-21	Seasonal Dependence of the Meridional Wind. . . . .	87
III-22	Gradient in the Meridional Neutral Wind at Chatanika on 18 November 1981 . . . . .	88
III-23	Early Morning Enhancement of Exospheric Temperature at Chatanika. . . . .	90

## ACRONYMS

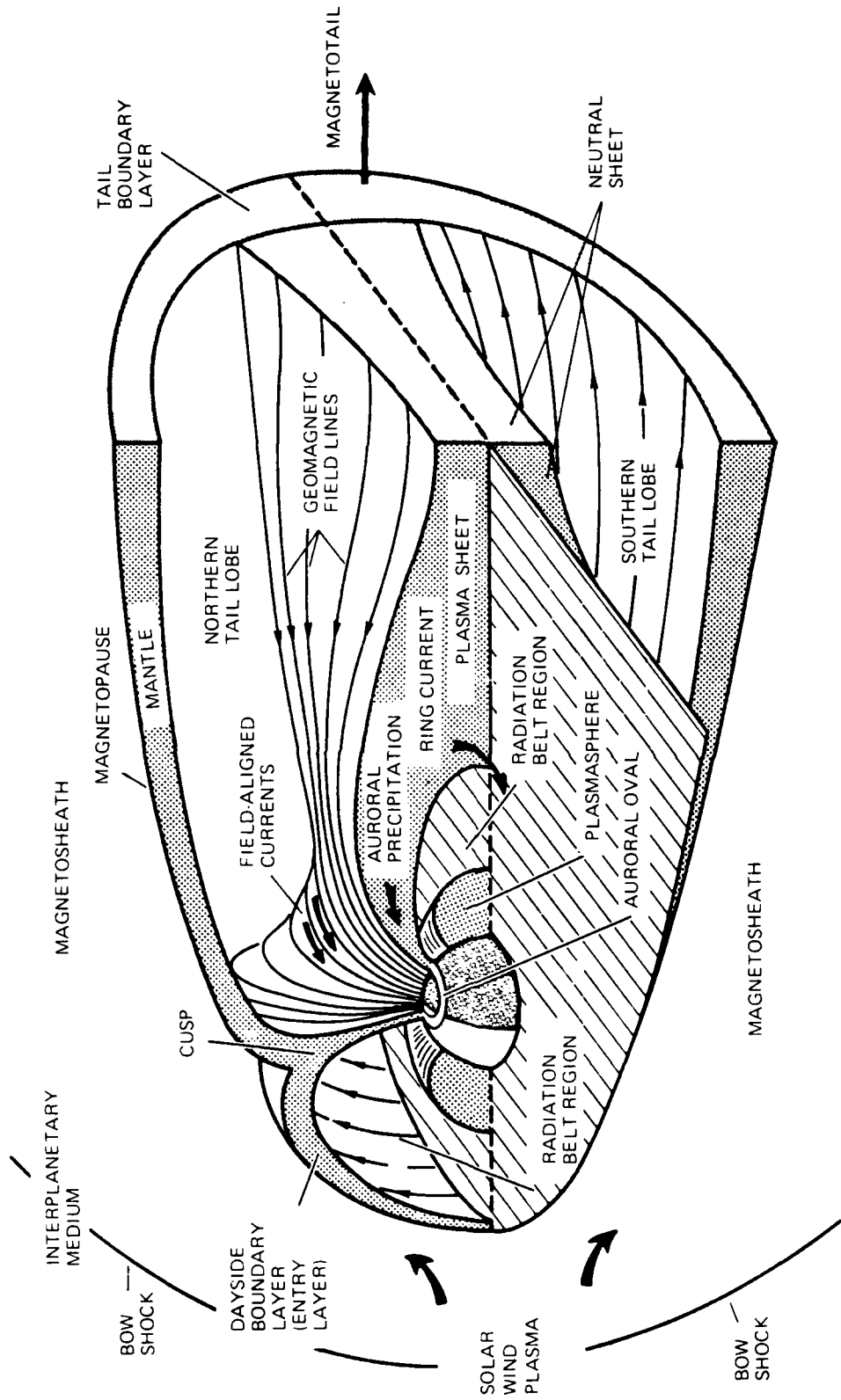
AED	Advanced Electronic Design
BPS	Boundary Plasma Sheet
CPS	Central Plasma Sheet
DE-1	Dynamics Explorer-1 Satellite
DE-2	Dynamics Explorer-2 Satellite
EISCAT	European Incoherent-Scatter
GISMOS	Global Incoherent-Scatter Measurements and Observations of Substorms
GTMS	Global Thermospheric Mapping Study
IMF	Interplanetary Magnetic Field
LT	Local Time
MITHRAS	Magnetosphere Ionosphere Thermosphere Radar Studies
NCAR	National Center for Atmospheric Research
SABRE	Sweden and Britain Radar Experiment
STARE	Scandinavian Twin Auroral Radar Experiment
TGCM	Thermospheric Global Circulation Model
URSI	International Union of Radio Science
USU	Utah State University
UT	Universal Time

## I INTRODUCTION

### A. The Magnetospheric-Ionospheric-Thermospheric System

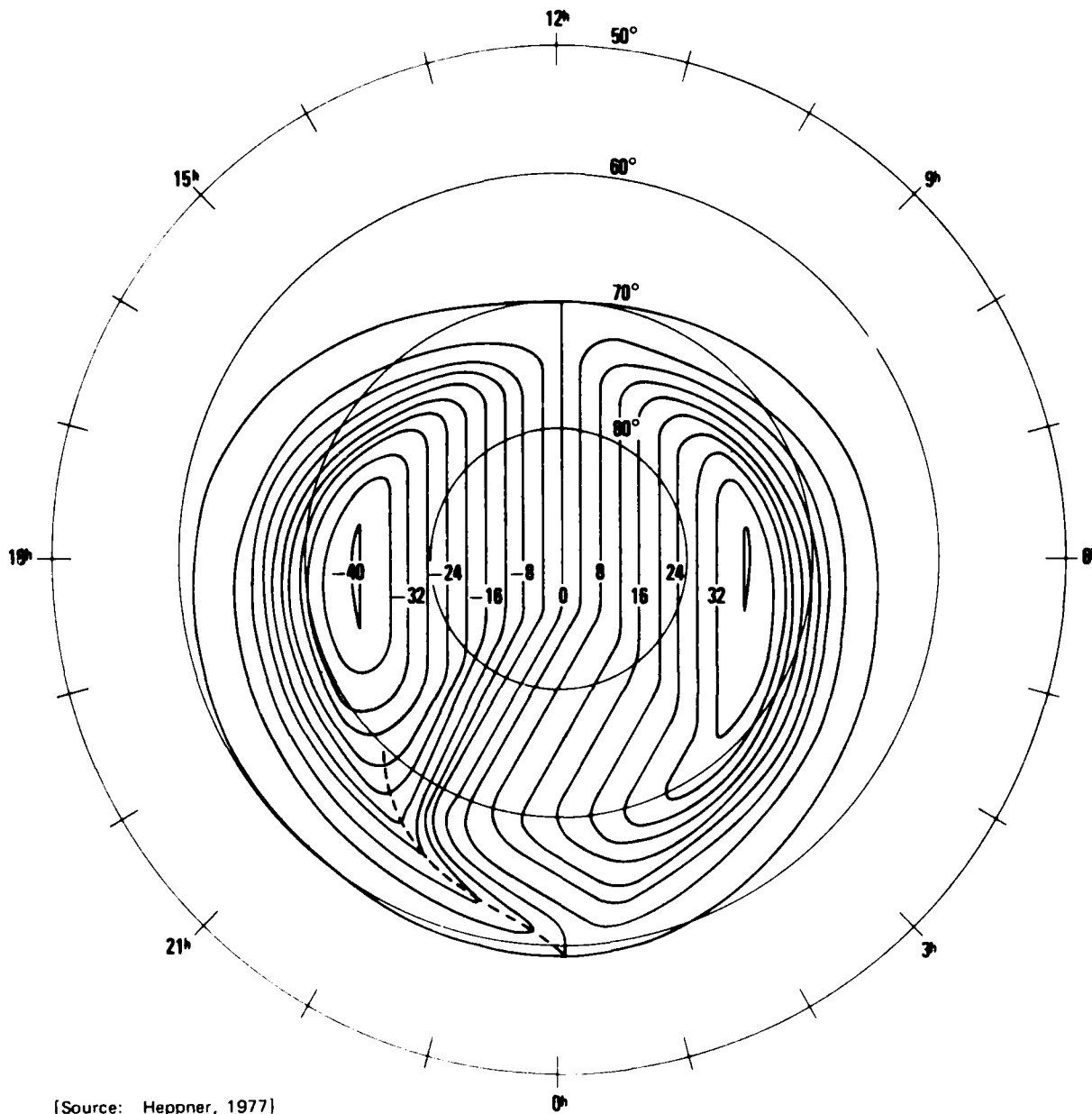
Since the realization in 1958 that the solar wind exists, a model has developed of the outer limits of our environment and the interactions among its components. The solar wind, dragging the solar and interplanetary magnetic field (IMF) with it, interacts with the earth's magnetic field to form the comet-shaped magnetosphere, Figure I-1. It also sets up a dawn-to-dusk electric field across the tail of the magnetosphere, and it helps to populate the magnetosphere with charged particles. The magnetosphere is closely associated with the ionosphere and neutral atmosphere at high latitudes because of the topology of the magnetic field. The polar-cap field lines extend to the magnetopause (the outer boundary layer) and out into the tail lobes. The auroral-region field lines extend to the boundary plasma sheet and central plasma sheet on the nightside and to the cleft on the dayside. The field lines just equatorward of the auroral region connect to the ring current. These associations lead to strong interactions among the magnetosphere, ionosphere, and neutral atmosphere. Most of which are concentrated in the D, E, and F regions of the ionosphere, and the mesospheric and thermospheric portions of the neutral atmosphere.

Because, to a first approximation, the magnetic field lines are equipotentials, the electric field in the magnetosphere maps along the field lines into the ionosphere, causing the ambient electrons and ions in the northern and the southern high-latitude regions to drift such that two convection cells are formed, Figure I-2, that cover the polar cap and auroral region. The ions, thus set into motion, collide with



[Courtesy of J. Roederer, University of Alaska, 1981]

FIGURE I-1 SCHEMATIC REPRESENTATION OF THE MAGNETOSPHERE



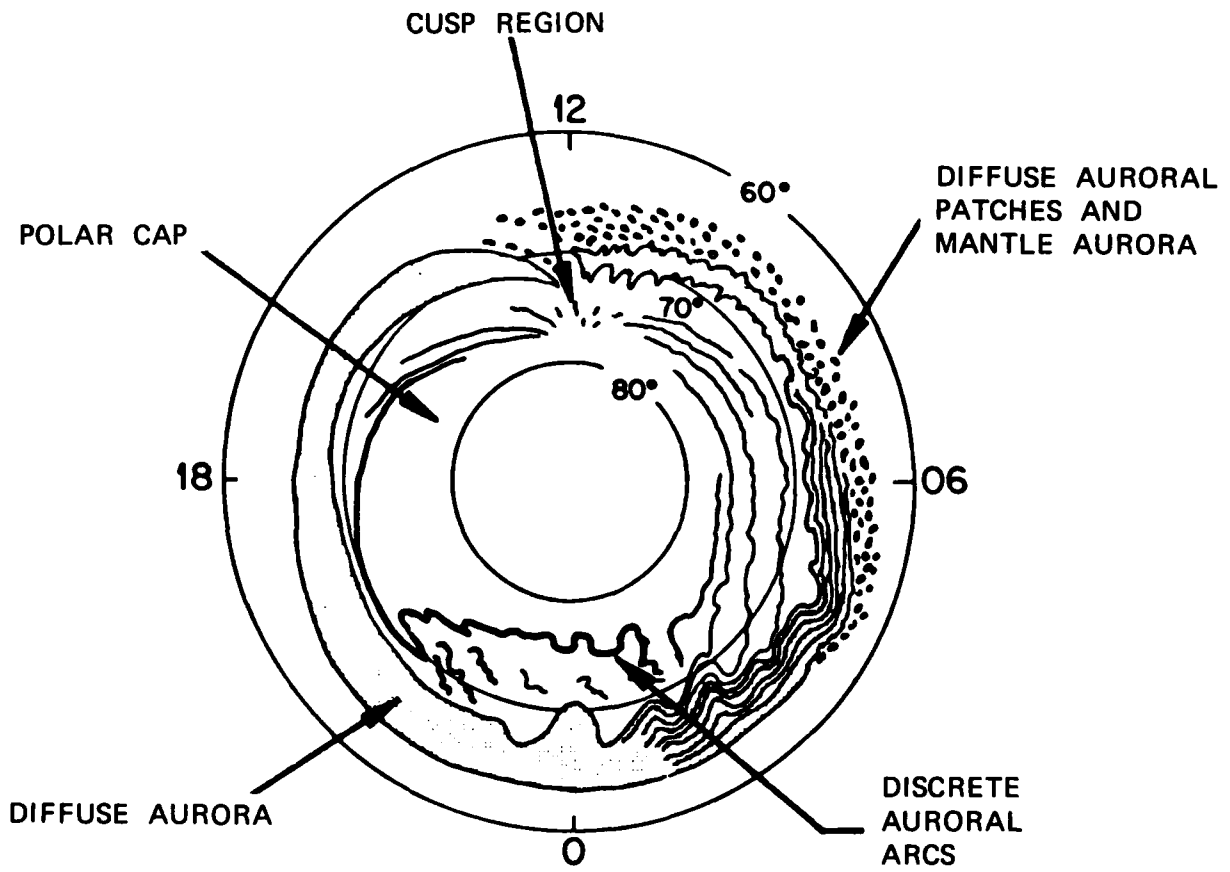
[Source: Heppner, 1977]

FIGURE I-2 EMPIRICAL MODEL OF THE IONOSPHERIC CONVECTION CELLS IN THE NORTHERN HEMISPHERE. They are shown in magnetic coordinates for an observer on the earth. The contours are for electrostatic potential with 4-keV steps. The dashed line is the Harang discontinuity.

neutrals, heating both the neutrals and ions (Joule heating) and transferring momentum to the neutrals (ion drag). The neutrals are set into motion as a result of both the Joule heating and the ion drag. In the E region, the ion motion is impeded by these ion-neutral collisions, while the electrons suffer very few collisions. The resultant difference between ion and electron velocities is the origin of the auroral electrojet currents, to which magnetometers respond. The same velocity difference further leads to the development of instabilities in the plasma, which give rise to the density irregularities used for the STARE and SABRE radars. In addition, the instabilities give rise to large electron heating. Energetic particles (mostly electrons) following the field lines from the cleft, central plasma sheet, and boundary plasma sheet precipitate into the atmosphere, forming the auroral oval, Figure I-3, in each high-latitude region. These precipitating particles deposit energy in the atmosphere at D-, E-, and F-region altitudes. In addition to exciting neutrals and ions, producing the auroras, the precipitating particles ionize the neutral gas, giving rise to electron density enhancements, as well as heat the ambient electrons and neutrals. The latter, like Joule heating, affects the neutral wind. In addition to the energetic particles, thermal particles flow in both directions along the field lines. These energetic and thermal particles carry field-aligned (Birkeland) currents, Figure I-4, that further couple the ionosphere and magnetosphere. These currents close in the ionosphere and in the magnetosphere.

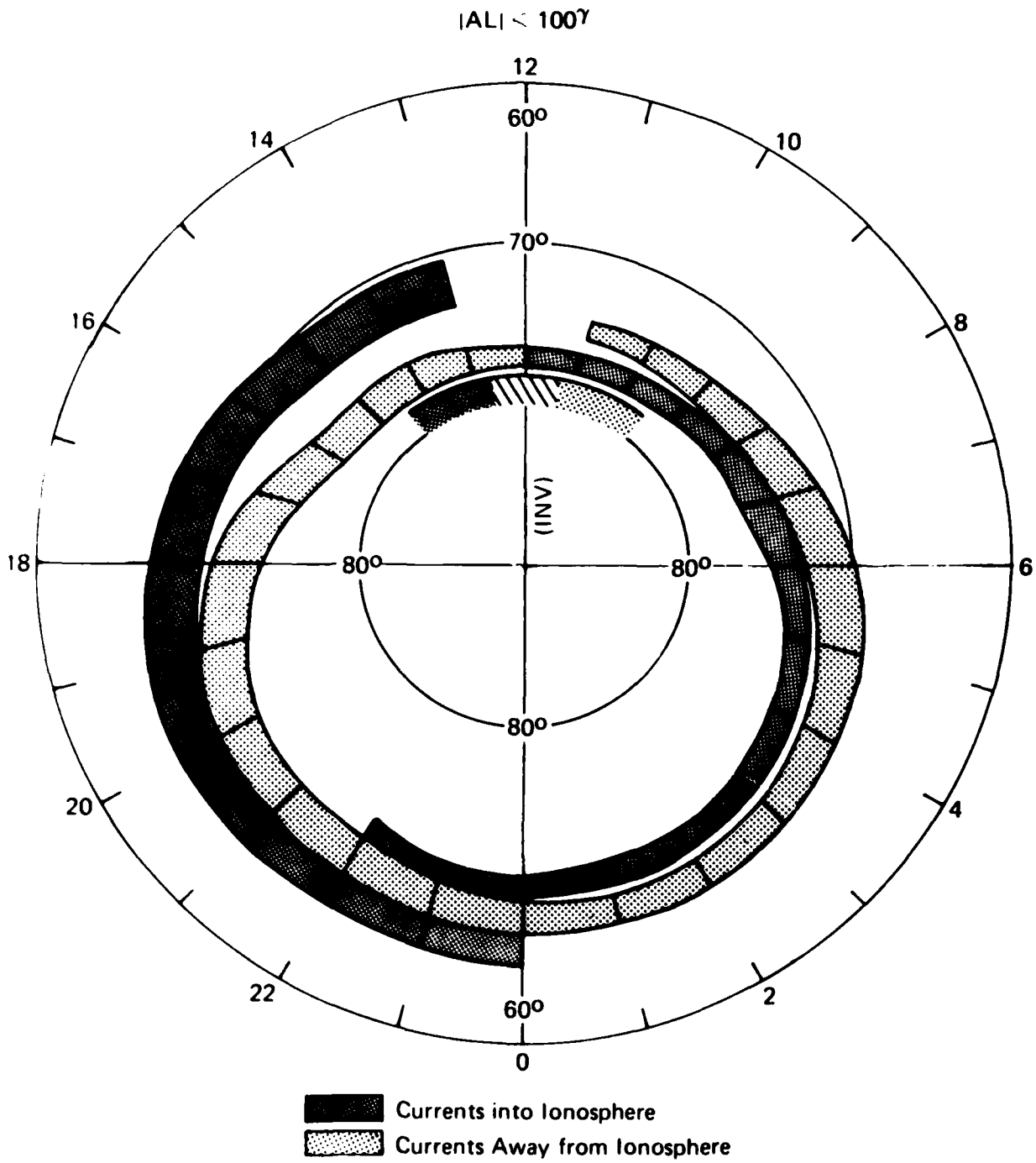
Many of these interrelations are presented schematically in the auroral diagram, Figure I-5. The geophysical parameters are shown in circles and rectangles with rounded corners. The physical processes that affect them are shown in rectangles (with square corners).

Transfer of energy and momentum from the magnetosphere occurs continuously and periods exist, called substorms, during which the



[Adapted from Akasofu, 1981]

FIGURE I-3 SCHEMATIC REPRESENTATION OF THE AURORAL OVAL SHOWING SEVERAL TYPES OF AURORA



[Source: Iijima and Potemra, 1978]

FIGURE I-4 SCHEMATIC REPRESENTATION OF THE LARGE-SCALE BIRKELAND CURRENTS



transfer increases impulsively and remains high for several hours. That the energy transfer alone can have major effects on the ionosphere and neutral atmosphere is apparent when we realize that the energy deposited above 90 km in a localized area can exceed that which would be deposited by the overhead sun by a factor of 10 to 100. Indeed, large effects do occur in every geophysical parameter: electron densities, electron and ion temperatures, neutral winds, neutral temperatures and densities.

In addition to these auroral phenomena in the high-latitude upper atmosphere, this part of the atmosphere already behaves very differently from midlatitudes because much of it is above the arctic circle where it can have as much as 24 hours of darkness or sunlight, depending on the season. This variable insolation, for instance, leads to major seasonal and hemispheric differences in the F-region densities and the E-region conductivities. Thus one of the challenges in this region is to distinguish between effects that are driven by or modulated by the solar wind and those that are driven or modulated by the solar EUV and UV radiation.

The interactions among the magnetosphere, ionosphere, and thermosphere lead to a vast array of phenomena, which are of great scientific interest. In addition, the changes that result in the ionosphere and thermosphere can have major effects on a variety of systems that involve the polar regions.

During periods of increased geomagnetic activity the best known phenomenon is the aurora. The emissions occur not only in the visible but also in the ultraviolet and infrared parts of the spectrum. They can present a confusing background that hampers locating other emission sources. Almost as well known are many radio or propagation phenomena. These include the disruption of HF radio communications, which also implies difficulty for direction finding and over-the-horizon radar. At

higher frequencies, these phenomena include the fading and scintillation of satellite signals. They also include variations in total electron content, on various time scales, that affect satellite ranging. The neutral density at high altitudes is increased, giving rise to increased drag on satellites. In the mesosphere, ozone is reduced. Speculation exists that tropospheric weather can be affected. Currents are induced in the lower ionosphere and at ground level. The former gives rise to magnetic-field fluctuations, the latter to potentially destructive currents on communication lines and power grids.

#### B. MITHRAS

The purpose of Project MITHRAS (an acronym for Magnetosphere Ionos-sphere Thermosphere Radar Studies) is to increase our understanding of these interactions and the resulting effects. The observations were made during a brief period when three radars could observe much of the auroral region, i.e., much of the auroral oval and equatorward portion of the convection pattern.

The individual radars are each very powerful research tools. An extensive set of ionospheric and neutral atmospheric parameters can be determined from the radar measurements. Many of these parameters are mentioned in Section III, in which we discuss the research results. Numerous altitudes can be probed, yielding profiles of these parameters. The fact that altitude profiles are obtained is important because what is observed at one altitude is often related by transport, diffusion, or conduction to what happens at other altitudes. Moreover, the altitude range observed at most radars can include the region between 80 and 150 km that is inaccessible to satellites and only accessible to rockets for a few minutes. The high-latitude radars can probe a wide spatial area within seconds or minutes. Thus, for instance, they can establish the location of a measurement with respect to a convection or precipita-

tion boundary. Finally, they can determine the time evolution of the parameters. Individual profiles require typically 5 s to 1 min. However, an experiment usually consists of many profiles in different directions, leading to an experiment time resolution of 5 min to 40 min. A radar can probe the same region for periods that typically range from 8 hrs to 72 hrs. In contrast, a satellite will return to the same latitude about every 90 min. Depending on the orbit, a satellite may take weeks to sample 24 hrs of local time (thereby mixing together many effects such as season and geomagnetic activity), or it may stay fixed in local time (LT).

Despite the great capability of an individual radar, a number of problems exist that can best be addressed simultaneous observations with by as many radars as possible. When one radar detects a change in a parameter, such as convection velocity, as a function of time, it is not clear whether the change arose because the phenomenon evolved [a variation in universal time (UT)] or because the radar moved with respect to a steady-state pattern with spatial gradients [a variation in local time (LT)]. Because LT is equivalent to longitude, this quandry is also referred to as a space-time ambiguity.

Another situation that introduces LT-UT differences is that the high-latitude phenomena are affected by two sources of energy input: the solar UV and EUV energy input depend on local time and geographic latitude, or equivalently, longitude and latitude; the magnetospheric energy and momentum transfer depend on local magnetic time and geomagnetic (invariant) latitude. Because the geographic and geomagnetic poles do not coincide, these coordinate systems do not coincide. The result is that at each location on the earth, there is a different mixture of inputs related to these two energy sources. Observationally, this means that sites at the same latitude (geographic or geomagnetic) will measure different values corresponding to different mixtures of

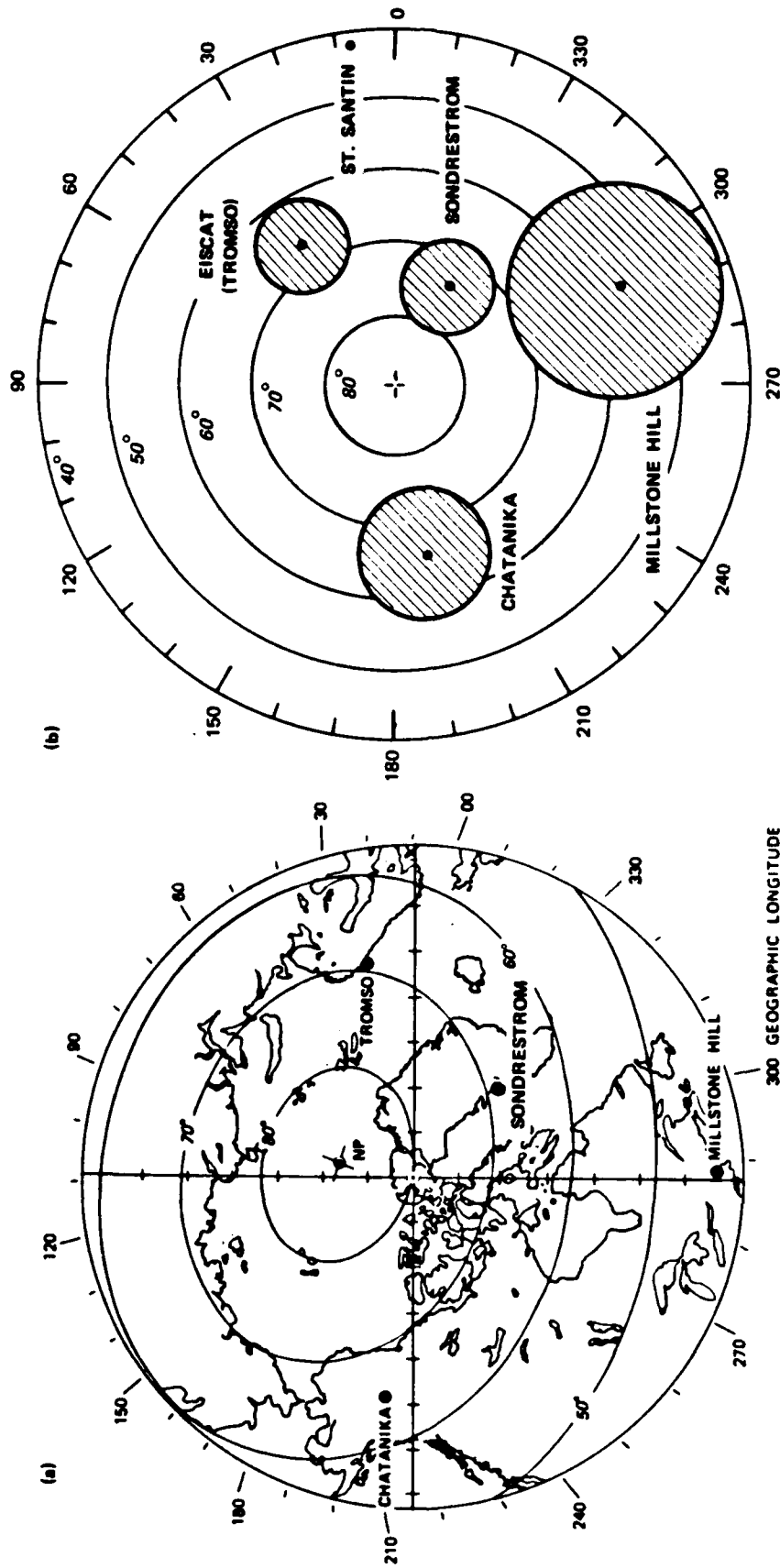


FIGURE I-6 RELATIVE LOCATIONS OF THE INCOHERENT-SCATTER RADAR FACILITIES.

(a) The relative locations in geomagnetic coordinates superimposed on a map of the northern polar region. Geomagnetic latitude is indicated at 5° intervals on two meridians. The geographic north pole (NP), latitude, and longitude are all indicated.

(b) The relative locations and fields of view in invariant latitude and geomagnetic longitude. The fields of view are estimated at the 500-km altitude level.

inputs. Accordingly, it also means that a UT variation will be imposed on observations made at a given site as the geomagnetic pole, hence auroral oval, moves about the geographic pole.

The first phase of MITHRAS [de la Beaujardiere et al., 1982, 1984b] was an observation program, between May 1981 and June 1982, based on three incoherent-scatter radars that could observe the northern high-latitude region between about  $57^{\circ}$  and  $73^{\circ}$  invariant latitude ( $\Lambda$ ): Chatanika, Millstone Hill, and EISCAT (the European Incoherent-SCATter radar). These latitudes typically embrace the auroral oval in the midnight sector and are equatorward of it in the noon sector. This period was unique because three such radars were at almost equally separated longitudes, Figure I-6. It began just before the beginning of observations at EISCAT and ended shortly after the dismantling of the Chatanika radar for its move to Sondre Stromfjord, Greenland. During this limited period, the AFOSR support enabled roughly three simultaneous 24-hr observations per month for 10 months. (The catalog of observations is given in Appendix A.) As seen in Figure I-6, the new configuration of Millstone Hill, Sondrestrom, and EISCAT, starting in 1983, is very different. With the radars closer together, it is more suited for detailed studies. It also differs in that Sondrestrom is at a higher geomagnetic latitude than the other two; Sondrestrom is under the oval near noon and in the polar cap from dusk until dawn.

In addition to this unique property during MITHRAS for LT-UT studies, the observing period was characterized by its proximity to solar-cycle maximum and its overlap with the brief lifetime of the Dynamics Explorer-2 (DE-2) satellite. The opportunity to obtain simultaneous and coordinated data from three radars widely spaced around the auroral zone was the driving reason for the timing of the MITHRAS experiment. The uniqueness of the other two characteristics only became apparent after the fact. The possibility of overlapping with DE-2 was

considered fortunate, and its observations were coordinated with those of the radars. However, we anticipated that the satellite would remain in orbit longer than it did. Being near the solar-cycle maximum was very fortunate, as well. Because of the high electron densities during this period, the radar data set is of very high quality. Thus, these data were unique in more ways than were originally expected.

The radar measurements were supplemented by those from STARE (the Scandinavian Twin Auroral Radar Experiment), the Fabry-Perot interferometer network, the global magnetometer network, the DE-1 and -2 satellites, the NOAA-6 and -7 satellites, the IMP-8, ISEE-1 and -3 spacecraft, and the mid- and low-latitude incoherent-scatter radars. They were further extended with older data from Chatanika and, recently, with data from Sondrestrom. These data were necessary to determine background or average conditions and to extend the coverage into the polar cap.

The second phase of MITHRAS concerns data reduction and analysis. This document is a report of work involving SRI personnel, alone and in collaboration with others, over a three-year period on this second phase. Part of the work consisted of collecting, reducing, and displaying data, as well as the development of new analysis procedures. These activities are discussed in Section II. The other part is the research, which included the analysis and interpretation of radar and other data. It also includes the comparison of data with the results of model calculations. Because of the many instruments and the model calculations, this research has often involved collaboration with other scientists, both nationally and internationally. This research is reviewed in Section III. The initiative for these projects has either come from individual researchers or has been the outgrowth of three workshops held to discuss the project. These workshops proved very valuable for interesting a varied group of researchers who possess a wide range of experi-

mental and theoretical backgrounds in the MITHRAS data set. The minutes of these meetings were presented in the Interim Progress Report [Wickwar et al., 1984a]. A list of researchers who participated in the workshops or studies are listed in Appendix B. The research efforts have led to a considerable number of presentations, reports, and publications. They are listed in Appendix C.

## II DATA CONSIDERATIONS

Some unusual, but anticipated, data-handling problems have arisen from the effort to bring together the large body of data from many ground-based and spacecraft sensors required for Project MITHRAS. A highly adaptable tape format had to be developed to exchange data among the MITHRAS participants. To explore the large amount of data for good situations for further study, it has been necessary to develop an extensive set of display programs, mostly in color. These have been used to make an overview of the data set and have been used in the scientific analyses. To the extent possible, all the radar and correlative data have been brought together in a data library and catalog at SRI International. To take full advantage of these MITHRAS data, we have had to extend the analysis capabilities considerably in the F region where most of the data were acquired. To look for the regular patterns of variation, we have developed binning and averaging programs to use on large bodies of data.

### A. Data Exchange

In a project that involves many sources of data, one of the most important considerations is to be able to exchange and manipulate the data easily. While this comment appears obvious, the task of implementing it is far from trivial. Since the beginning of the project, we have worked closely with the URSI Incoherent-Scatter Working Group and the Incoherent-Scatter Data Base, which has been set up by the National Science Foundation at the National Center for Atmospheric Research (NCAR) in Boulder, Colorado. Indeed, the MITHRAS work on data exchange became the beginning of the formal international data base; the MITHRAS data exchange format [de la Beaujardiere et al., 1982] that we developed under this contract was the model for the NCAR data base. The format

has now evolved and been adopted for the NCAR data base, as well as by the Europeans for the EISCAT data.

Because of MITHRAS, we have played a very active role in data exchanges. It has also meant that we have been able to obtain and readily plot the data from the other radars and from a number of other instruments with which we need to compare measurements. It has also facilitated exchange of data with theoreticians and modelers. We expect that in the future this format will be adopted by an even wider segment of the aeronomy community.

#### B. Data Display

The radars produce an enormous amount of information. This is apparent when we realize that the measurements can be reduced and analyzed to produce many physical parameters as a function of altitude, latitude, and time. The problem of displaying the data is further exacerbated because some of the parameters, such as the electron density, can vary in magnitude over such a very wide range that they are hard to display.

Perhaps, if we knew precisely for what we were looking, this would not matter. But this is an observational science and we are still very much exploring the high-latitude region. We, therefore, needed to examine as many of the parameters from as much of the data as possible. Indeed, it is in doing so that we have found a number of unexpected results--for example, the great variation of nighttime F-region electron density at the different longitudes, very high electron temperatures near the convection reversal in the afternoon convection cell, and, on occasion, coincidence between energetic particle precipitation and F-region electron-temperature enhancement.

To help in displaying the data, we purchased, as part of Project MITHRAS, a color terminal and SRI purchased a camera. We developed an extensive series of color display programs. The color terminal is an Advanced Electronic Design (AED) model 767 which has a 1024 × 1024 × 8

bit memory, and a viewing window of 768 x 575 pixels. Eight bits per pixel allow the simultaneous use of 256 colors from a palette of almost 17 million different colors.

The color camera is a Dunn 631 system. It receives the three-color video signals from the AED terminal and is also connected to the main computer by a serial link.

We developed and documented general-purpose software to drive these two instruments [Leger, 1983]. This user's guide describes the operation and special commands for the AED terminal together with illustrative examples.

To display the data in color, the first practical problem was to develop a color scale. With the ability to use 256 colors, it is possible to make what appears to be a continuous scale. However, it is easier to examine data where discrete steps exist. Therefore, a criterion in developing a color scale was to have a large enough color change at each step to distinguish between colors. Another criterion was to have a "logical" change in color across the scale so that we would not have to refer back to the scale to determine if a color step represented an increase or decrease.

With much experimentation, two scales were developed. The first has 25 steps; the second has 20. The 25-step scale is used for most of the data. The 20-step scale is used for velocity data, which can be positive or negative. For both scales it was necessary to vary both the hue and intensity to separate the colors. The "logical" progression in hue is in the following order: black, blue, cyan, green, yellow, red, and magenta. The subset from blue to red is the usual spectrum obtained by dispersing white light. Furthermore, with the exception of black, the pattern is a cyclic progression of primary colors from blue to green, green to red, and half way from red to blue. To avoid confusion between the highest and lowest values, the cycle is not completed back to blue. The intensity settings for the three primary colors were given

in Wickwar et al. [1984a]. They may be useful to other groups beginning to use color.

The region probed by the radar can often be represented as a prism, as pictured in Figure II-1. The axes are altitude, latitude, and time. During the MITHRAS observation campaign three main experiment modes were used, MITHRAS 1, 2, and 3 [de la Beaujardiere et al., 1982, 1984b]. The MITHRAS 1 and 3 experiments fit this representation well. In the MITHRAS 2 Experiment, time resolution is increased at the expense of latitude coverage and the separation between the two planes defining the triangle becomes very small.

In terms of this three-dimensional solid, it is apparent that we can put planes through the solid in several ways to get useful two-dimensional representations of the data. We have developed the software to do this. The capabilities are illustrated with examples using MITHRAS-3 data from Chatanika observations on 27 January 1982.

The first cut through the data is a latitude cut. Figures II-2(a) through II-2(d) show the electron density, electron temperature, ion temperature, and line-of-sight ion velocity, respectively. The data were acquired during an elevation scan taking 15 min. The data were accumulated for 55 s and reduced to the basic parameters shown. Depending on the quality of the data and what one is looking for, the accumulation or integration time could be shorter or longer. The axes are altitude and invariant latitude, where each degree of invariant latitude is approximately 100 km in the magnetic north/south direction at the earth's surface. Because the earth's surface has been flattened in this display, the radar line-of-sights appear curved. This cut is particularly good for showing the relation between E- and F-region phenomena and for showing the relative latitudinal locations of structures and boundaries. These figures show E-region ionization, indicating energetic particle precipitation between 64 and 67 A. The elevated F-region electron temperatures in coincidence with enhanced electron density also indicate soft particle precipitation between

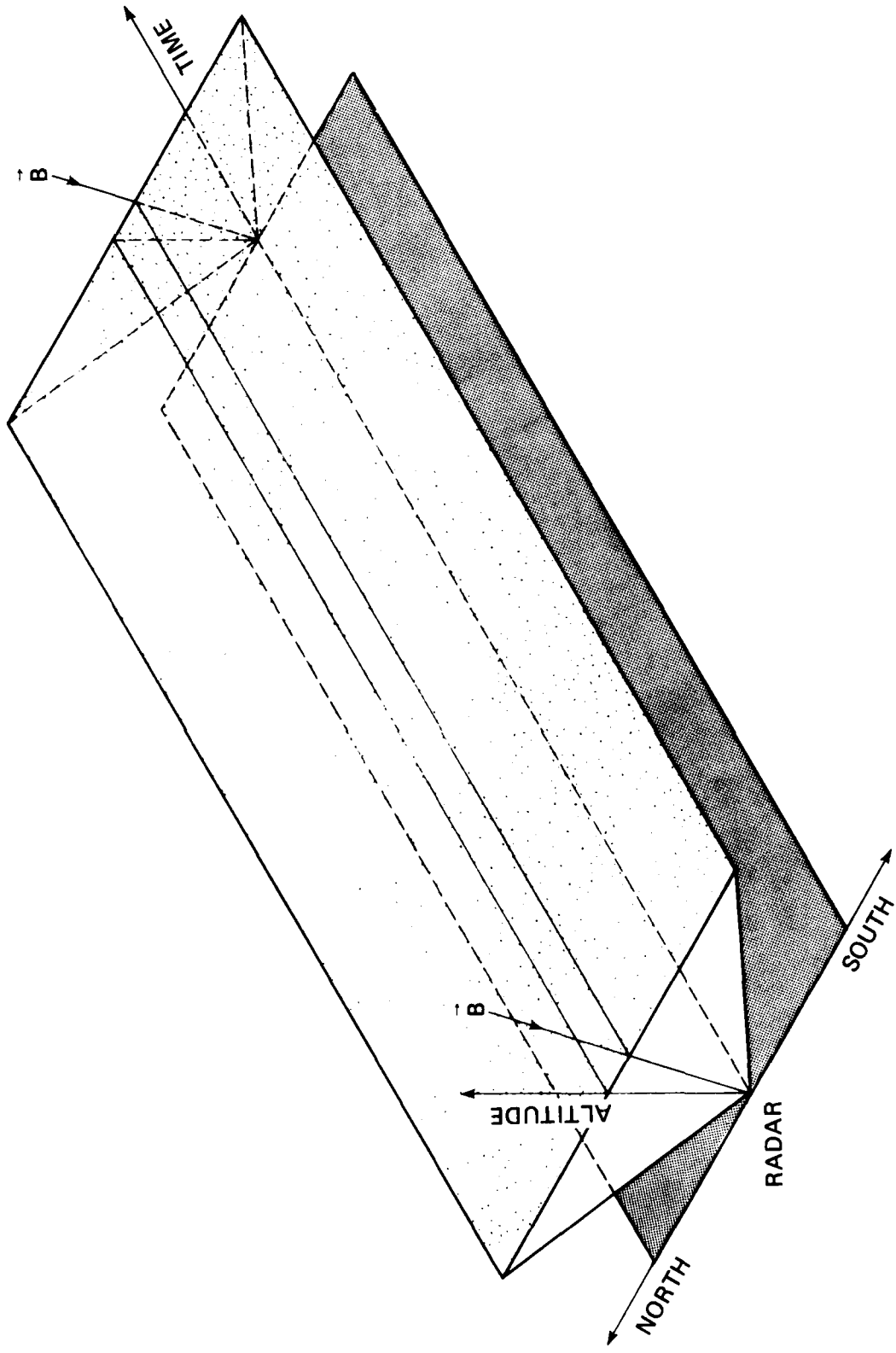
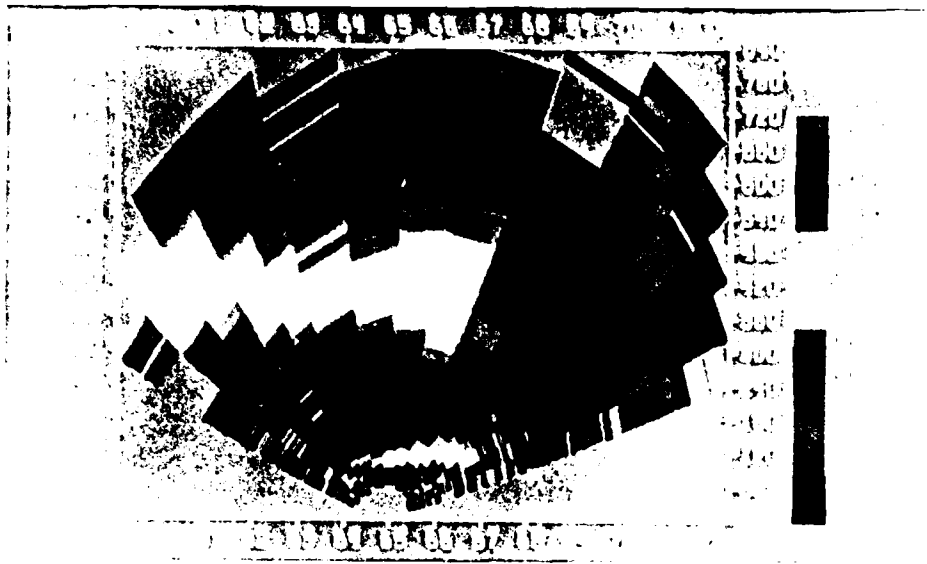
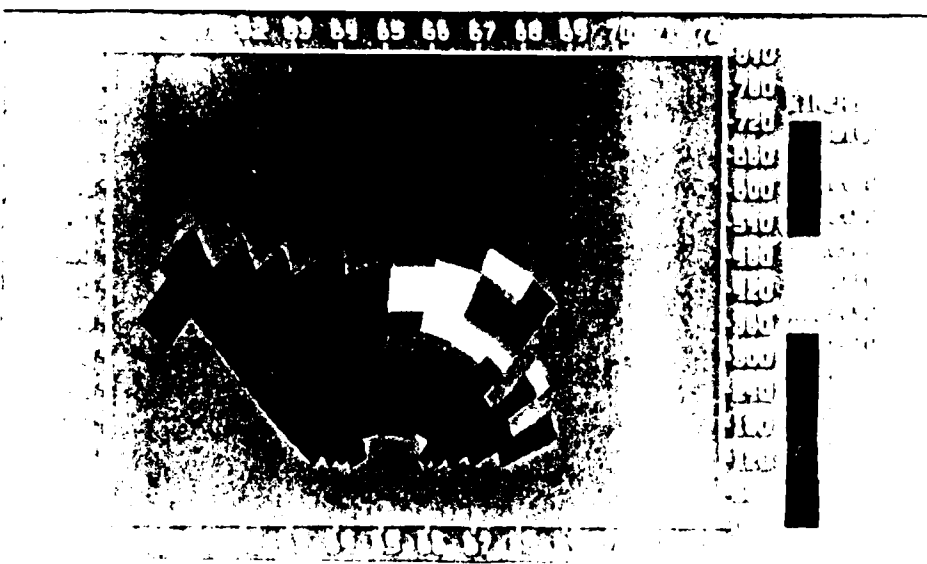


FIGURE II-1 PRISMATIC REPRESENTATION OF THE REGION IN SPACE AND TIME PROBED BY A RADAR

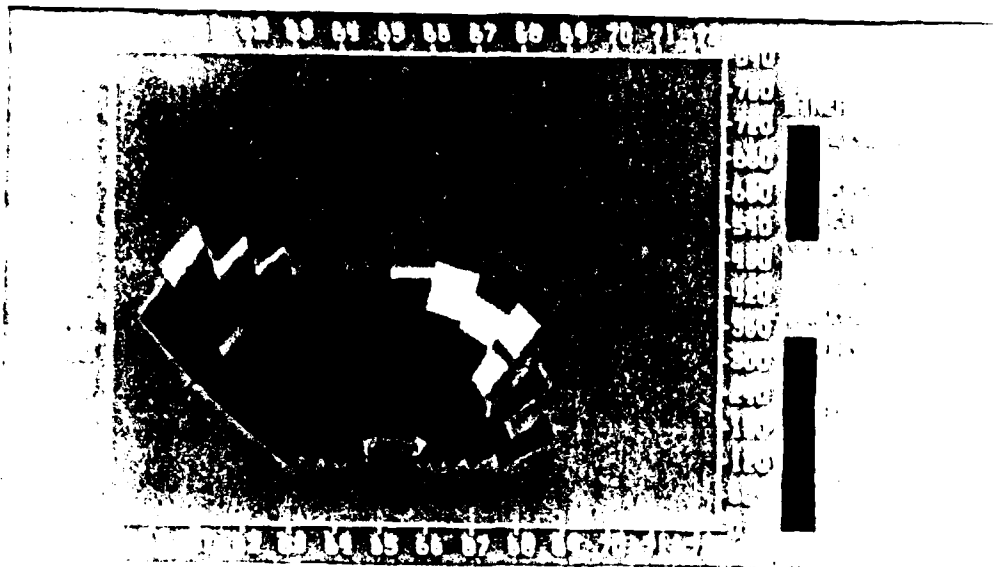


(a) ELECTRON DENSITY —  $\text{cm}^{-3}$

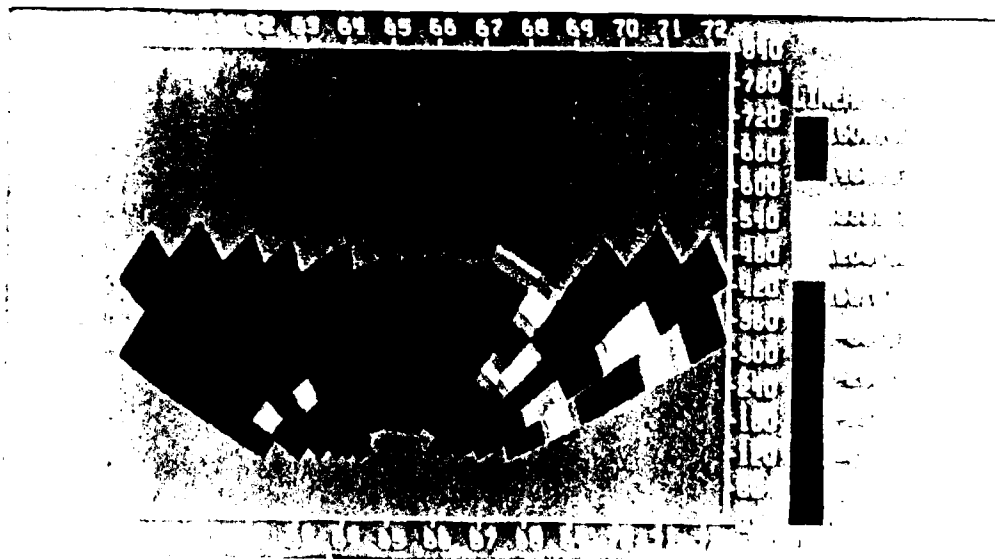


(b) ELECTRON TEMPERATURE — K

FIGURE 11-2 CUT IN MAGNETIC MERIDIAN PLANE AT CHATANIKA BETWEEN 1558 AND 1612 UT (0558 AND 0612 AST) ON 27 JANUARY 1982



(c) ION TEMPERATURE — K



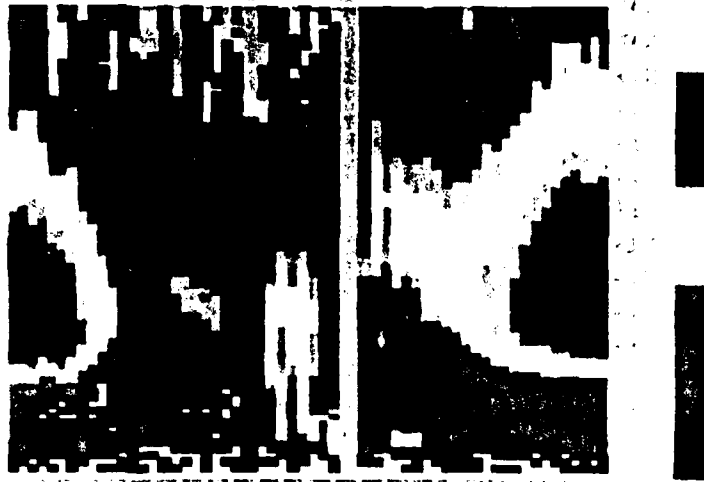
(d) LINE-OF-SIGHT ION VELOCITIES (positive is away from radar) — m/s

FIGURE II-2 (concluded)

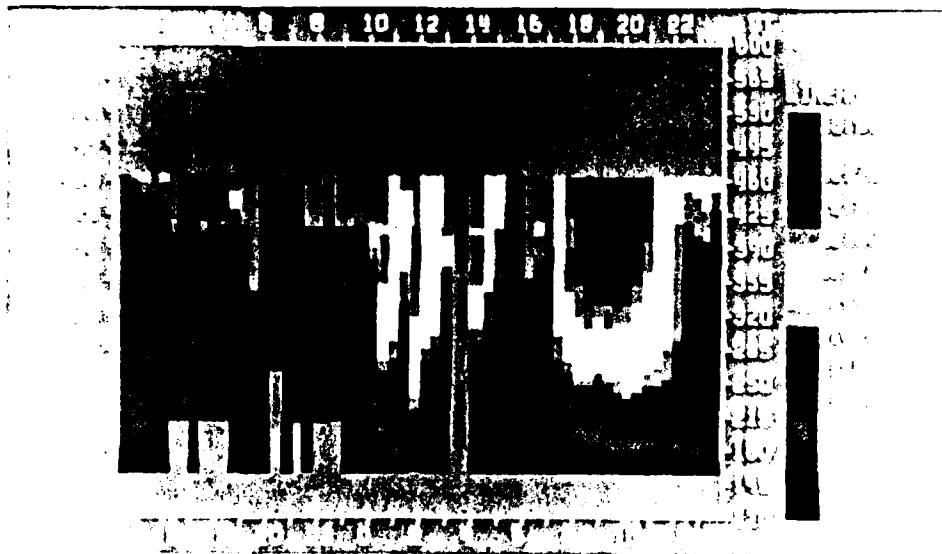
65 and 67 A. Poleward of 67 A, the hard and soft precipitation drop dramatically and Joule heating of the ions sets in. In these representations structures appear vertical when the inputs are aligned along the magnetic field. If a structure were not vertical, it would be a warning that the phenomenon was varying rapidly in time compared to our scan rate.

The second cut through the solid is a plane along the magnetic field direction, with altitude and time as the two coordinates. Figures II-3(a) through II-3(c) show the electron density, electron temperature, and ion temperature. Note the relation between E- and F-region parameters. The F-region density enhancement before midnight is not accompanied by energetic particle precipitation that creates an E region, whereas the F-region density enhancement after midnight is accompanied by energetic particle precipitation. Similarly, note the covariation or lack of covariation among parameters. For instance, no electron temperature increase accompanies the density increase before midnight, whereas one accompanies the increase after midnight. (The implication is that the density increase before midnight was created elsewhere and transported to where it was observed. In contrast, the density increase after midnight was being created locally.) Another feature that stands out is the rapid way in which the various parameters turn on and off such as shortly after local midnight as the radar moves from one region to another or as particle precipitation and convection turn on and off. That some of these changes are caused by crossing boundaries will be more obvious in the next cut.

The third cut through the solid is a horizontal plane at a specified altitude. The axes are latitude and time. The plot may be rectangular or curved to form a clock dial. Examples of electron density at 250, 350, and 450 km are shown in Figures II-4(a) through II-4(c). Examples of electron and ion temperature at 350 km are shown in Figures II-5(a) and II-5(b), respectively. This display is particularly good for showing regions and boundaries. For instance, an ionization trough develops shortly after 1400 LT and extends through the midnight

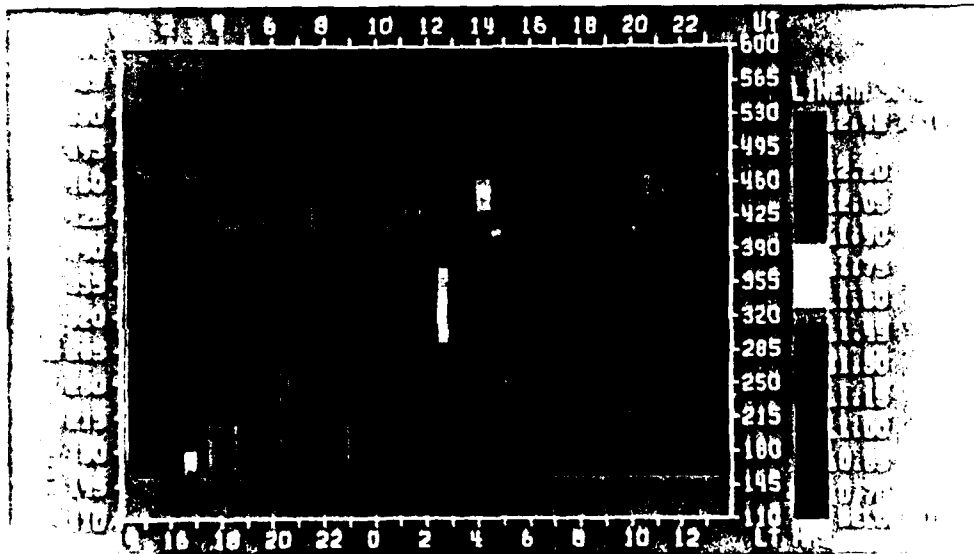


(a) ELECTRON DENSITY —  $\text{cm}^{-3}$



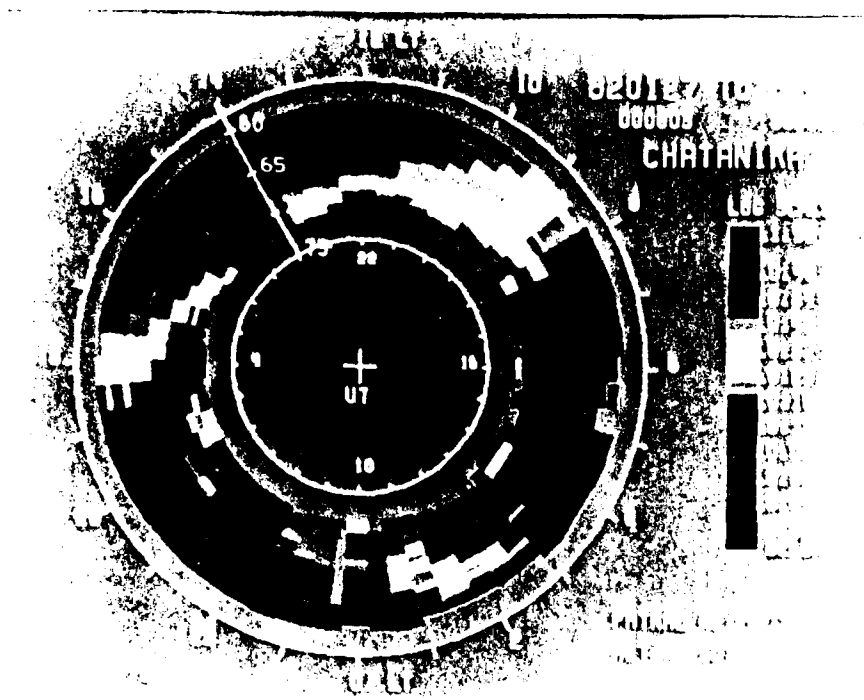
(b) ELECTRON TEMPERATURE — K

FIGURE II-3 CUT ALONG MAGNETIC FIELD AT CHATANIKA ON 27 JANUARY 1982

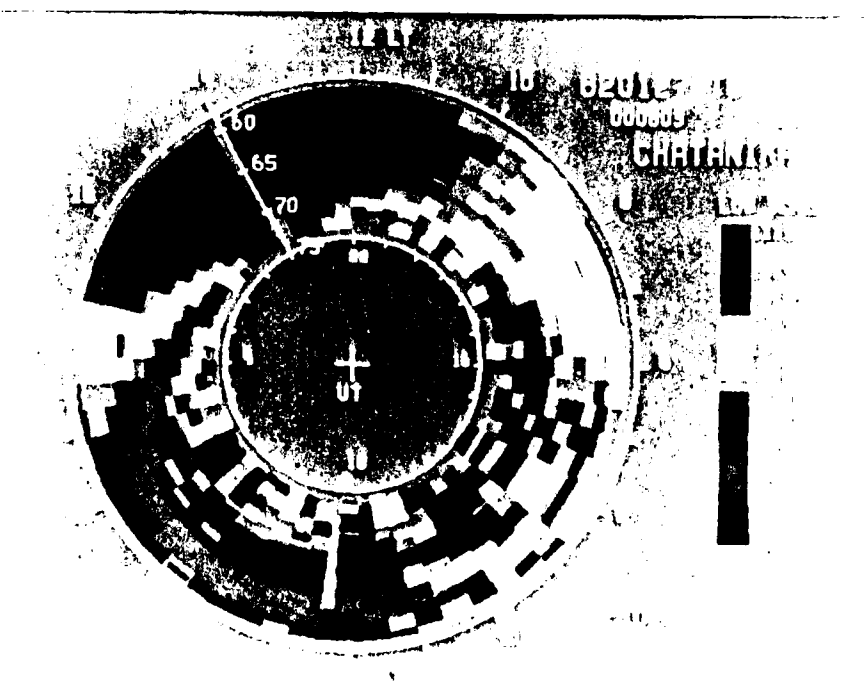


(c) ION TEMPERATURE — K

FIGURE II-3 (concluded)

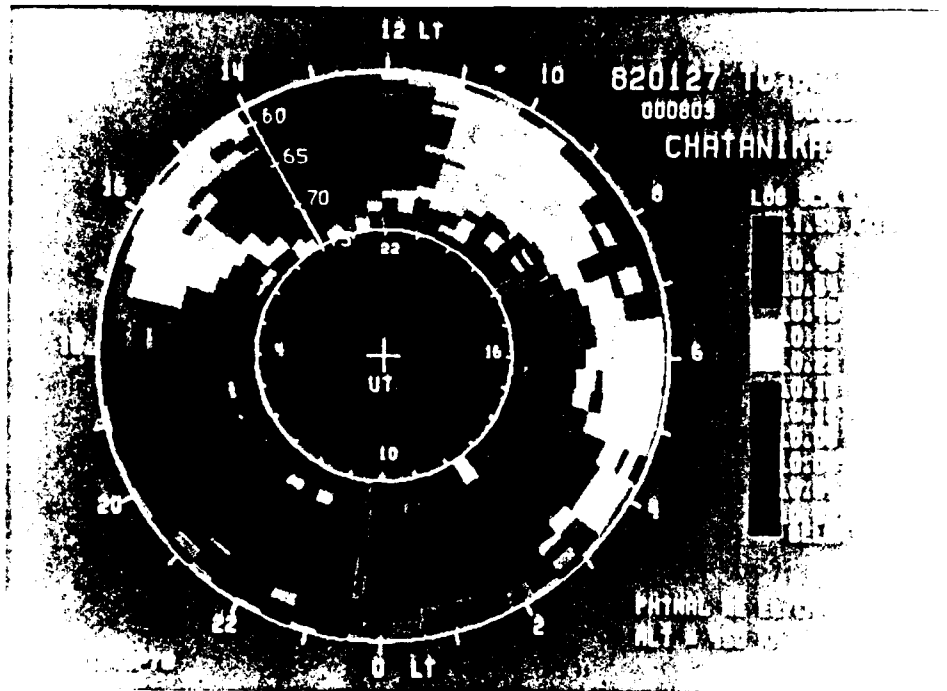


(a) 250 km



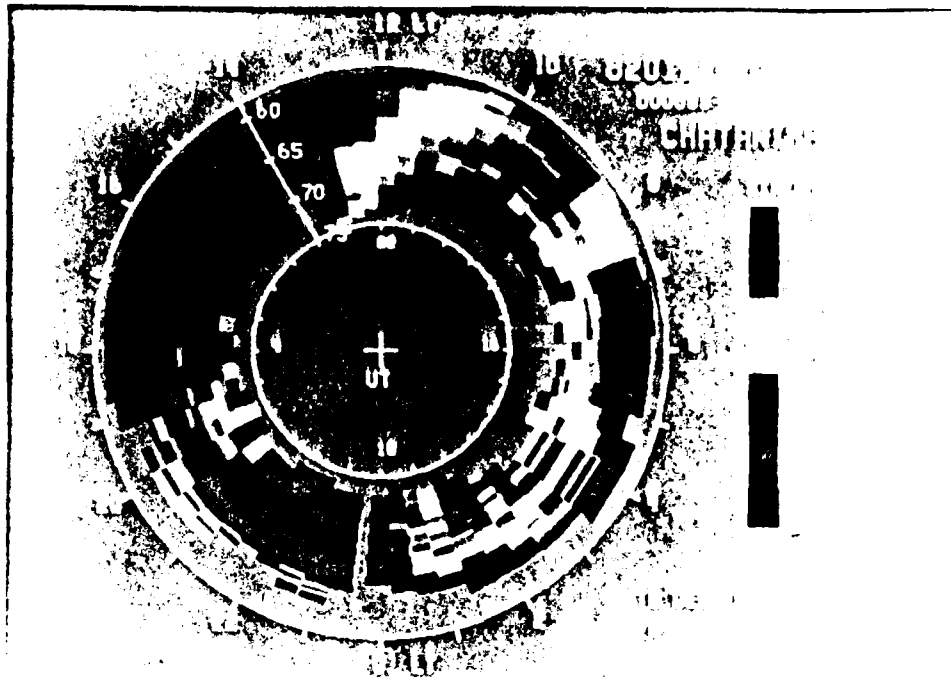
(b) 350 km

FIGURE II-4 CUT AT FIXED ALTITUDE FOR ELECTRON DENSITY AT CHATANIKA ON 27 JANUARY 1982

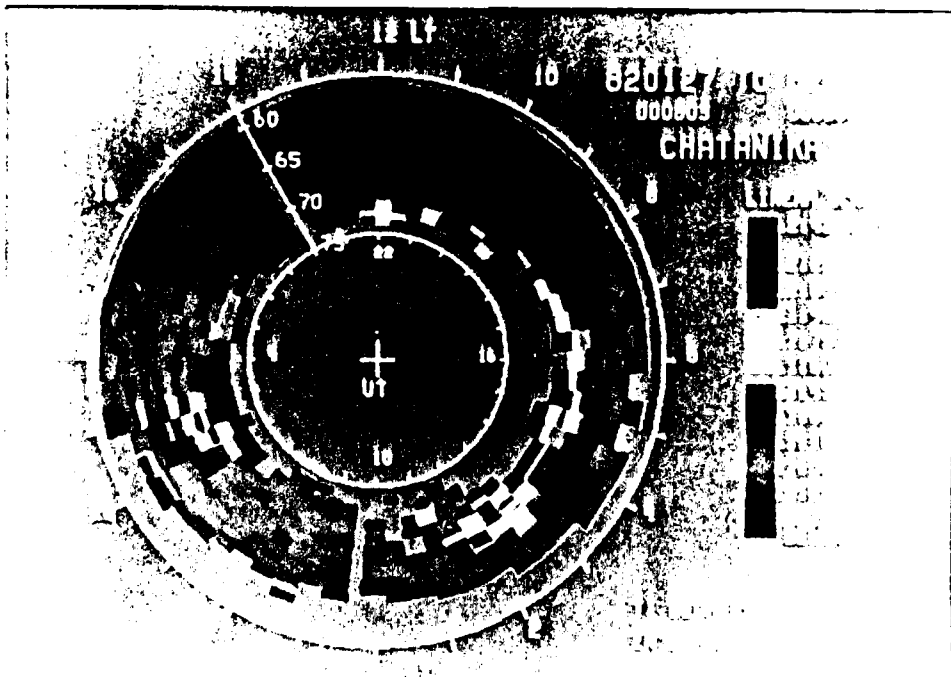


(c) 450 km (the units are  $\text{cm}^{-3}$ )

FIGURE II-4 (concluded)



(a) ELECTRON TEMPERATURE — K



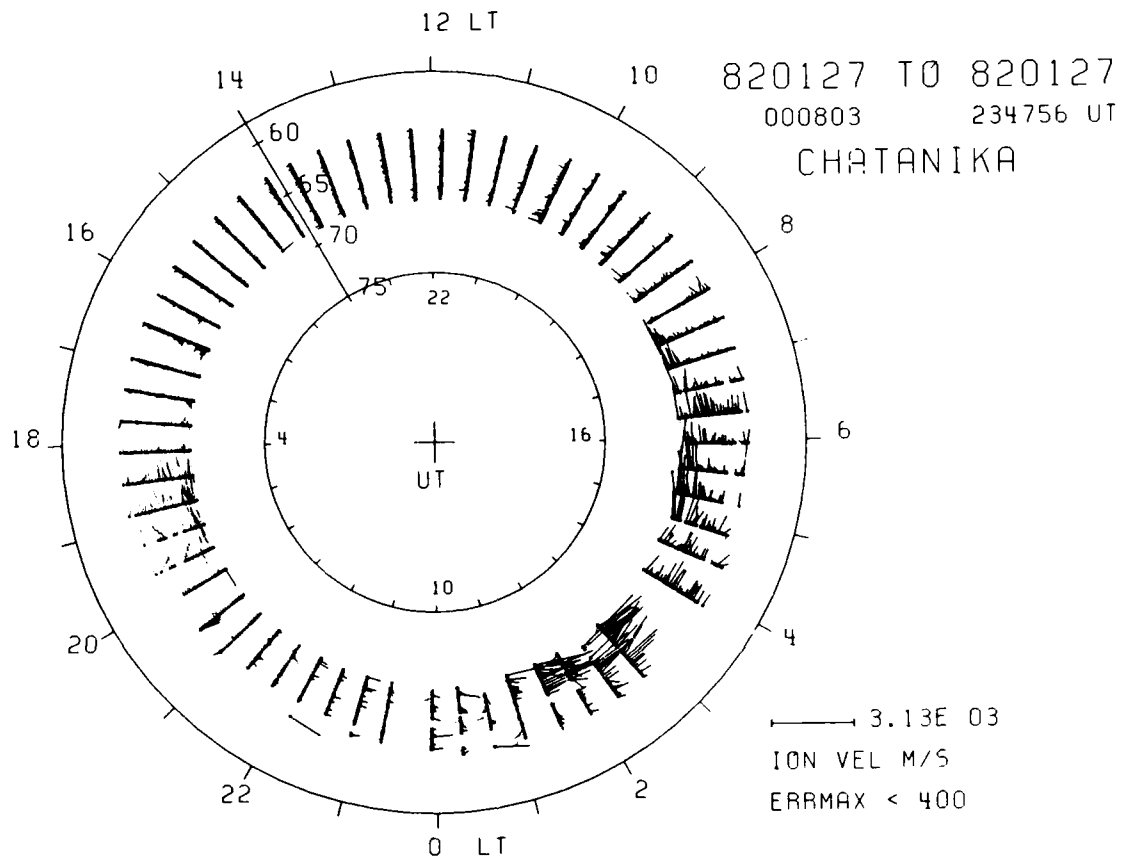
(b) ION TEMPERATURE — K

FIGURE II-5 CUT AT 350 km AT CHATANIKA ON 27 JANUARY 1982

sector. The way the latitude of the trough boundary varies in time can be compared to the convection velocities, Figure II-6, and the solar zenith angles, Figure II-7, all presented in exactly the same format. It is readily apparent that the trough is a magnetospheric related phenomenon, i.e., a phenomenon related to convection, not to solar insolation. Indeed, the trough appears in the region of sunward convection in the evening convection cell. Poleward of the trough, there is considerable patchy ionization. Between 1900 and 2000 LT, the elevated electron temperatures strongly suggest that the patches arise from precipitation. After that, the low temperatures suggest that the patches were produced elsewhere and convected into the field of view. They could have been produced just poleward of the observations or all the way across the polar cap near noon. After midnight, the radar moves under the region of sunward convection in the morning cell. It encounters both Joule heating (elevated  $T_i$ ) and particle precipitation (coincidence in the occurrence of elevated  $N_e$  and  $T_e$ ).

We have presented examples of the three major ways of surveying the data, which correspond to the software packages that were developed under MITHRAS. In the examples, we have shown the four basic parameters derived from the radar measurements. Most of the derived parameters can be similarly displayed. In addition, by using the exchange format discussed above, we can obtain and display data from other radars in the same way. As an example, in Figures II-8(a) through II-8(c), we show electron densities from Chatanika, Millstone Hill, and EISCAT for 18 November 1981 [de la Beaujardiere et al., 1985a]. Major differences in the diurnal pattern are readily apparent. They are discussed in the next section in terms of transport across the polar cap. It is also apparent that the high nighttime densities in the F region at Chatanika and EISCAT are very structured.

In addition to these presentations, we have added the ability to include some correlative data, such as IMF, on the same plot. An example of convection velocities and IMF is presented in Section III. We have also added the ability to bin and plot in the usual ways a large



**FIGURE II-6 ION-CONVECTION VELOCITIES AT CHATANIKA ON 27 JANUARY 1982.** The format is the same as in Figure II-5. The conventions for the vectors are that the tail is at the time of the measurement, that the head is in the direction of the ion velocity, and that the vector is only plotted if the uncertainty in its magnitude is less than 400 m/s. For example, at 0600 UT the ion drift is greater than 1 km/s toward magnetic west at  $67^\circ\Lambda$ , while at 1245 UT the ion drift is approximately 2 km/s toward magnetic east at  $67^\circ\Lambda$ .

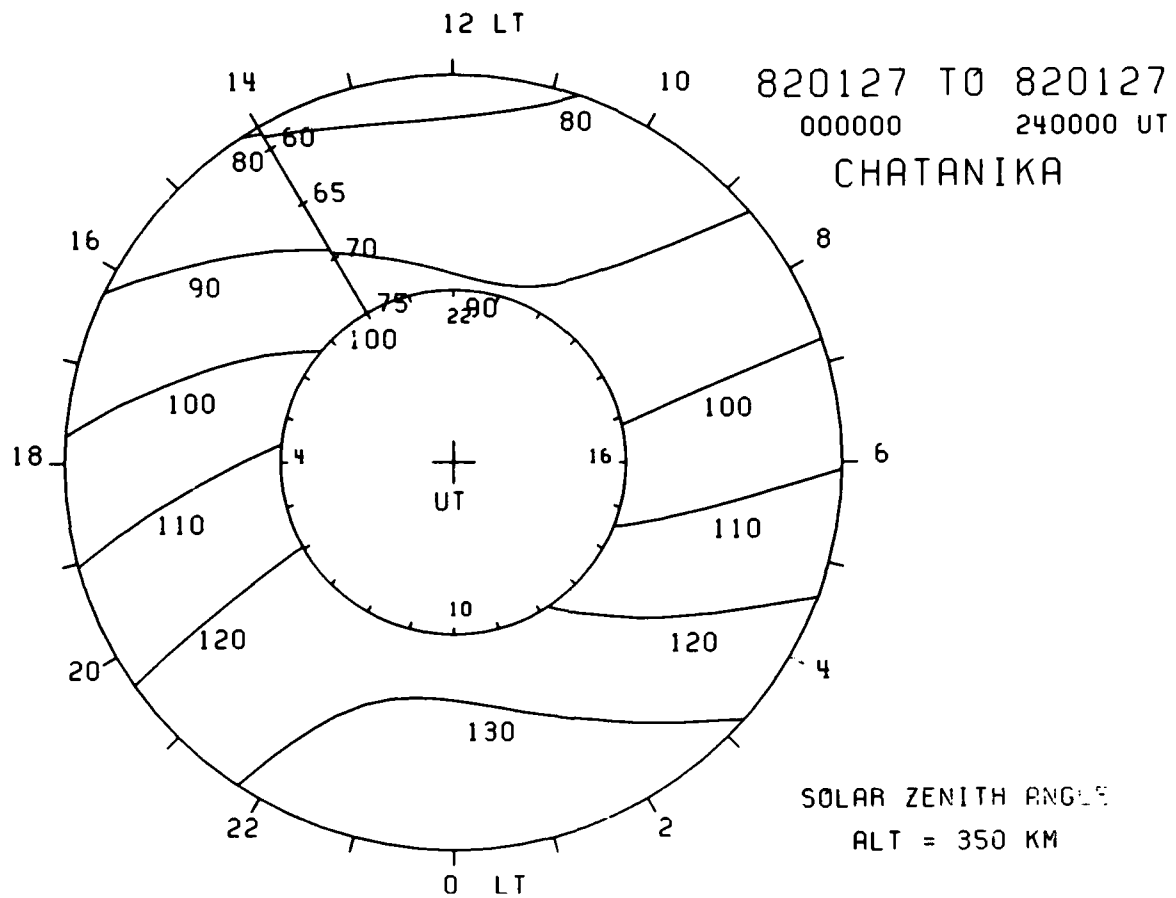
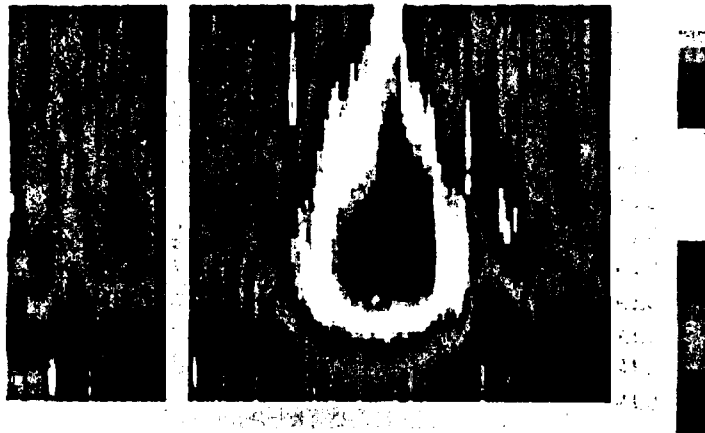
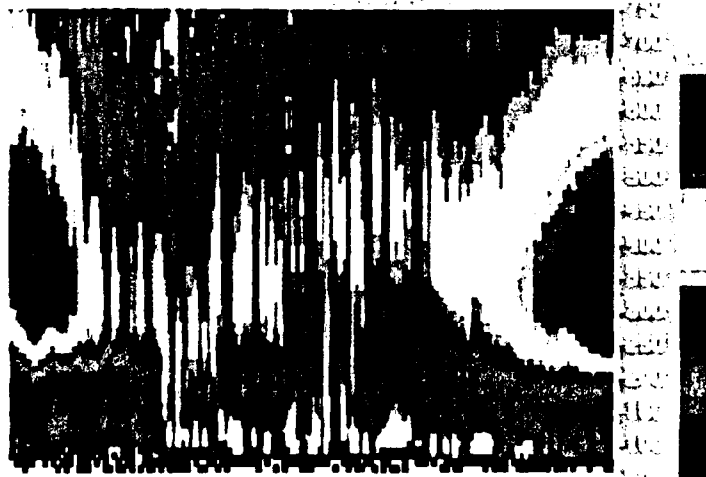


FIGURE II-7 SOLAR ZENITH ANGLES AT CHATANIKA ON 27 JANUARY 1982. The format is the same as in Figures II-5 and II-6. An altitude is needed for the invariant latitude calculation.

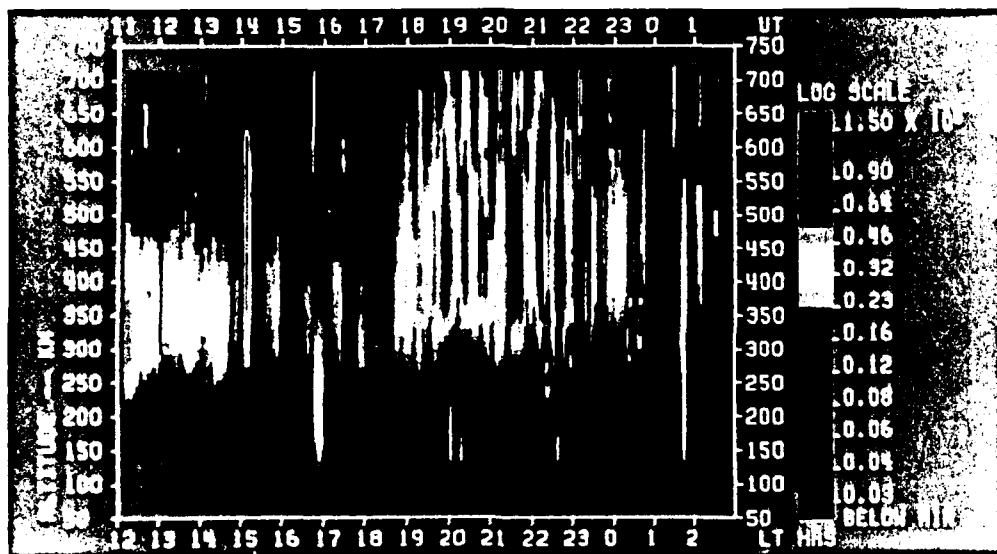


(a) MILLSTONE HILL AT 342° AZIMUTH AND 12° ELEVATION



(b) CHATANIKA ALONG THE MAGNETIC FIELD

FIGURE II-8 ELECTRON DENSITIES AT THREE RADARS ON 18 NOVEMBER 1981



(c) EISCAT ALONG THE MAGNETIC FIELD (the units are  $\text{cm}^{-3}$ )

FIGURE II-8 (concluded)

sample of data so then we can examine average behavior instead of particular cases. An example of the variation of convection velocity with IMF By direction is presented in de la Beaujardiere et al. [1985b; 1986].

In conclusion, software was devised to display the data in three phases from the four-dimensional volume formed by the space and time coordinates. This software has provided us with a powerful tool for examining the various high-latitude phenomena.

### C. Data Analysis

Before MITHRAS, our research efforts concentrated on the relatively easy-to-analyze E-region data from the Chatanika radar. They were principally used to learn about energetic electron precipitation and such electrodynamic parameters as conductivities and currents. Although Chatanika provided much F-region data as well, the only parameter routinely used was the easy-to-derive convection velocity. However, the fact that there are only small amounts of E-region data from the EISCAT experiments, and that there are none from Millstone Hill in the auroral region has prompted us to develop analysis procedures for using the other F-region parameters for studying auroral related phenomena: soft-particle precipitation, downward heat flux, electron-energy-loss rates, optical emissions, and meridional neutral wind.

When low-energy electrons, those having energies less than 400 eV, precipitate into the atmosphere, they penetrate to F-region altitudes only. In doing so, they ionize the neutral gas and heat the ambient electrons. Because of the long chemical lifetimes, on the order of one to several hours, F-region ionization can be transported great distances (Section III.B). Therefore, increases in density need not indicate particle precipitation. However, the electron gas heats up and cools in the order of a few seconds to a few tens of seconds, which suggests that electron temperature is a better parameter for indicating soft-particle precipitation.

However, the electron temperature alone is not a good indicator of energy deposition by either soft particles or other sources. If the electron density is low, a given energy input may increase the electron temperature greatly. If the density is high, that same energy input will raise the temperature far less. Thus, when we examine electron densities and temperatures, we find that, if two regions (at the same altitude) have the same electron density, and one has a higher temperature, then more energy is deposited into that region. Similarly, if one region has both a higher density and a higher temperature, then greater energy is deposited into that region. However, if one region has a lower density and a higher temperature than another, it is impossible to say from a qualitative argument alone into which region the greater energy is deposited.

Another difficulty with a qualitative analysis is that it does not tell which of several possible mechanisms, solar EUV, particle precipitation, or heat conduction, contributes to the energy deposition. Most of these problems can be solved by the proper quantitative analysis of the data. In conjunction with the Sondrestrom radar project, we have developed the software to make the above analysis more quantitative.

We have developed least-squares fitting procedures to smooth the electron- and ion-temperature profiles [Kofman and Wickwar, 1984]. We have also devised new methods for estimating the neutral temperature (and its asymptotic value, the exospheric temperature) [Alcayde et al., 1983a; Wickwar and Kofman, 1984]. Using these profiles and a model of the neutral atmosphere, the energy loss rates from electrons to ions and neutrals can be calculated. As part of that calculation, the downward heat flux into the electron gas near 500-km altitude can also be derived [Kofman and Wickwar, 1984]. In addition, the emission at 6300 A from atomic oxygen and at 5200 A from atomic nitrogen can be calculated for thermal excitation and dissociative recombination.

Thus we can determine the total energy loss rate, which has to be equal to the net energy input to the electrons from all sources, local and otherwise. This is very helpful for determining the location of

soft-particle precipitation. Although most of the energy of precipitating particles may not be carried by soft particles, they are important for creating F-region ionization, existing F-region optical emissions, producing metastable species that can be transported great distances, and for affecting the thermospheric wind system. We can also determine the energy delivered to the electron gas from above by heat conduction. Although it is not clear whether the energy is deposited just above our maximum altitude by very soft particles or whether it is conducted from far out in the magnetosphere, this is a new capability that we have never had before in the auroral region.

We have significantly improved in the procedure with which we can derive the horizontal neutral wind in the magnetic north-south direction. Our ability to calculate this parameter as of the beginning of MITHRAS was discussed in Wickwar et al. [1984c]. Since then, we have improved the actual calculation, added the ability to use the Jacchia 1971 model and to vary the assumed exospheric temperature, and developed procedures with which to find the derivatives of the temperatures, which are needed to determine the diffusion velocity properly. Our meridional-neutral-wind calculations have now been developed to the point where they are a very useful tool for ionospheric and thermospheric studies.

The derivation of analytic temperature profiles are useful for additional F-region analyses. We can now calculate the excitation of the  $O(^1D)$  state of atomic oxygen, which leads to emission at 630 nm, from dissociate recombination and from collisions with thermal electrons [Wickwar and Kofman, 1984].

We have, in addition, been able to improve the derivation of the meridional neutral wind [Wickwar, 1984]. Instead of estimates, the calculation now uses the electron- and ion-temperature gradients in the diffusion calculations.

In conclusion, we have thus considerably extended and improved our ability to use the F-region data from the radar observations to learn about the physical processes occurring in the F region.

### III RESEARCH

Appendix C lists a large number of publications and presentations involving MITHRAS. These are the result of new observations, efforts to develop and validate new analysis procedures, studies of coincident radar and satellite observations, and steps in an ordered progression from simple to complex comparisons with theory. In this section, we place these works in the larger context that we outlined in Section I, thereby giving a "logical" review of the research.

We start with the work that pertains to the magnetosphere, namely, the convection pattern and the precipitation. From there, we turn to the ionosphere, i.e., the F-region electron density and the factors affecting it, the electron temperature, and the ion temperature. Finally, we discuss the neutral atmosphere, in particular, the neutral wind and temperature.

#### A. Magnetosphere

Two major manifestations of the coupling of the magnetosphere to the ionosphere and neutral atmosphere can be detected with the radars. The first is the electric field that is mapped down the field lines from the magnetosphere to the upper atmosphere; the second is the precipitation of electrons and ions from the magnetosphere.

##### 1. Convection

As stated above, convection plays a key role in the coupling of the magnetosphere to the ionosphere and neutral atmosphere. Above about 180 km both ions and electrons convect in the  $\vec{E} \times \vec{B}$  direction. A number of effects occur as a result of collisions between ions and neutrals. Momentum is transferred to the neutrals, dragging them along with the ions. In the E region, the ion motion is impeded by collisions with

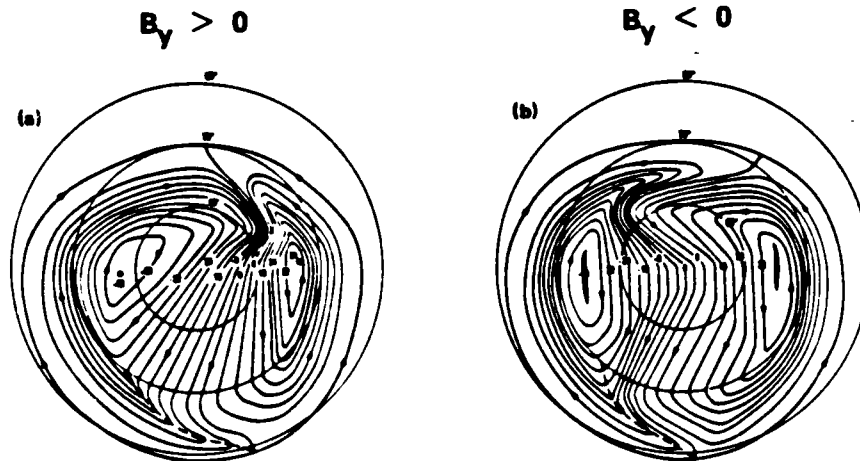
neutrals. Therefore, the ions and electrons do not travel at the same velocity and auroral electrojet currents are generated. In the E and F regions, the ion-neutral collisions produce Joule heating. The energy from Joule heating can be very large. We will look at some of the effects in a later subsection.

Our interest here is on convection itself, not its consequences. We will describe a number of MITHRAS studies that were designed to determine the convection pattern, what affects it, and how it evolves. Some of these relied on simultaneous, but widely separated, observations by the high-latitude radars; others depended on observations from the highest possible latitudes, from Sondrestrom.

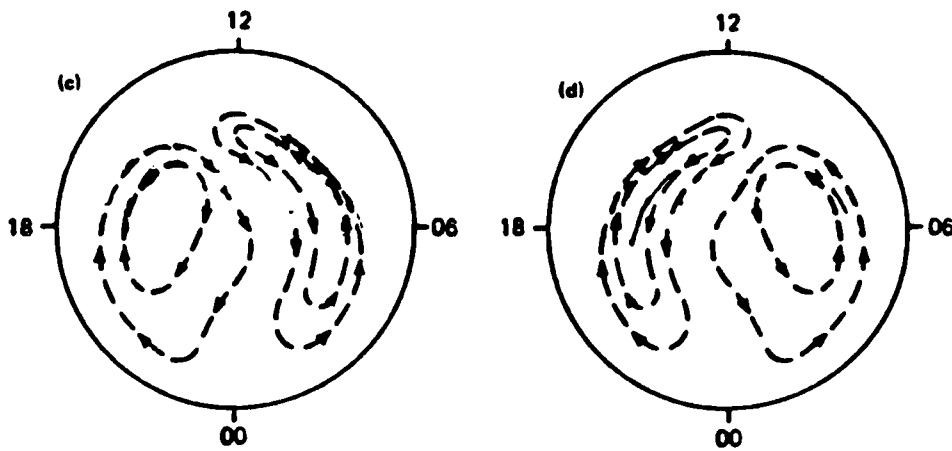
#### a. Global Convection Pattern

The plasma convection pattern in the polar regions is, to a first approximation, in the form of two convection cells; the flow is anti-sunward across the polar cap and sunward along the auroral oval [Figures III-1(a) to (d)]. However, considerable uncertainty and controversy still exist concerning important aspects of plasma convection. What is the exact shape of the convection pattern? What is the relative importance of the dawn and dusk cells, what are the precise shapes of the cells, and is the overall pattern rotated toward early hours? Is this pattern substantially modified during substorms or is it simply intensified? Recently, several researchers have suggested that the pattern may be more complex, consisting of three, four, or even five cells intricately distributed over the high-latitude region [Zanetti et al., 1984; Potemra et al., 1984; Reiff and Burch, 1985; Burch et al., 1985]. These more complex patterns are reproduced in Figure III-1(e) through (n) for several IMF orientations, along with the simpler two cell patterns of Friis-Christensen et al. [1985].

It is well established that the IMF strongly influences the global convection pattern. However, in spite of a large number of observations--ground based as well as spaceborne--the precise role of each of the three components of the IMF is still not well known. The role of

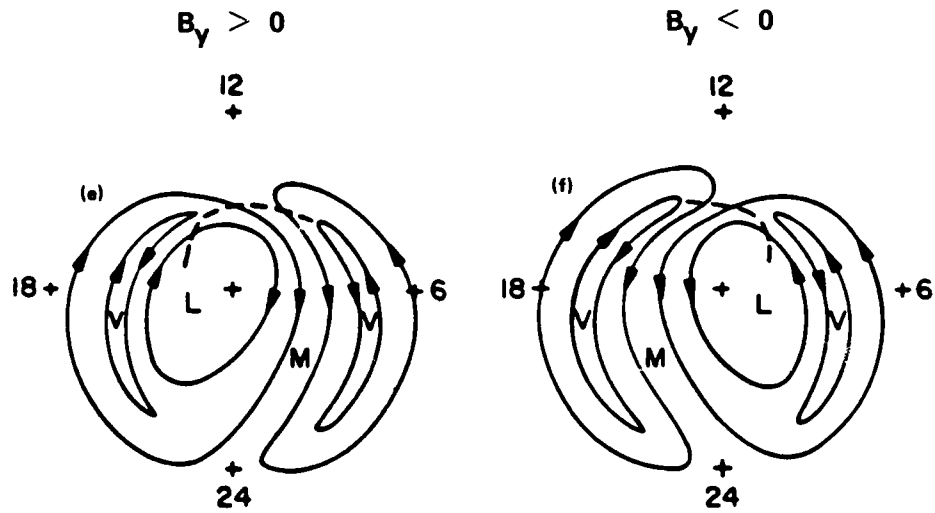


[Source: Heppner, 1984]

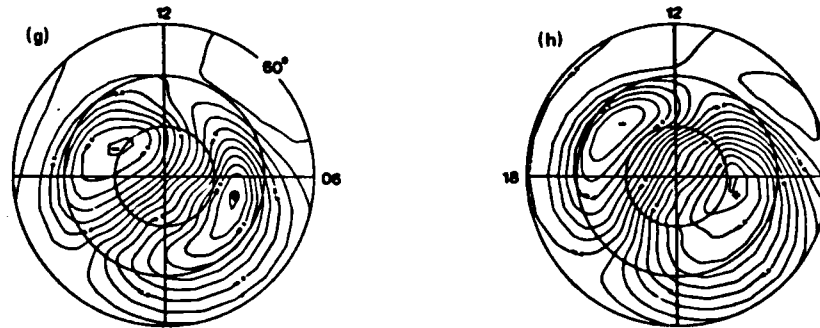


[Source: Potemra, et al., 1979]

FIGURE III-1 RECENTLY PROPOSED CONVECTION PATTERNS.  
 $B_z$  not specified.



[Source: Reiff and Burch, 1985]



[Source: Friis-Christensen, et al., 1985]

FIGURE III-1 (continued) RECENTLY PROPOSED CONVECTION PATTERNS.  
 $B_z$  is negative.

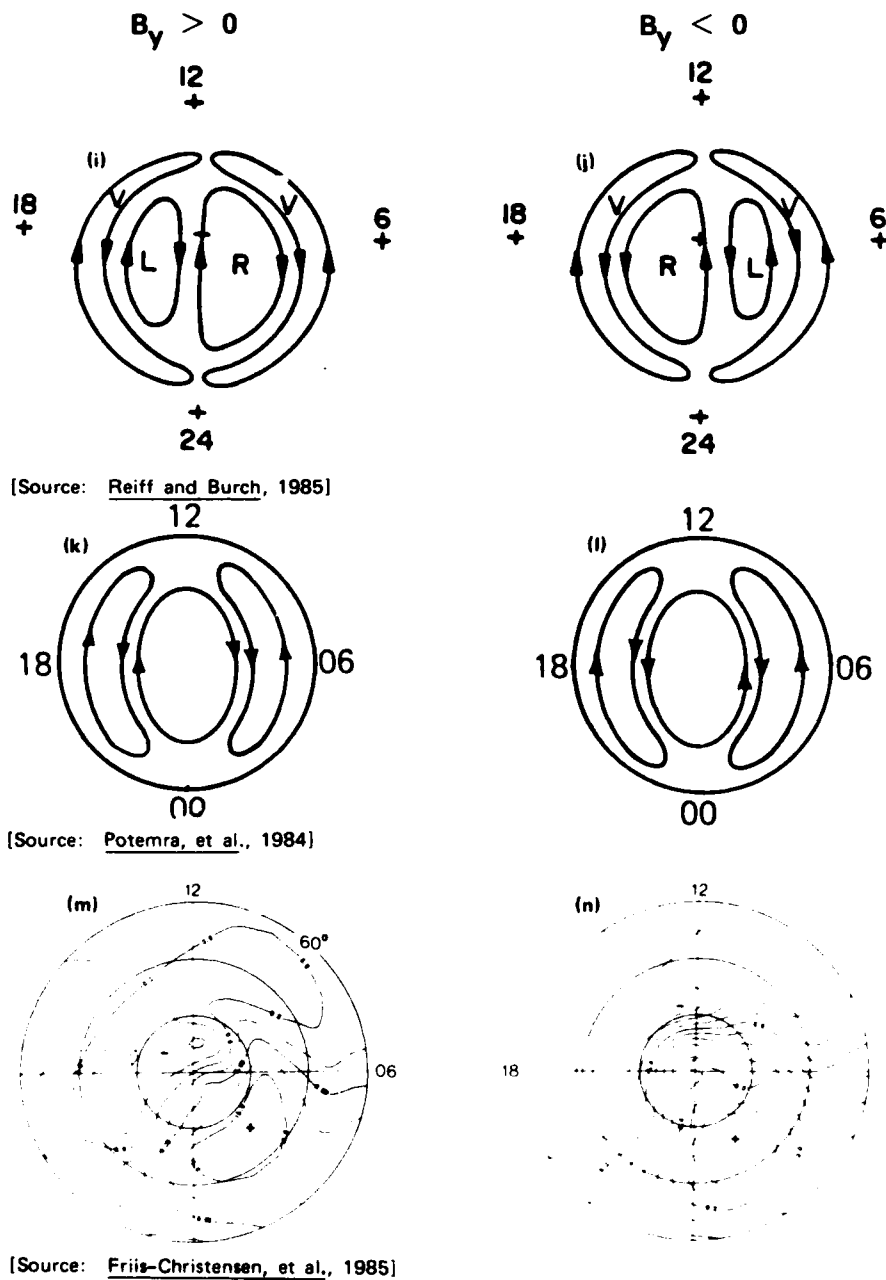
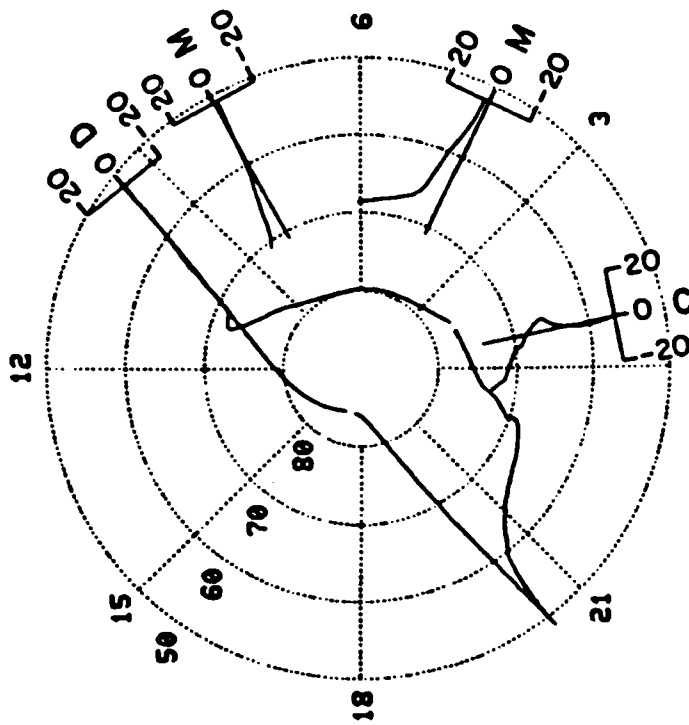


FIGURE III-1 (concluded) RECENTLY PROPOSED CONVECTION PATTERNS.  
 $B_z$  is positive.

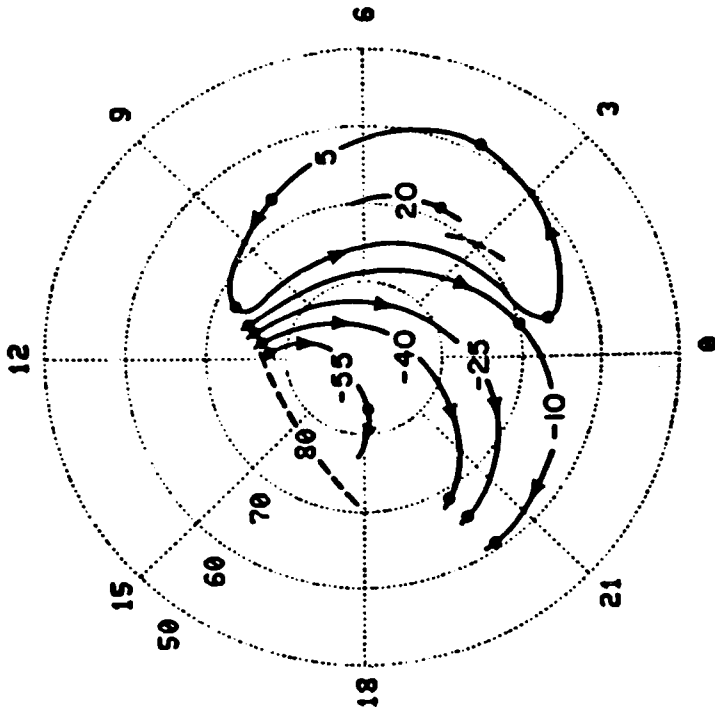
the  $B_y$  component has recently received considerable attention both from a theoretical standpoint [Crooker, 1979; Banks et al., 1984; Reiff and Burch, 1985; Lyons, 1985], and an experimental standpoint [Heelis, 1984; Potemra et al., 1979; Potemra et al., 1984; Zanetti et al., 1984; Burch et al., 1985; Jorgensen et al., 1984; Clauer et al., 1984; McCormac and Smith, 1984; Friis-Christensen et al., 1985]. However, the uncertainty about how the convection is affected by IMF  $B_y$  is still large. This point is illustrated by the variety of patterns that have been proposed in three recent publications on the subject, which are used as sources for Figures III-1(e) through (n).

One reason for such uncertainty is that it is not possible to measure the plasma convection everywhere at the same time. Satellite measurements cover a wide range of latitude, but only along one line. Ground-based measurements with the incoherent-scatter radars have the advantage of providing time variations of the convection, but the field of view is small compared to the overall convection pattern. At present, the most effective way to determine the global pattern is to combine data from several radars with data from satellites. Such an analysis was done in collaboration with Heelis [Heelis et al., 1983]. Vector velocity measurements from DE-2 were combined with MITHRAS radar data. Instantaneous "snapshots" of the polar convection were derived at the time of each northern polar pass during a period of fairly stable conditions (25 October 1981). One of these snapshots is reproduced in Figure III-2, which shows the electrostatic potential distribution. In the F-region, the plasma flows along these equipotentials. We see from Figure III-2 that the afternoon convection cell was roughly circular and of much larger extent than the morning, crescent-shaped cell. During these observations the IMF  $B_z$  was negative and  $B_y$  positive. This orientation corresponds to the conditions for the patterns of Figures III-1(a), (c), (e), and (g) and the observed convection matches the common portions of patterns (c) and (e) fairly well.



[Source: Heelis, et al., 1983]

(a) ELECTROSTATIC POTENTIAL DISTRIBUTIONS. THERE ARE BOTH EAST AND WEST CONTRIBUTIONS FROM MILLSTONE HILL.



(b) INFERRED POTENTIAL CONTOURS. THE CROSS POLAR CAP POTENTIAL IS ABOUT 80 kV. THE DASHED LINE IS THE POLEWARD BOUNDARY FOR AURORAL PRECIPITATION ENERGY FLUX LESS THAN  $0.25 \text{ erg/cm}^2$  DETERMINED FROM THE NOAA 6 AND 7 SATELLITES.

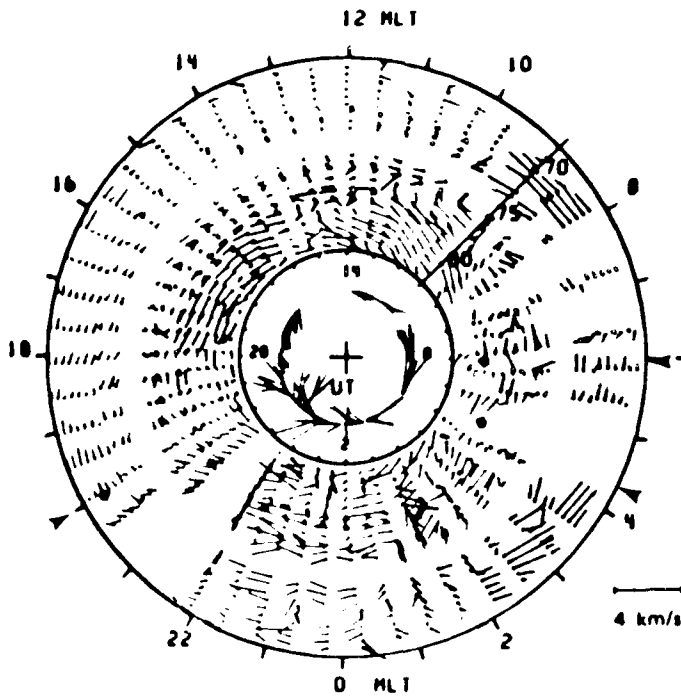
FIGURE III-2 CONVECTION PATTERN AT 1050 UT ON 25 OCTOBER 1981 BASED ON OBSERVATIONS BY DE-2, CHATANIKA, AND MILLSTONE HILL. The IMF  $B_y$  was positive;  $B_z$  was negative.

Further studies of the instantaneous convection pattern are needed, particularly for other IMF conditions and for a denser set of observations such as is obtained using Millstone Hill, Sondrestrom, and EISCAT.

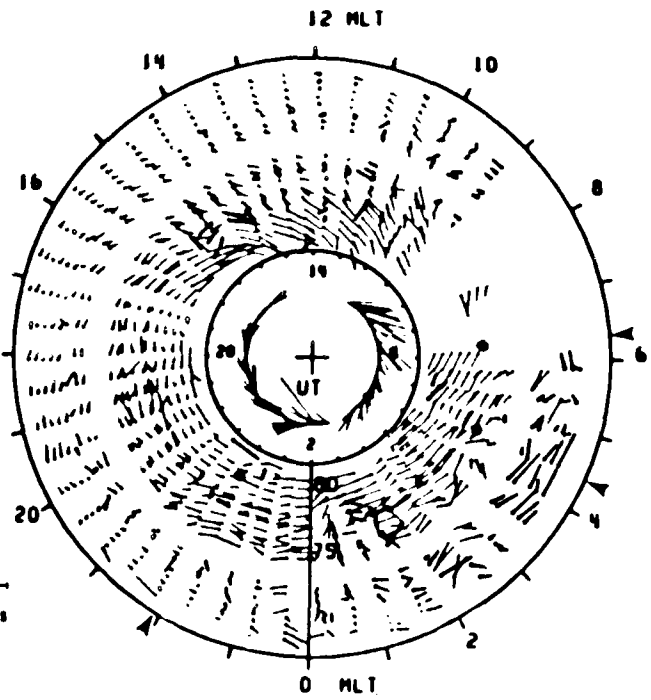
b. Effect of the IMF  $B_y$  Component

Although little doubt exists that the IMF  $B_y$  component strongly influences the whole convection pattern, most studies have concentrated on the daytime pattern. In fact, all the patterns shown in Figure III-1 are based mostly on daytime observations. In contrast, little attention has been given to the  $B_y$  effect on the nightside of the convection since the early observations of Heppner [1972] and Mozer et al. [1974].

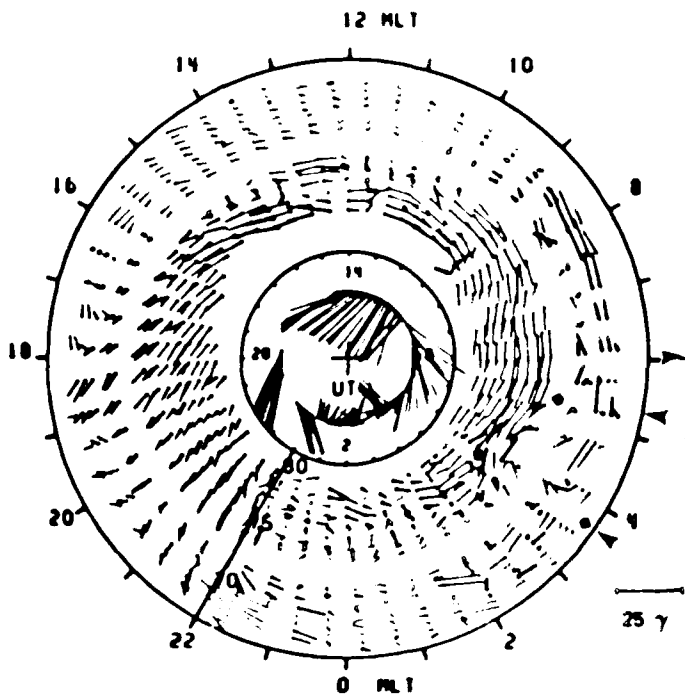
In three separate studies, the Sondrestrom radar 24-hour runs have been analyzed to determine how  $B_y$  affects the nighttime convection [de la Beaujardiere et al., 1985b,c; 1986]. In the first study, four events on 23 and 24 April 1983 were examined. In the other studies, two years of observations from 1983 and 1984 were examined, both individually and statistically. Velocity vectors from the first study are shown in Figure III-3. These days were selected because they are representative of features observed on many days. The IMF  $B_z$  and  $B_y$  vectors (GSM coordinates) are displayed in the inside circle. Red is for westward velocities and positive  $B_y$ ; blue is for eastward velocities and negative  $B_y$ .  $B_z$  is positive toward the center of the circle. Averaged vector velocities are shown in Figure III-4. These figures show that the  $B_y$  component of the IMF strongly influences the nightside polar convection. Its effect is quite complex. The convection for one orientation of  $B_y$  is not the mirror image of the other orientation. This asymmetry is in disagreement with the schematic patterns proposed by Potemra et al. [1979; 1984] and Reiff and Burch [1985], but it is present in the empirical models by Heppner [1984] and Friis-Christensen et al. [1985] (Figure III-1). A positive  $B_y$  seems to organize the velocities such that, at all local times, they are predominantly westward within the radar field of view. Figure III-3(b) offers a clear example of this; the radar appears to remain under a large westward vortex for 24 hours.



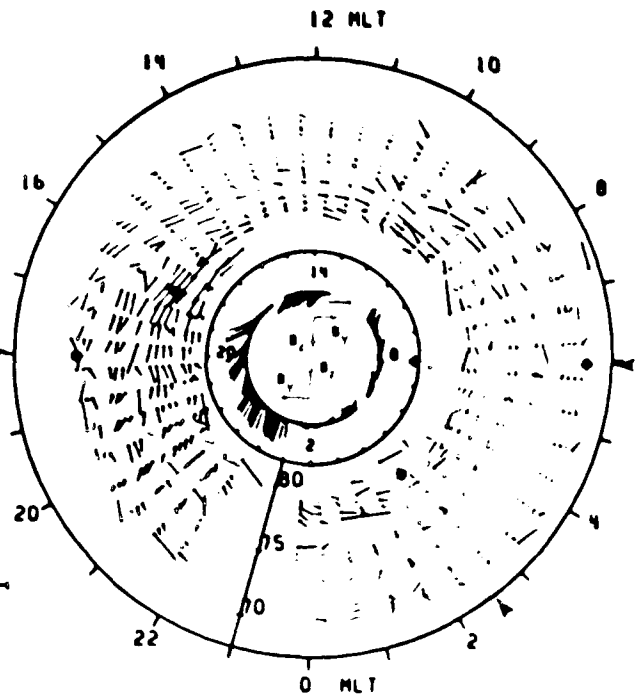
(a) 23-24 APRIL 1983



(b) 13-14 JULY 1983



(c) 23 JULY 1983



(d) 18 JANUARY 1984

FIGURE III-3 IMF BY INFLUENCE ON CONVECTION

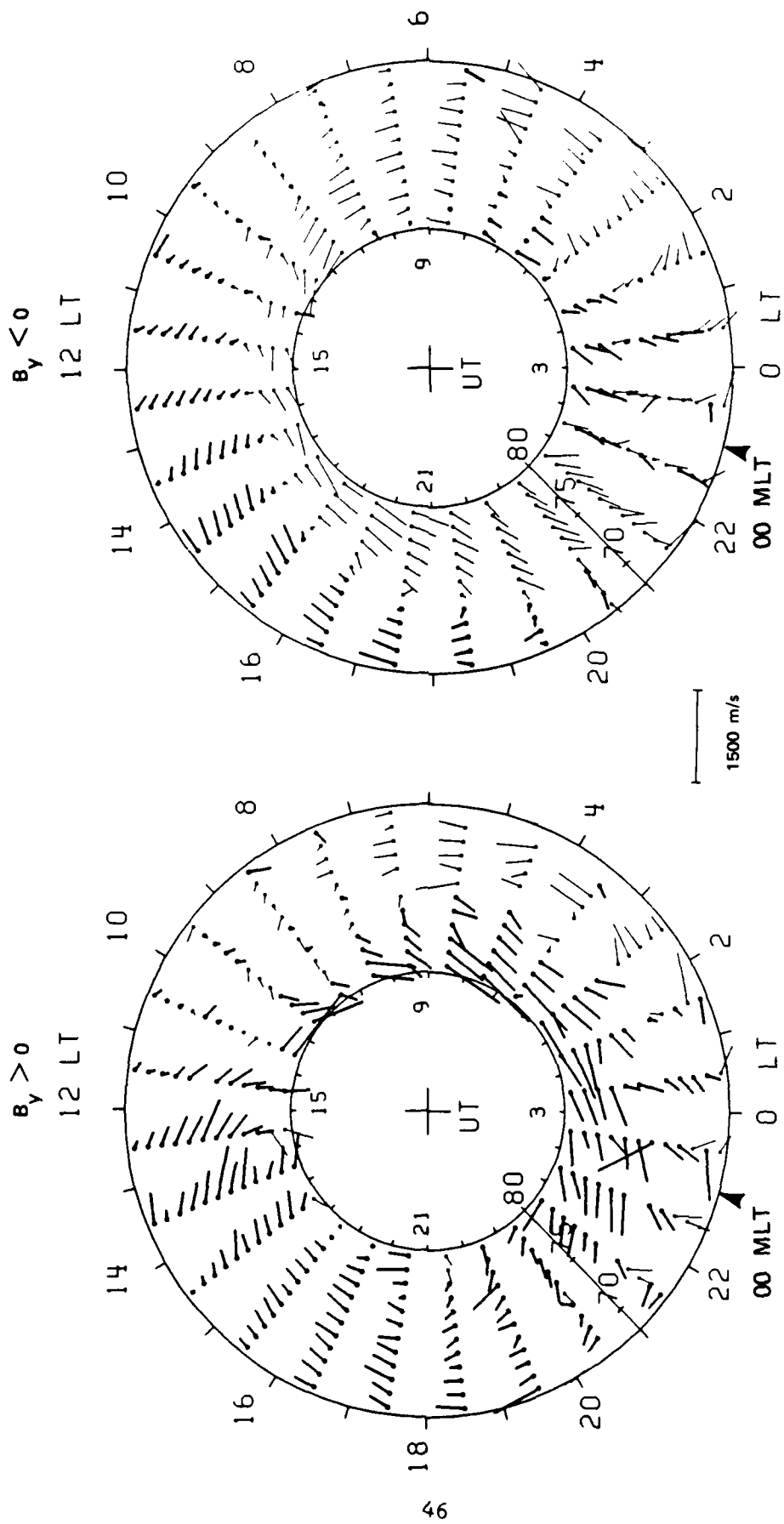


FIGURE III-4 AVERAGE ION DRIFTS MEASURED BY SONDRSTROM RADAR FOR  $B_y > 0$  AND  $B_y < 0$ . The heavy lines denote westward velocities, and the thin lines eastward velocities. Magnetic midnight is at 0200 UT and local midnight at 0300 UT.

Between dusk and midnight, on 23 and 24 April 1983, sunward flow is observed within the polar cap [Figure III-3(a)]. In the midnight and dawn sectors, when  $B_y$  is negative, the plasma velocities often appear random [18 January, Figure III-3(d)]. For large negative  $B_y$ , the afternoon cell appears shifted toward early hours such that large southward velocities are observed about three hours before midnight [23 July, Figure III-3(c)]. The only times when the predominant velocity component is southward are in the premidnight hours, when  $B_y$  is large and negative.

Thus, the  $B_y$  effect of the IMF on convection is very clear and very dramatic. This avenue of MITHRAS research should be continued and extended. The data exist to do so. The lower latitude data from Chantanka, pertaining mostly to sunward convection and the region around the Harang discontinuity, should be examined.

The effects of other factors should also be determined. The first, and most obvious, is season. The seasonal dependence of currents (ionospheric as well as field-aligned currents) is well established, but little work has been done on seasonal dependence of polar cap convection velocities or, equivalently, electric fields. Other factors include the various activity indices. Such parameters would be either magnetic activity indices such as Kp, AE, AU, or global-energy indices such as the auroral oval radius [Gussenhoven et al., 1983] or the auroral precipitation energy index [Hill et al., 1982]. The various energy-related parameters of the solar wind, such as  $B_z$ ,  $VB_z^2$ , or  $\epsilon$ , should also be correlated with the observed electric fields.

c. Data/Theory Comparison with Utah State University Group

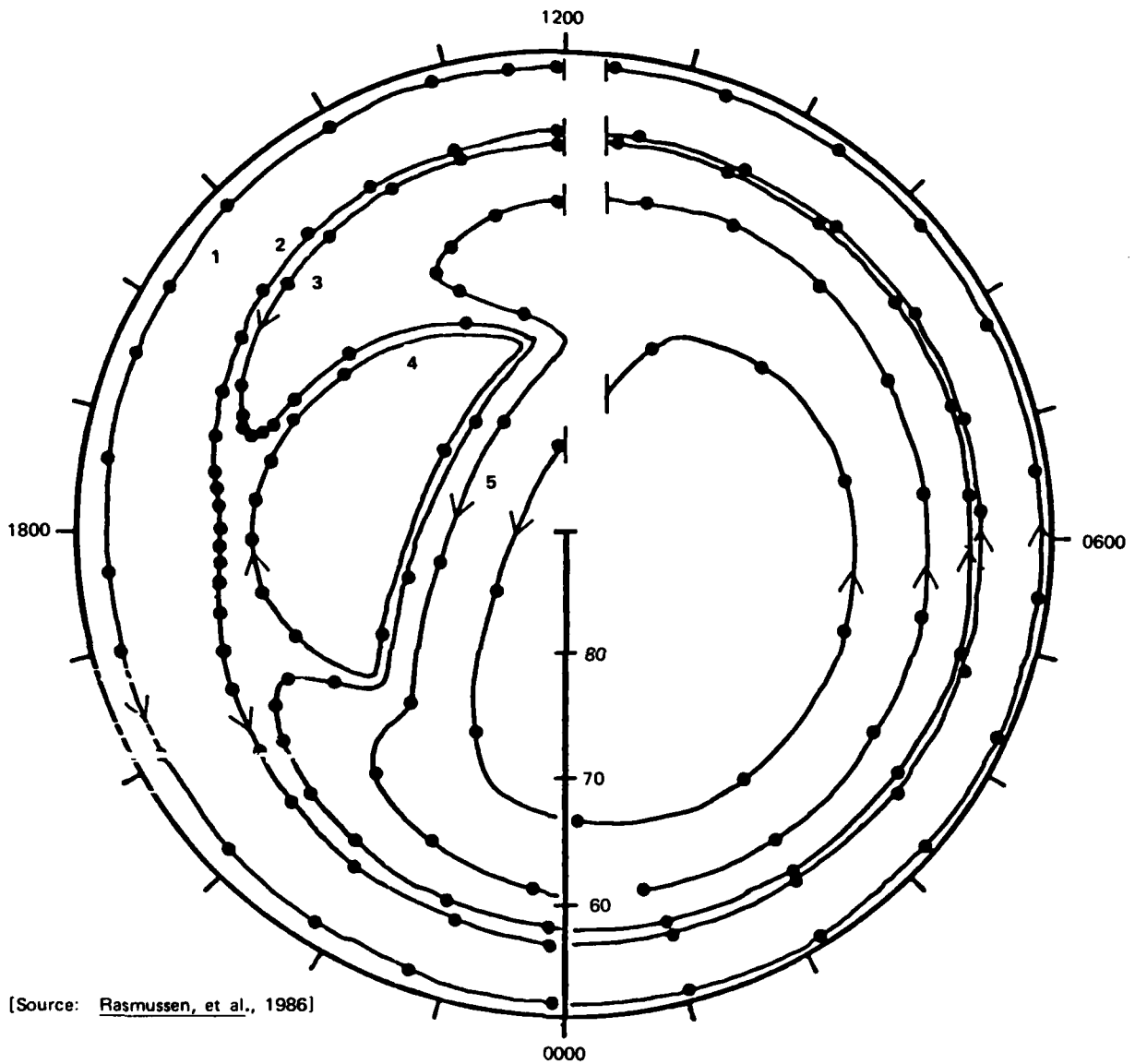
Another method for determining the large-scale convection pattern is used by R. Schunk, J. Sojka, and C. Rasmussen at Utah State University (USU). The pattern is derived by adjusting the parameters of an analytic expression for a two-cell representation, such as those of Volland [1978] or Heelis [1984], until a good fit is achieved. In a collaborative study between USU and SRI, Rasmussen et al. [1986] have

applied the technique to the MITHRAS data of 27 and 28 June 1981 from Chatanika, Millstone Hill, and STARE. Despite small disturbances (or substorms), they were able to fit one pattern remarkably well to the whole set of velocity data. This pattern is reproduced in Figure III-5. It is in a frame of reference that does not rotate with the earth. The validity of this pattern is strongly supported by the fact that the derived F-region electron densities calculated with the USU global ionospheric model, which depend greatly on the convection pattern, agree closely with the observations. This  $N_e$  comparison will be discussed later.

This indirect technique for inferring the large-scale convection pattern is very effective and more such studies should be pursued. We started a study for 17 and 18 November 1981. The constraints are greater for this period because we have vector ion velocities from all three MITHRAS radars. In addition, we have the meridional component of the thermospheric neutral wind from both Chatanika and EISCAT, as well as two lower-latitude radars--St. Santin and Arecibo. This period is a particularly valuable one to model because it has already been examined in detail in two separate works [Caudal et al., 1984; de la Beaujardiere et al., 1985a].

d. Determination of the Electrostatic Potential Distribution from Magnetometers

The magnetic disturbances measured from a worldwide network of magnetometers can, in principle, be used to deduce the global convection [Kamide et al., 1981; Kamide and Richmond, 1982]. Several inversion methods have been used to deduce the electrostatic potential from the magnetic perturbation vectors [Friis-Christensen et al., 1985 and references therein]. If it could be established that this method can reliably determine the global convection pattern, it would be very powerful because the electric potential could be deduced globally and with good temporal resolution. However, this technique is severely limited by the fact that the results strongly depend on the ionospheric conductivities.



[Source: Rasmussen, et al., 1986]

FIGURE III-5 SELECTED PLASMA STREAM LINES PREDICTED FOR 27 AND 28 JUNE 1981 AS A RESULT OF FITTING CONVECTION VELOCITIES AT CHATANIKA, MILLSTONE HILL, AND STARE. The direction of motion is indicated by arrows; one-hour intervals are indicated by dots. The coordinate system is magnetic local time versus magnetic latitude; the frame of reference is quasi-inertial.

Model conductivities based on statistical averages have to be used because of the paucity of measurements. Despite the great number of magnetometers distributed over the globe, problems can also arise because the data have to be interpolated between the magnetometer stations. This interpolation can introduce significant errors. Therefore, the question still remains as to how meaningful the results of this technique are.

The multiradar experiments can provide very useful observations for improving various aspects of the inversion technique. Work was started on this collaborative project using MITHRAS data in two ways: first to provide a check on the inferred plasma convection, and second, to provide measurements of conductivities that can be incorporated into the calculations. Particle measurements from the NOAA, DMSP, P78-1, DE-2, and HILAT satellites were used to provide estimates of the conductivities. The days selected were 25 October 1981, 26 October 1981, 11 November 1981, 8 December 1981, and 18 to 19 January 1984. So far, Y. Kamide, S.-I. Akasofu, and B.-H. Ahn (Kyoto Sangyo University, University of Alaska, and Kyangpook National University, respectively) have collected, calibrated, digitized, rotated, and verified the magnetometer data from over 100 sites for most of these days. A plot of stacked magnetic disturbances from about 60 stations is shown in Figure III-6 for 11 November 1981. A first attempt at the derivation of the potential function was done before the end of this contract. As a result, A. D. Richmond (NCAR) has modified the inversion technique so as to include the measured conductivities and electric fields whenever and wherever they exist.

e. Electric Fields at Subauroral Latitude

We have studied subauroral electric fields that have been observed in the afternoon or evening sector during several MITHRAS experiments. In particular, on 18 November 1981 [Caudal et al., 1984] and 11 November 1981 [Senior, 1982; Senior et al., 1986]. These electric fields give rise to large sunward ion drifts that occur equatorward of the auroral

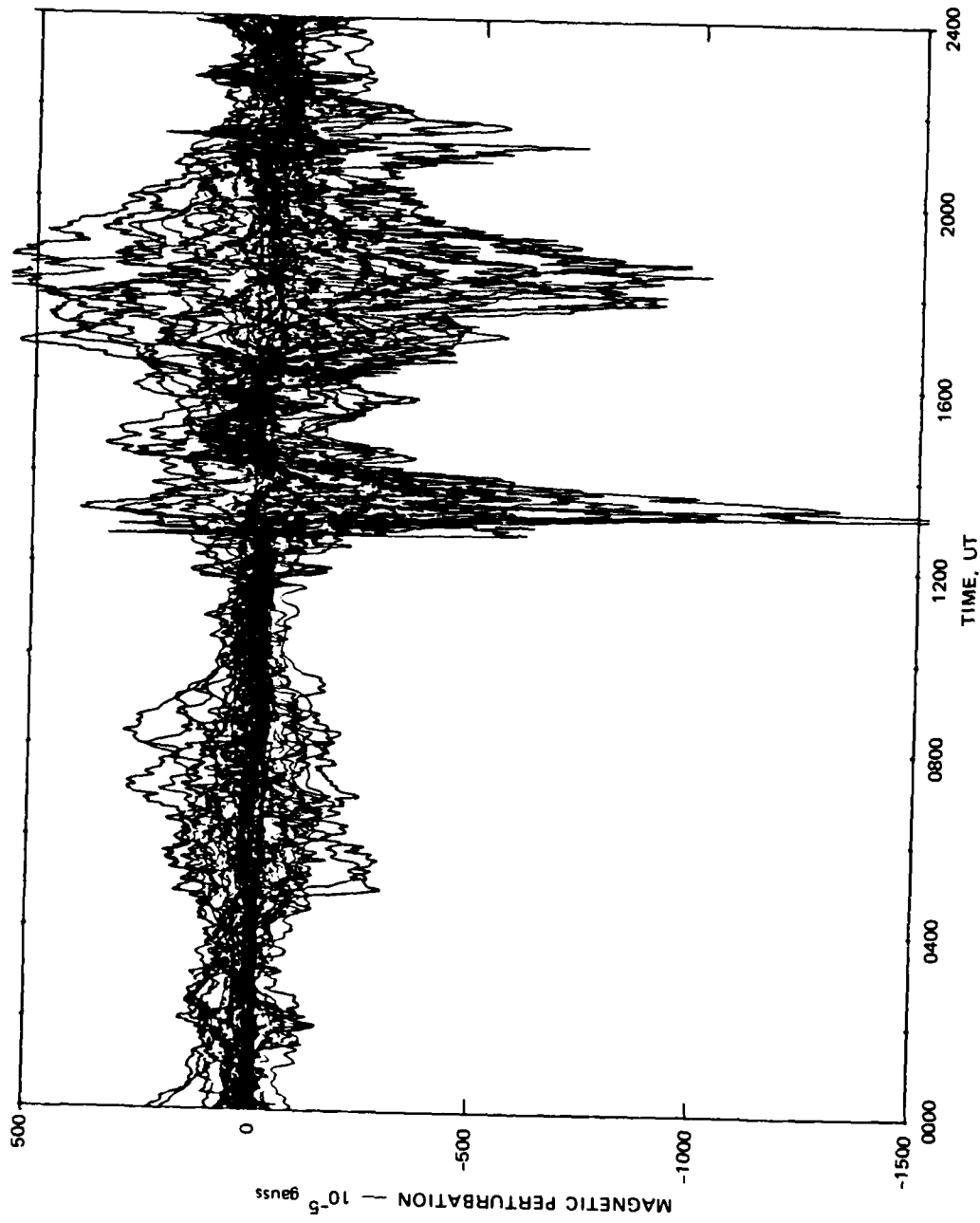


FIGURE III-6 STACK PLOT OF THE MAGNETOMETER PERTURBATIONS IN THE GEOMAGNETIC NORTH DIRECTION FROM APPROXIMATELY 60 HIGH-LATITUDE STATIONS ON 11 NOVEMBER 1981. The upper and lower envelopes give the AU and AL indices, respectively.

precipitation. These fields occur because in the afternoon sector, the equatorward boundary for proton precipitation is not collocated with that for electron precipitation but is equatorward of it. This effect has been explained in terms of the crosstail electric field in the magnetosphere causing a sunward displacement of the inner edge of the ring current [Schild et al., 1969; Vasyliunas, 1972]. The Region-2 Birkeland currents flow between these two boundaries. They close in the ionosphere, in a region of reduced conductivity. As a consequence of the low conductivity, large subauroral electric fields are established [Smiddy et al., 1977]. Verification of this explanation requires a careful study of boundaries for proton and electron precipitation in relation to the convection pattern.

Analysis of the observations from 11 November [Senior et al., 1986] was mostly performed while Senior was at SRI, working on the MITHRAS project. This particular case was selected because there were coincident DE-2 and NOAA-6 satellite passes. The satellite measurements provide parameters that are essential to complement the Chatanika data: field-aligned currents as well as proton and electron precipitation spectra. Figure III-7, from Senior et al. [1986], illustrates these observations. The figure depicts the equatorward boundary of the diffuse aurora and of the electric field, measured by the Chatanika radar. The Region-1 and Region-2 Birkeland currents, measured by DE-2 are also shown.

#### f. Substorm Studies

Substorms are the manifestations of energy transfer from the magnetosphere to the ionosphere. This transfer can be an explosive release of energy that has been previously accumulated in the tail [McPherron, 1979; Rostoker et al., 1980] or, alternatively, can be directly driven from the solar wind energy [Akosofu, 1980]. But the relative importance of these two components is not known. Whether it is a driven system or a storing-unloading of energy, this energy transfer is in fact a complex superposition of a variety of processes. A summary of a substorm

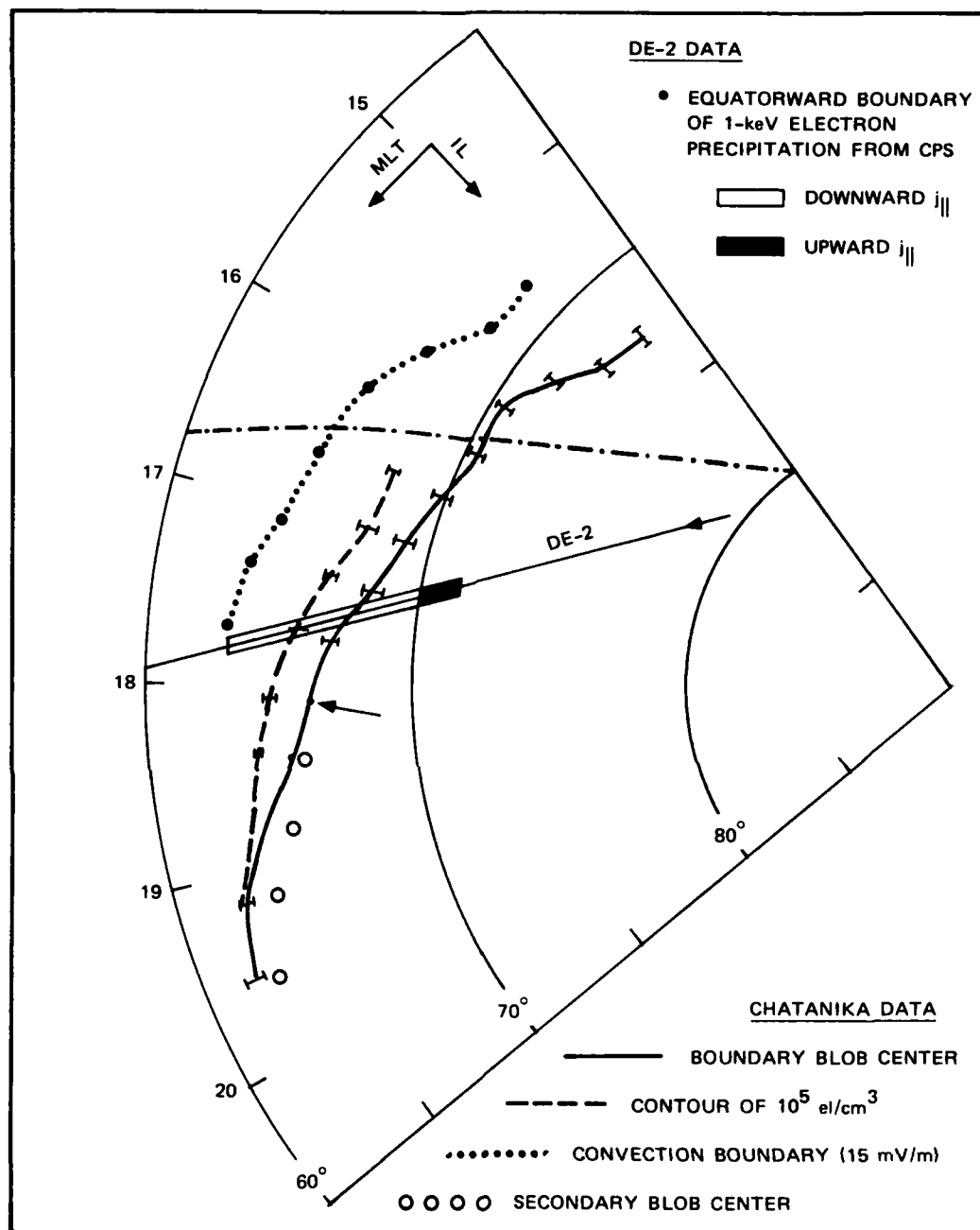


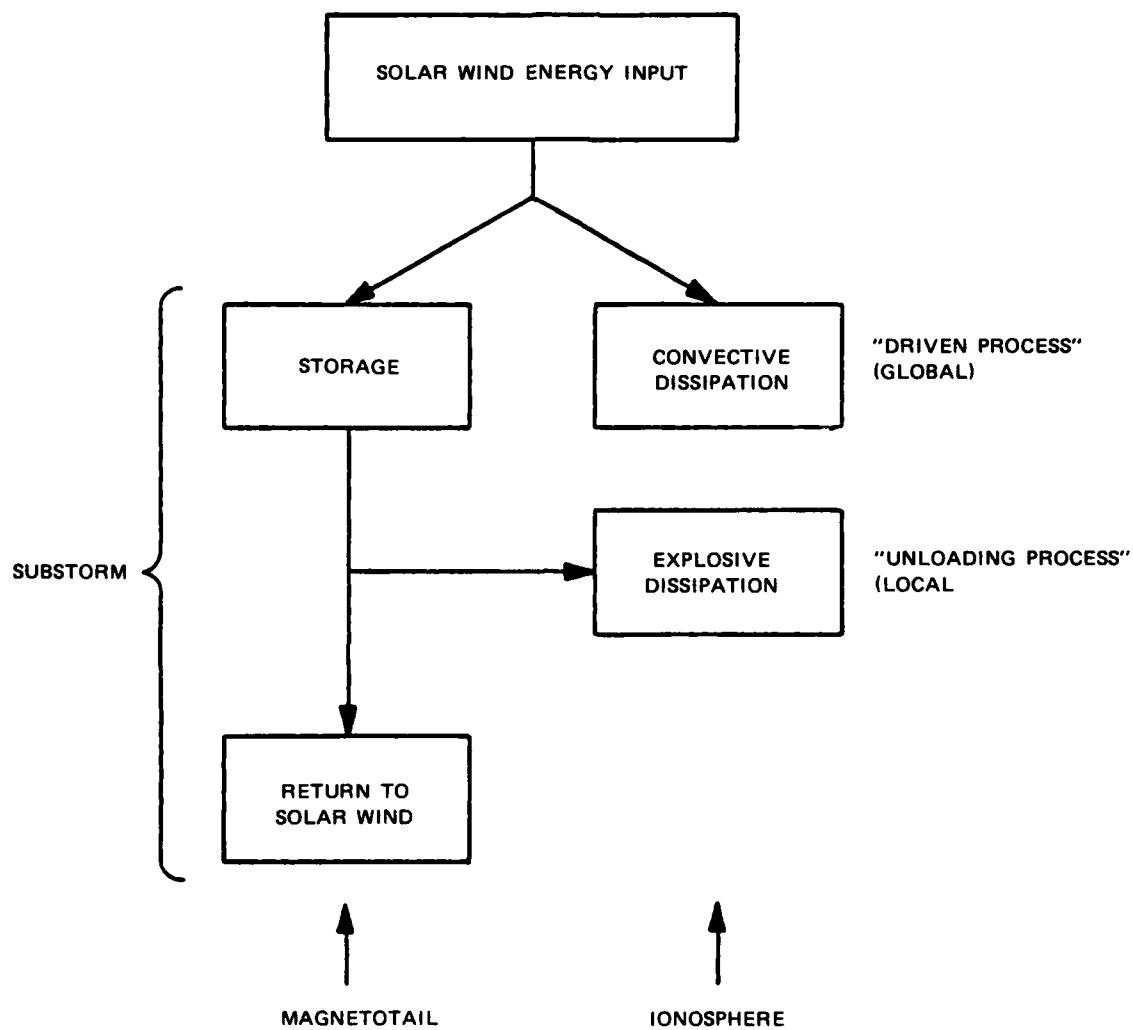
FIGURE III-7 DETAILED CHATANIKA AND DE-2 OBSERVATIONS IN THE EVENING SECTOR AURORAL ZONE ON 11 NOVEMBER 1981. The location and alignment of the boundary blob with the convection and diffuse aurora boundaries strongly suggest that it is related to the equatorward edge of the central plasma sheet.

sequence is shown in Figure III-8 [NASA, 1984]. It follows from this figure that a complete description of substorms has to rely on a variety of observations in the solar wind, magnetosphere, and ionosphere. The difficulty in making the appropriate measurements coincidentally, and at enough points within these regions, has hampered the understanding of how these processes operate. The MITHRAS observations provide a very important set of data for these studies.

The advantage of the radar data is that the radars provide continuous coverage at several locations and that they can provide the parameters that are needed to define both the electrodynamic and precipitation aspect of the energy transfer. For example, radars can determine the electric fields and the ionospheric and Birkeland currents, as well as the energy dissipation parameters such as Joule heating and particle precipitation.

Several MITHRAS studies examined the convection pattern behavior at two or three radar sites. In the first of these [de la Beaujardiere et al., 1983], the convection velocities at Chatanika, Millstone Hill and STARE were examined during five periods of geomagnetic disturbances on 27 to 28 June 1981. At the same local time, independent of longitude, similar behavior occurred. In the dawn and dusk sectors, the convection intensified; in the midnight and noon sectors it appeared to reverse. When Chatanika and EISCAT were in the dawn and dusk sectors, respectively, the convection intensified at both locations, almost simultaneously, at the onset of a magnetic disturbance or substorm.

The analysis of a series of magnetic disturbances was also carried out for the experiment on 27 January 1982 [Fontaine et al., 1983; de la Beaujardiere et al., 1984a]. Again, an intensification of the convection pattern was found in the dusk and dawn sectors. In the noon period, the convection region was poleward of the region probed by the Chatanika radar. However, significant precipitation of energetic particles was observed in the noon sector above Chatanika at the time of the magnetic disturbance. Precipitation by low-energy particles, which deposit their energy in the F region, was examined on this day and found



[Source: NASA, 1984]

FIGURE III-8 A SUMMARY OF THE SUBSTORM SEQUENCE SHOWING THE ROLES OF THE MAGNETOTAIL AND THE IONOSPHERE AND ALSO SHOWING THE ASPECTS OF SUBSTORMS THAT ARE REGARDED AS DRIVEN AND UNLOADING PROCESSES

to occur in conjunction with the magnetic disturbances in the dusk and dawn sectors. This was the first attempt at using a new method to infer the existence of low-energy precipitation.

Caudal et al. [1984] performed a careful comparison of convection velocities from three MITHRAS radars for 18 November 1981. The convection was quite steady during this experiment. On this stable background, perturbations were observed. When EISCAT was under the afternoon cell and Chatanika under the morning cell, the velocity variations were correlated.

These studies show that during substorms sunward convection is increased in the dawn and dusk regions and often velocity reversals are observed near noon and midnight. It is too early to say whether this behavior is due to an increase in convection velocities, an expansion of the convection cells, or a reconfiguration of the pattern.

Later studies related the convection changes to changes in the IMF. It was seen that, within about 10 min following a southward turning of the IMF, the electric field intensifies in the dawn and dusk sectors [de la Beaujardiere et al., 1983, 1985b,c; Clauer et al., 1984]. An example of timing of events associated with a change in the IMF orientation is shown in Figure III-9, reproduced from de la Beaujardiere et al. [1985c]. Fifteen minutes after the IMF turned southward, the convection intensified and, to the north of Sondrestrom, changed direction. Then, after another 15 min, a sharp onset of a negative bay was observed in the midnight sector. The onset of a negative bay at the radar local time occurred much later, one hour after the IMF orientation changed. These and other radar observations indicate that the convection intensifies before the onset of a substorm expansive phase. But, is this intensification part of the substorm growth phase? Is it simply an intensification of an existing pattern or does it correspond to a significant change in the overall convection pattern?

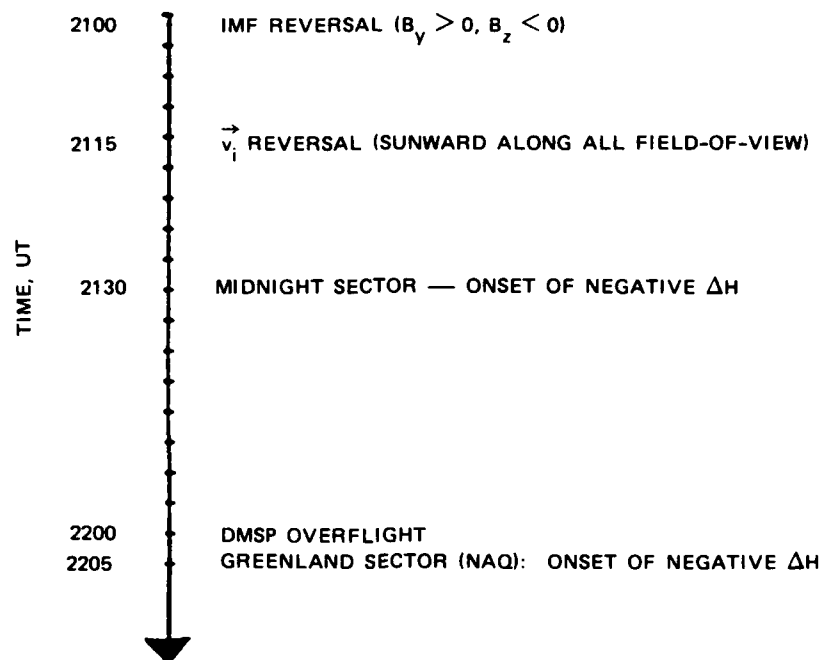


FIGURE III-9 SEQUENCE OF EVENTS FOLLOWING IMF CHANGE AT 2100 UT ON 23 APRIL 1983

Thus, a number of case studies have shown the potential for using the radars to learn about substorm processes and have provided information about convection velocities and particle precipitation. The radars are a very powerful tool for substorm studies. They enable convection and particle precipitation to be examined simultaneously over a range of latitudes. Because of these capabilities, this line of research can continue to provide significant advances.

## 2. Precipitation

A second major aspect of coupling between the magnetosphere, on the one hand, and the ionosphere and neutral atmosphere, on the other, is the precipitation of energetic particles. This precipitation leads to auroral emissions; produces D-, E-, and F-region ionization; can modify the electric fields; and deposits a substantial amount of energy in the upper atmosphere. Indeed, the energy deposition can be very significant in local areas, compared to that which the overhead sun would deposit. Thus it can have large effects in the upper atmosphere.

Our interest in this section is on the precipitation itself, not its consequences. The interpretation of the MITHRAS data has revealed where various types of precipitation occur, under what conditions, and at what energies.

The radars have proved well suited for this study. Chatanika, Sondrestrom, and EISCAT are sensitive to the precipitation of electrons with energy between a few tens of eV and 100 keV, because the electron density profile can be measured from the F region down to the D region. When combined with photometers or spacecraft, they provide information on proton precipitation. In addition, they enable the precipitation to be examined in the larger context of the convection pattern. This is particularly important because precipitation and convection are closely linked, although in the past they have almost always been studied separately.

a. Relation of Precipitation and Convection

One approach to examining particle precipitation is to relate where one type of precipitation is located with respect to another. This approach was followed by Winningham et al. [1975; 1978] with satellite data. They were able to relate their observations to the known particle populations in the magnetosphere. They identified two principal types of precipitation: boundary- and central-plasma-sheet precipitation (BPS and CPS, respectively). An extension of this approach is to relate the particle precipitation to the convection pattern. An analysis of this sort was performed for the cleft region by Reiff et al. [1978].

The relative locations of various types of precipitation and of convection can be deduced from radar observations. Initial efforts were made with Chatanika data using ion velocities and E-region densities in the evening sector by Robinson et al. [1982] and in the early morning sector by Senior et al. [1982] and Kamide et al. [1984]. The first paper showed the diffuse aurora from the CPS in the sunward convection region and auroral arcs from the BPS near the convection reversal. The second paper showed that arcs were present in the sunward convection region. However, most of the time these data were limited to the regions of sunward convection on the night side of the earth.

For MITHRAS, this research has been extended by including data from Sondrestrom. Because this radar is farther north, the convection reversal can be seen more often. Under this contract, the early afternoon sector has been examined by Wickwar and Kofman [1984], and Kofman and Wickwar [1984] using new procedures to determine the presence of low-energy electrons. Considerable soft- and hard-particle precipitation has been found in the vicinity of the convection reversal in the afternoon convection cells. The precipitation occurs in the region where the gradient of the current would be negative and it occurs almost entirely in the region of sunward convection. These particles probably originate in the BPS. At the BPS, and equatorward of it, there is often a diffuse auroral E layer, which probably arises from precipitation from the CPS.

## b. Very Energetic Particles

At the other end of the energy spectrum, the MITHRAS data contain information on more energetic particles, those that penetrate below 95 km--often to 75 km. Figure III-10 shows the resultant D-region densities observed on a quiet and on an active day. Eighteen days have been examined in order to study the behavior of energetic electron precipitation and of D-region electron density. Under quiet conditions, the densities vary slowly in time with a low-altitude cutoff between 85 and 90 km near noon. In winter, the altitude cutoff appears similar near noon, but the densities are lower. Often energetic auroral precipitation occurs near midnight or near dusk or dawn. Near dusk there is a tendency for a distinct layer to appear near 95 km. At dusk and dawn, the radar should have been equatorward of the diffuse aurora and significant convection; hence, inside the plasmasphere. Significant energetic precipitation was observed on some days near noon. Thus, it appears that energetic precipitation originates from three separate source regions.

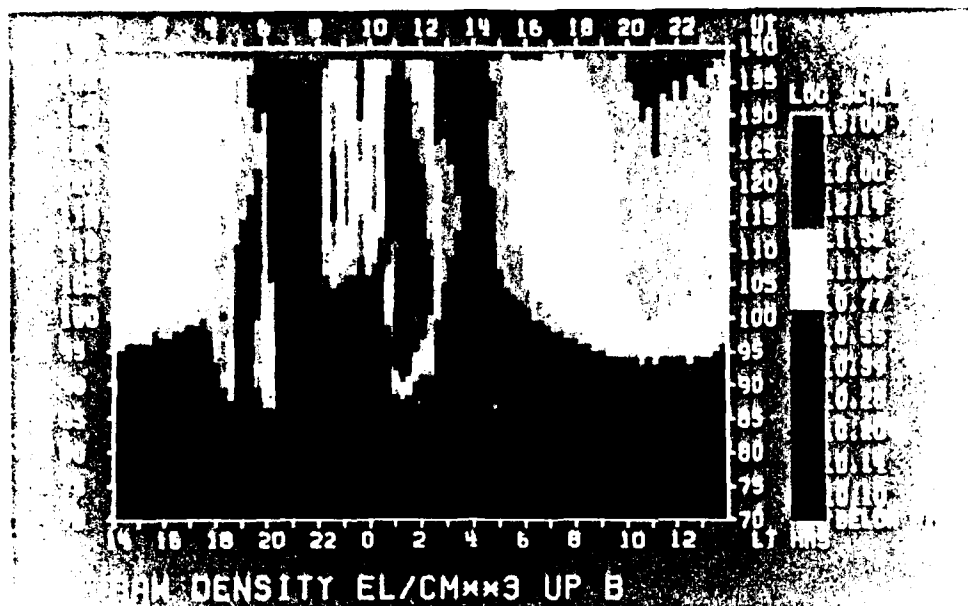
On some days, the energetic precipitation occurs for limited periods, but on others it is present for many hours. When this energetic precipitation occurs, it appears uniform over the extent of the region probed by the radar (50 to 75 km).

## B. Ionosphere

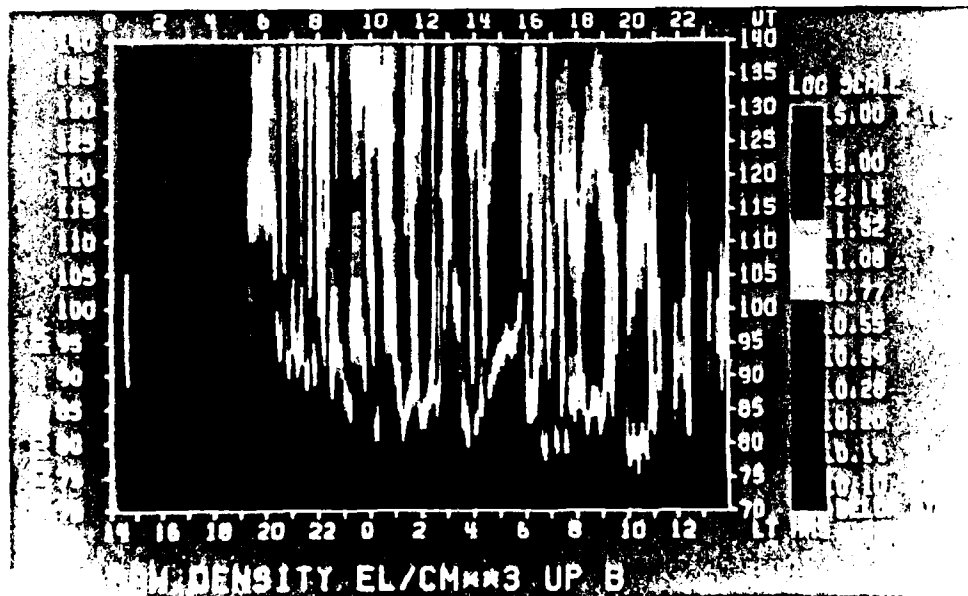
In this subsection, we discuss studies involving the effects of convection and particle precipitation on the electron density, the electron temperature, and the ion temperature. We also discuss some of the physical processes that affect these quantities.

### 1. Electron Density

The F-region electron density at high latitudes varies greatly as a result of several competing factors. Ionization is produced by solar EUV and by soft-particle precipitation. Plasma may be convected over



(a) 9 JULY 1980



(b) 18 NOVEMBER 1981

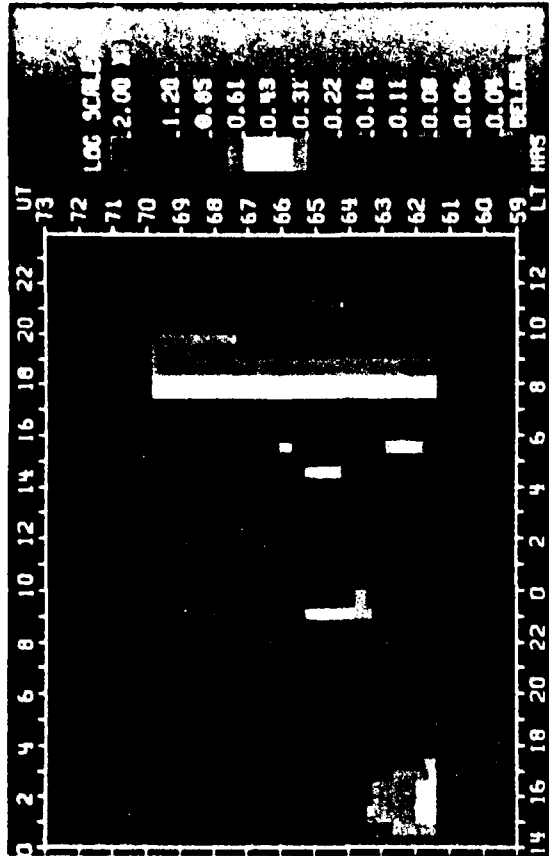
FIGURE III 10. PENETRATION OF ENERGETIC PARTICLES TO D-REGION ALTITUDES AT CHATANIKA

large distances. The F layer can shift up or down in altitude depending on the direction of the meridional component of the neutral wind, the zonal component of the electric field, or an impressed electric field parallel to the magnetic field. The altitude profiles are modified when the electrons or ions are significantly heated by particle precipitation or Joule heating, respectively. The ion chemistry can be greatly modified as a result of large differential velocities between ions and neutrals, which hasten the change from atomic to molecular ions, or as a result of changes in the neutral composition that are produced by Joule heating.

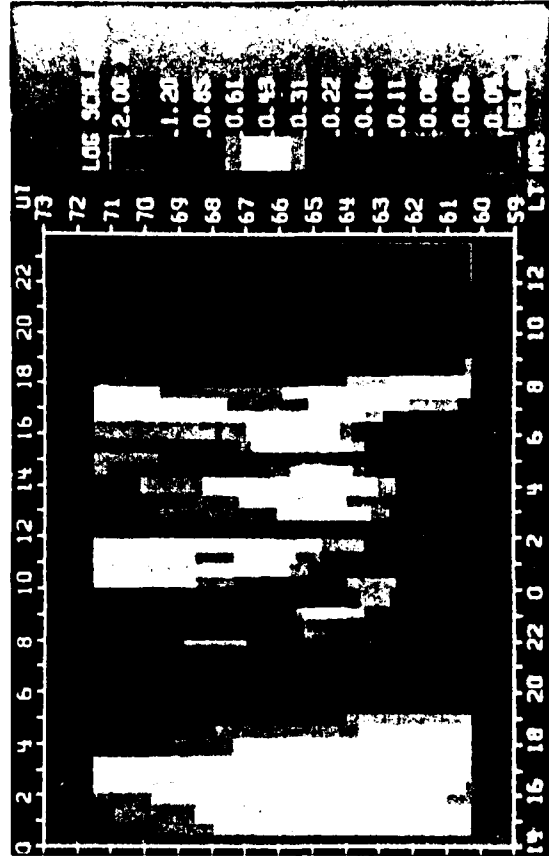
a. Daytime Density Depletion

At high latitudes, we tend to think that most of the variations in F-region electron density occur at night as a result of particle precipitation. Although dramatic changes do occur then, very significant ones also occur during the day, which are more difficult to explain. Such decreases have been seen in ionosonde and satellite data [Prolss, 1980]. The MITHRAS data contain several examples when the daytime density is reduced from one day to the next by a factor of four. Figure III-11 shows a very significant depletion at two altitudes during the daytime on 25 October 1981. The densities are at their usual levels the day before and the day after.

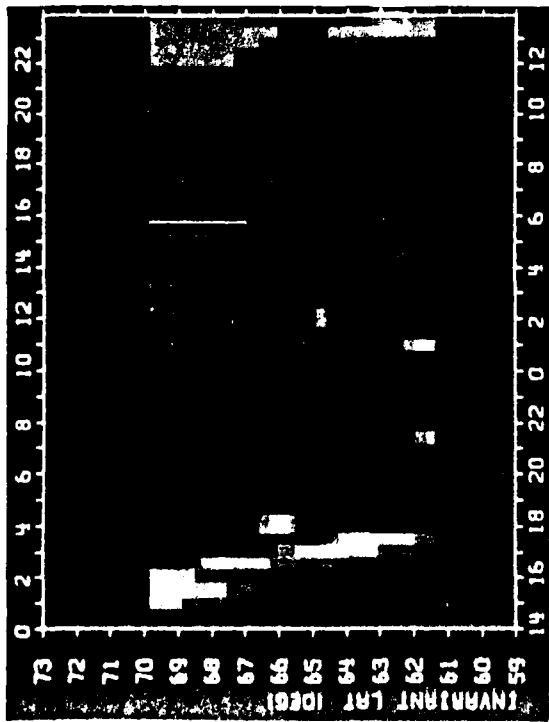
These variations are large enough and the data comprehensive enough to be amenable to detailed study. The hypothesis is that some processes linked to magnetic activity have increased the concentration ratio of  $N_2$  to O at F-region altitudes, with the result that the daytime electron-production rate is reduced and the loss rate increased. This would have happened if there had been significant Joule heating poleward of the radar, followed by equatorward transport of the neutrals. The chemical part of this mechanism is essentially the same one used to account for larger electron densities in winter than in summer (the winter anomaly) and for greater electron densities at solar cycle maximum than at solar cycle minimum. The phenomenon and the mechanism are most likely related



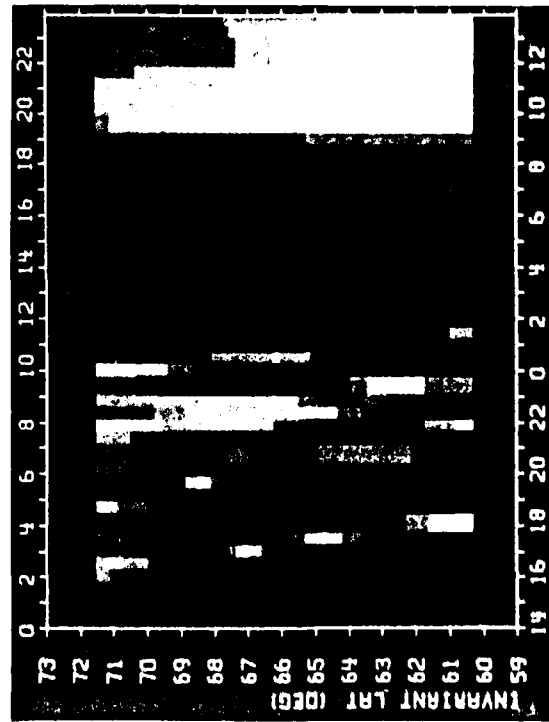
(a) ELECTRON DENSITY AT 250 km IN UNITS OF  $\text{cm}^{-3}$



(b) ELECTRON DENSITY AT 350 km IN UNITS OF  $\text{cm}^{-3}$



(a) ELECTRON DENSITY AT 250 km IN UNITS OF  $\text{cm}^{-3}$



(b) ELECTRON DENSITY AT 350 km IN UNITS OF  $\text{cm}^{-3}$

FIGURE III-11 DAYTIME DENSITY DEPLETION AND RECOVERY AT CHATANIKA DURING 48 HOURS ON 25 AND 26 OCTOBER 1981

to the much smaller density increases and decreases at midlatitudes after a magnetic storm.

b. Longitudinal or UT Density Variations

Because of the separation of the geographic and geomagnetic poles, the effects of solar EUV and magnetically controlled phenomena occur in regions that are partially displaced from one another. This displacement is even more complex because the auroral oval is shifted about  $3^{\circ}$  antisunward of the magnetic pole [Gussenhoven et al., 1983]. These offsets lead to a complicated relative motion of the auroral zone with respect to the geographic pole. In turn, this motion leads to longitudinal or UT variations in the electron density behavior. Such variations have been predicted [Knudsen, 1974; Sojka et al., 1982] and observed [Sato and Rourke, 1964].

One of the important MITHRAS observations was that in the middle of the night in fall and winter, the F-region density at EISCAT was greater than at Chatanika and the density at Chatanika was greater than at Millstone Hill, Figure III-12. These longitudinal variations have been examined in considerable detail by de la Beaujardiere et al. [1985a]. The data are consistent with the idea that ionization produced in the vicinity of the noon auroral oval and cleft can be transported across the polar cap and that the production of ionization near the cleft by solar EUV varies because of the offset between the geomagnetic and geographic poles. In other words, the relative location of the terminator and auroral oval varies with longitude.

Several other UT variations have been observed in the MITHRAS data set. One involves the rate of density increase at dawn and decrease at sunset. At Chatanika, the increase is slow and the decrease rapid. At EISCAT, the reverse is true. Another is the noon density, which is often larger at Chatanika than at EISCAT. A third is the E-region electron density, with the result that the conductivities appear to be systematically greater at EISCAT than at Chatanika.

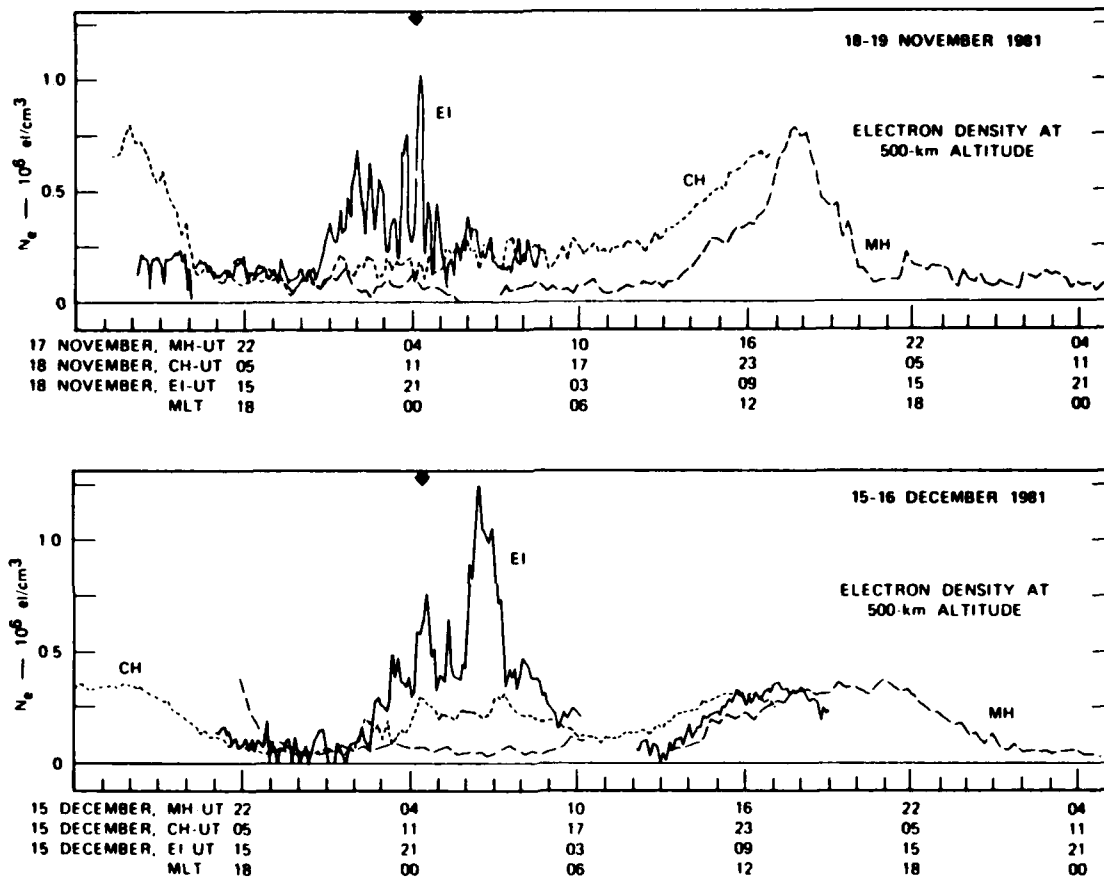


FIGURE III-12 MAGNETIC-LOCAL-TIME DEPENDENCE OF THE F-REGION ELECTRON DENSITY AT MILLSTONE HILL, CHATANIKA, AND EISCAT ON 18 AND 19 NOVEMBER 1981 AND 15 AND 16 DECEMBER 1981. The densities are from an altitude of 500 km and an invariant latitude of approximately  $64^\circ$ .

### c. Trough and Other Large-Scale Structures

There are several large-scale F-region density features that are closely associated with the convection pattern. As such, they may also have a longitudinal dependence. The best studied is the trough [Muldrew, 1965], an electron density depletion that has a limited latitudinal extent. There can be multiple depletions. The "main trough" or "midlatitude trough" is in the evening or nighttime sectors, but depletions occur at any local time [Grebowsky et al., 1983].

The trough has been examined extensively with data from Millstone Hill [Evans et al., 1983a, 1983b; Holt et al., 1983]. They discuss three major factors that appear to cause the observed depletion. The first is the stagnation hypothesis [Knudsen, 1974]. Because sunward convecting plasma in the evening sector spends a long time in darkness, the normal chemical decay has a long time to operate. The second is the subauroral electric field hypothesis [Evans et al., 1983a]. These fields, as already discussed, occur in the evening sector and lead to an increased rate for the charge exchange reaction  $O^+ + N_2 \rightarrow NO^+ + N_e$  [Banks et al., 1974; Schunk et al., 1975], which leads to an accelerated F-region decay. The third is the fossil hypothesis [Evans et al., 1983b]. It is similar to the previous hypothesis in that it depends on increased charge exchange followed by recombination to cause the decrease in ionization. It differs in that it depends on large electric fields during magnetic disturbances or substorms to create the depletion, which then persists and corotates once the disturbance has subsided and the region of increased convection has moved poleward.

The main trough is on the equatorward side of the auroral oval where it is observed in the region of sunward convection in the afternoon and evening sectors. But the effect of large ion velocities on the chemistry, which is involved in the second and third hypotheses, can occur elsewhere. Indeed, large reductions in density are often seen at Sondrestrom poleward of the auroral oval, in regions of strong anti-sunward convection. The velocities are often between 1 and 3 km/s.

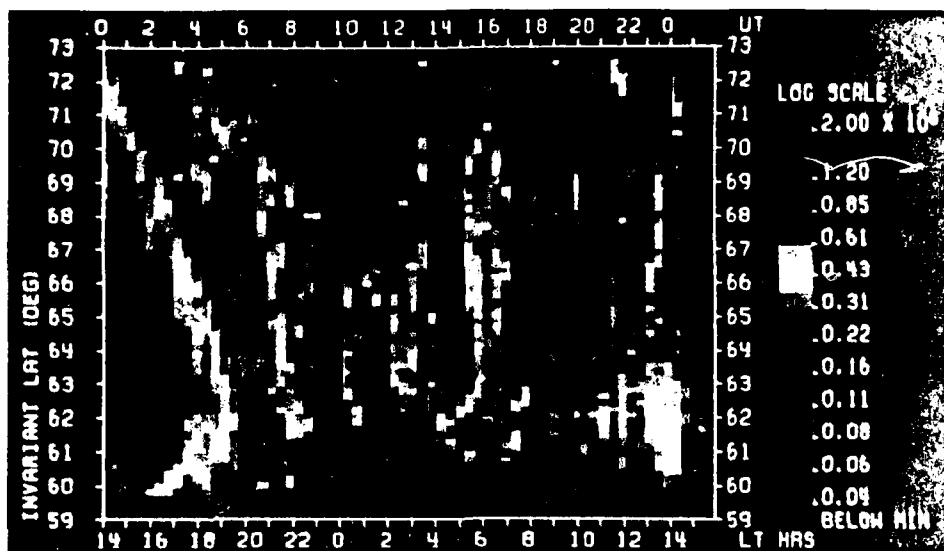
We have carefully examined a MITHRAS data set in which the midlatitude trough extended over several hours of local time (Figure III-13). This case study was done while Senior was at SRI. In it, Senior et al. [1986] found that the trough formation was consistent with the stagnation model developed by Spiro et al. [1978].

In the same study, we explained the formation of a ridge of ionization, which was observed to lay parallel to the main trough, along its poleward wall. We showed that this ridge of ionization (often called the boundary blob) could not arise from local production, but was the result of the large-scale convection.

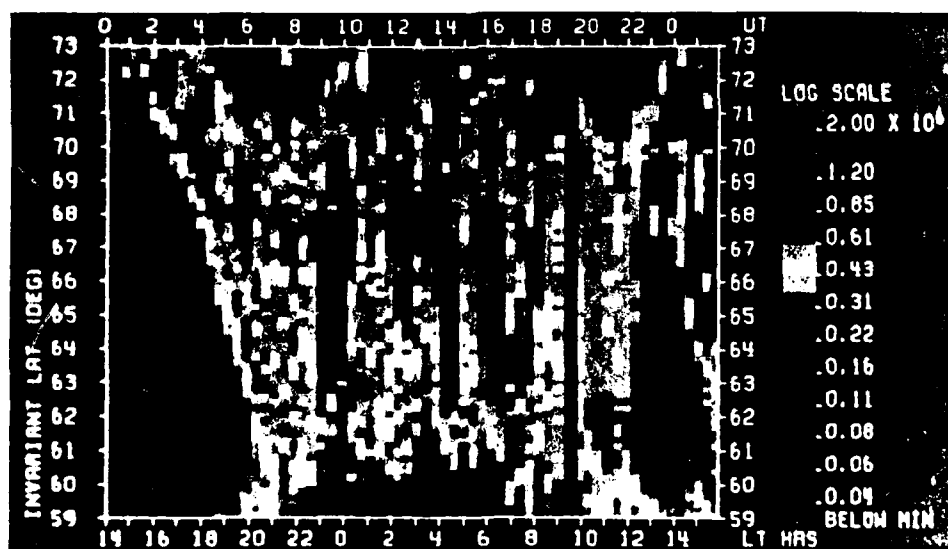
The MITHRAS observations are more comprehensive than those which were previously available. The data from Chatanika, Sondrestrom, or EISCAT have better latitudinal resolution than the data from Millstone Hill, which were used for the early radar trough studies. The data from Chatanika and EISCAT have a wide local-time separation. Data from Sondrestrom are from a higher latitude, enabling the trough and other structures to be seen at earlier times as well as enabling the depletions formed in regions of antisunward convection to be explained. More can be done with these data as procedures are developed for a detailed comparison between theory and observation. The status of these comparisons is discussed in the next section.

#### d. Comparison With Theory

The last aspect of our study of ionospheric densities concerns collaborative work with the USU group. As was mentioned in an earlier section, we just performed the first comparison of their model with data from several radars [Rasmussen et al., 1986]. This work combines the USU model ionosphere with data from 27 June 1981, principally from the Chatanika and Millstone Hill radars, but also includes data from the STARE radar and the NOAA-6 satellite. Despite the occurrence of several magnetic disturbances, it was possible to use a time-independent convection pattern. In general, good agreement was obtained between observation and theory, indicating that no major physical or chemical



(a) ELECTRON DENSITY AT 250 km IN UNITS OF  $\text{cm}^{-3}$



(b) ELECTRON DENSITY AT 350 km IN UNITS OF  $\text{cm}^{-3}$

FIGURE III-13 MAIN ELECTRON DENSITY TROUGH AT CHATANIKA ON 11 NOVEMBER 1981. The main trough moves equatorward from 72  $\Lambda$  at 0130 UT to 60  $\Lambda$  at 0700 UT. Several other regions of density depletion occur during the night.

process was left out or badly calculated. There were, however, a number of smaller discrepancies that should be looked at more carefully in future studies.

In this case study, the convection pattern and neutral wind pattern were held constant for 24 hours. Only ion velocities and electron densities were more extensive than in previous calculations in that velocities were available from two locations all the time and from three locations some of the time. Similarly, the electron densities were compared at several altitudes. A follow-up study was started for the same day to explore electron and ion temperature behavior.

From the experience gained in these studies, the next step, when funding is renewed, will be to allow the convection pattern to change continuously throughout the period being modeled. This will allow days with more variable geomagnetic activity to be examined. The other change that will have to be tried is varying the neutral wind pattern as a function of time. At that time, it will also become necessary to combine the ionospheric model with the thermospheric global circulation model (TGCM). It should then be feasible to carefully examine such phenomena as the daytime depletion, the several UT-longitudinal variations, and the troughs. The combination of the multiradar measurements and the global ionospheric modeling is very powerful, but the process is just beginning and the ability to use it to understand more complex situations is growing incrementally.

## 2. Electron Temperature

Another useful parameter to study in order to gain insight into coupling phenomena is the electron temperature. This parameter has the advantage over F-region density that the time constants for heating and cooling are on the order of a few seconds instead of tens of minutes. Therefore, it is a good indicator of energy input to the electrons. Generally, this energy input is from collisions with suprathermal electrons. These electrons may be photoelectrons produced by solar EUV or UV, or secondary electrons produced by energetic auroral precipitation.

Another source of energy input is heat flux down the magnetic field. The energy source may arise from processes far out in the magnetosphere or from auroral particles with such low energy that they penetrate to just above the field of view of the radar. The electrons are cooled by collisions with ions and neutrals as well as by heat conduction. Ultimately, most of the energy deposited in the electron gas is deposited in the neutral gas.

a. Elevated Electron Temperatures

We found that the F-region electron temperatures are significantly elevated in a  $2^{\circ}$  to  $3^{\circ}$  region near the convection reversal in the afternoon convection cell. We have seen this enhancement near noon and in the early afternoon at Sondrestrom [Kofman and Wickwar, 1984; Wickwar and Kofman, 1984]; and in the evening and near midnight at Chatanika [Fontheim et al., 1984; Wickwar et al., 1984d]. In these cases, significant energy is transferred to the electrons. This energy transfer is readily apparent qualitatively because the temperature and density both increase. It has been examined quantitatively by solving the electron-energy equation [Kofman and Wickwar, 1984; Wickwar et al., 1984d]. Under steady-state conditions, the rate of energy input to the electron gas  $Q_e$  is equal to the rate of energy loss from the electron gas  $L_e$  and the rate of energy loss from heat conduction. The energy input can be from ionization by solar EUV and UV or from collisions with auroral primaries and secondaries. The energy loss can be from collisions by the ambient electrons with ions and neutrals. The net energy input rate at a given height is equal to  $L_e$ . The radar data can be used to derive enough parameters to calculate  $L_e$  and the heat conduction term, which is closely related to the heat flux.

Under extreme conditions, the energy deposited between 180 and 500 km has reached  $1 \text{ erg/cm}^2 \text{ s}$ . If it were from soft electrons, they would have to have energies below 400 eV to have stopped in the

F region. Under these same conditions, the downward heat flux at 450-km altitude was  $0.3 \text{ erg/cm}^2 \text{ s}$ . More typical values were an order of magnitude smaller.

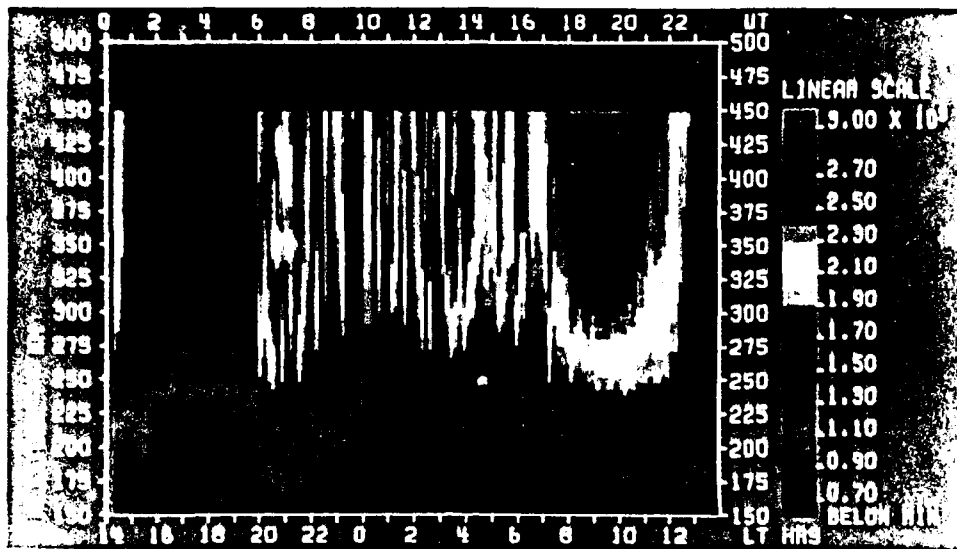
In MITHRAS data from Chatanika and EISCAT, we have found that there often is often a high correlation between the occurrence of energetic precipitation producing an auroral E region and the occurrence of elevated electron temperatures in the F region. This correlation is apparent in the data from the two parts of Figure III-14. Part (a) shows the F-region temperatures; Part (b) shows the E-region densities. We have started to interpret these observations to determine under what conditions the correlation exists and to determine whether the elevated electron temperatures arise because of soft particle precipitation or heat conduction.

b. Large Temperature Increases at the Afternoon Convection Reversal

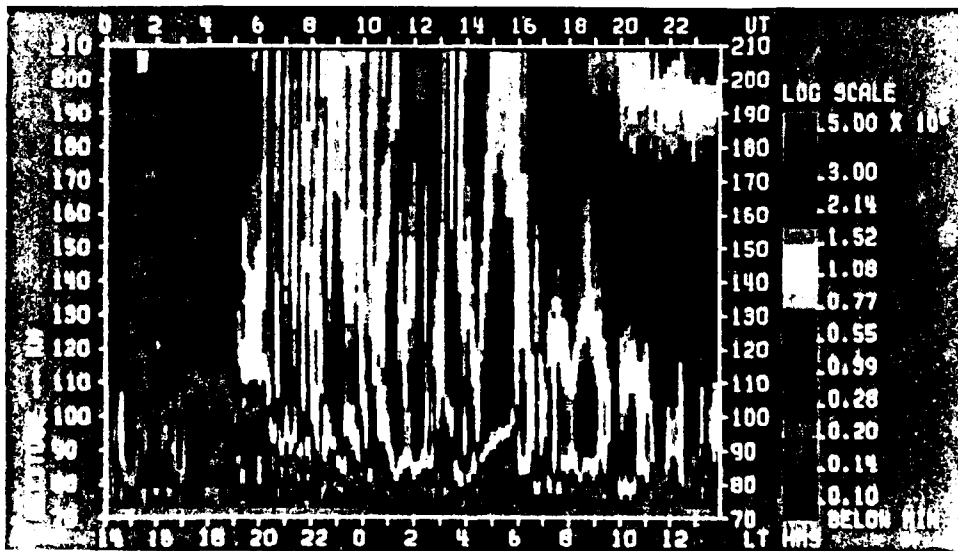
As mentioned above, the largest electron temperature increases have been seen near the convection reversal in the afternoon cell. Figure III-15 shows the extreme examples. The first is from near noon on 24 April 1983 at Sondrestrom [Wickwar and Kofman, 1984]. The second is from the evening on 5 March 1981 at Chatanika [Wickwar et al., 1984b]. In the second example, which was at night, an extremely bright red aurora covered the sky. In both cases, we obtained electron temperature as high as 6000 K at 500-km altitude. In addition to the high temperatures, we demonstrated that large downward heat fluxes were present on both days. The temperatures and fluxes are shown in Figure III-15.

We are now trying to understand why such large temperature increases were observed on these two days and not on other days. At this point, what we know is that magnetic activity was very high on both days. During the Sondrestrom observations, Kp was 6-; during the Chatanika observations, a large magnetic storm was in progress.

Other questions have arisen concerning the heat flux. Does it arise from very soft particles (about 10 to 20 eV) stopping at altitudes



(a) ELECTRON TEMPERATURE IN KELVIN



(b) ELECTRON DENSITY IN  $\text{cm}^{-3}$

FIGURE III-14 COMPARISON OF F-REGION ELECTRON TEMPERATURE AND E-REGION ELECTRON DENSITY ON 18 NOVEMBER 1981. A good correlation often exists at night.

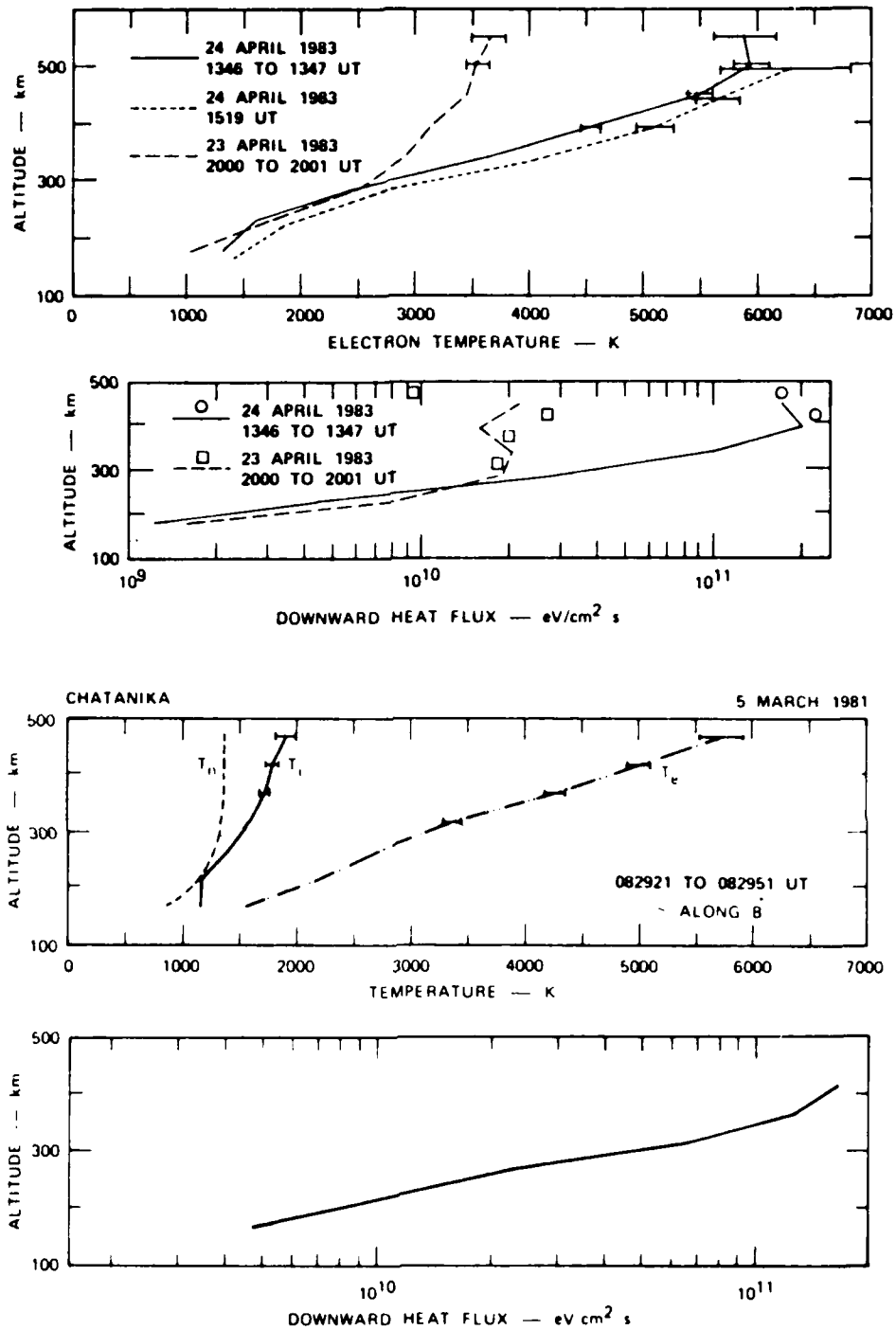


FIGURE III-15 ELEVATED ELECTRON TEMPERATURES AND LARGE DOWNWARD HEAT FLUXES IN THE AFTERNOON SECTOR. The top two panels show data from Sondrestrom (LT = UT - 3 hr). On 23 April 1983 the electron temperature and flux have typical values. On 24 April both are greatly elevated. The bottom two panels show data from Chatanika (LT = UT - 10 hr). Both the electron temperature and heat flux are greatly elevated.

just above 500 km, or does it arise from processes deep within the magnetosphere? Our approach to these questions is to make a very detailed comparison of the Chatanika data and one-dimensional model calculations. This collaboration has been ongoing with M. Rees and G. Romick (University of Alaska) and others.

A similar question is being addressed on several MITHRAS data sets using radar-determined temperatures in the topside ionosphere below 550 km and DE-2 determined temperatures at higher altitudes. The work has been conducted in collaboration principally with E. Fontheim of Michigan and L. Brace of NASA. This work follows a study using data from the August 1972 magnetic storm [Fontheim et al., 1978]. The present work is aimed at learning whether an anomalous thermal conductivity is needed to explain the very high electron temperatures [Fontheim et al., 1984].

c. Excitation of the Red Line of Atomic Oxygen

One of the ways that hot electrons lose their energy is in collisions with neutrals. We have studied the possibility that hot electrons could excite atomic oxygen to the  $^1D$  state followed by emission at 630.0 nm. In examining the radar data from Sondrestrom, we found that thermal excitation did appear capable of producing several kilo Rayleighs of red-line emission [Wickwar and Kofman, 1984]. These intensities are comparable to what have been observed in cleft auroras. Our findings are important because we found that the electron temperatures were much higher than assumed by previous works [Link et al., 1983; Roble and Rees, 1977]. Indeed, the electrons are hot enough that thermal excitation becomes a significant excitation mechanism.

We then performed the same calculations with data from 5 March 1981, the day with several periods of intense red aurora. We again found that hot electrons could account for several kR of red-line emission. Temperature and heat flux profiles were already shown in Figure III-15. Unlike the Sondrestrom observations, when it was sunlit, the Chatanika observations were at night, when there were simultaneous

photometric observations by researchers from the University of Alaska and the Lockheed Palo Alto Research Laboratory. The optical observations have been cross calibrated and we are making a detailed comparison of intensities deduced from the radar data and those that were measured.

Preliminary results are shown in Figure III-16 for data obtained along the magnetic field line. The optical data (curve labelled "Photometer") were selected from very rapid meridian scans such that the fields of view and integration times were as closely matched as possible to the radar measurements. This ability to compare radar and optical data properly is an important analysis capability. We calculated the 630.0-nm intensities from two mechanisms (curve labelled "Radar" in Figure III-16). The first is based on chemistry [Wickwar et al., 1974; Cogger et al., 1979]; the second is based on collisions with hot ambient electrons [Wickwar and Kofman, 1984]. When auroral activity was very low, the background intensity owing to the recombination of ions accounts for much of, if not all, the observations. The largest intensities coincide with the periods of greatest electron temperature, when the thermal excitation mechanism accounts for the observations. Thus, we have confirmation that thermal excitation can be an important emission mechanism. Under intermediate conditions, i.e., with lower electron temperatures, the dominant excitation mechanism is presumably from impact of the atomic oxygen by the low-energy precipitating electrons and their secondaries.

Because of the importance of thermal excitation, the ratio of the 630.0-nm intensity to that of other auroral emissions is not as good a way of determining the precipitating electron energy spectra as has been assumed for the last decade. This finding has important implications for a number of studies because the ratio of intensities at 6300 Å and 4278 Å has become a standard technique for estimating a Maxwellian distribution for energetic auroral electrons.

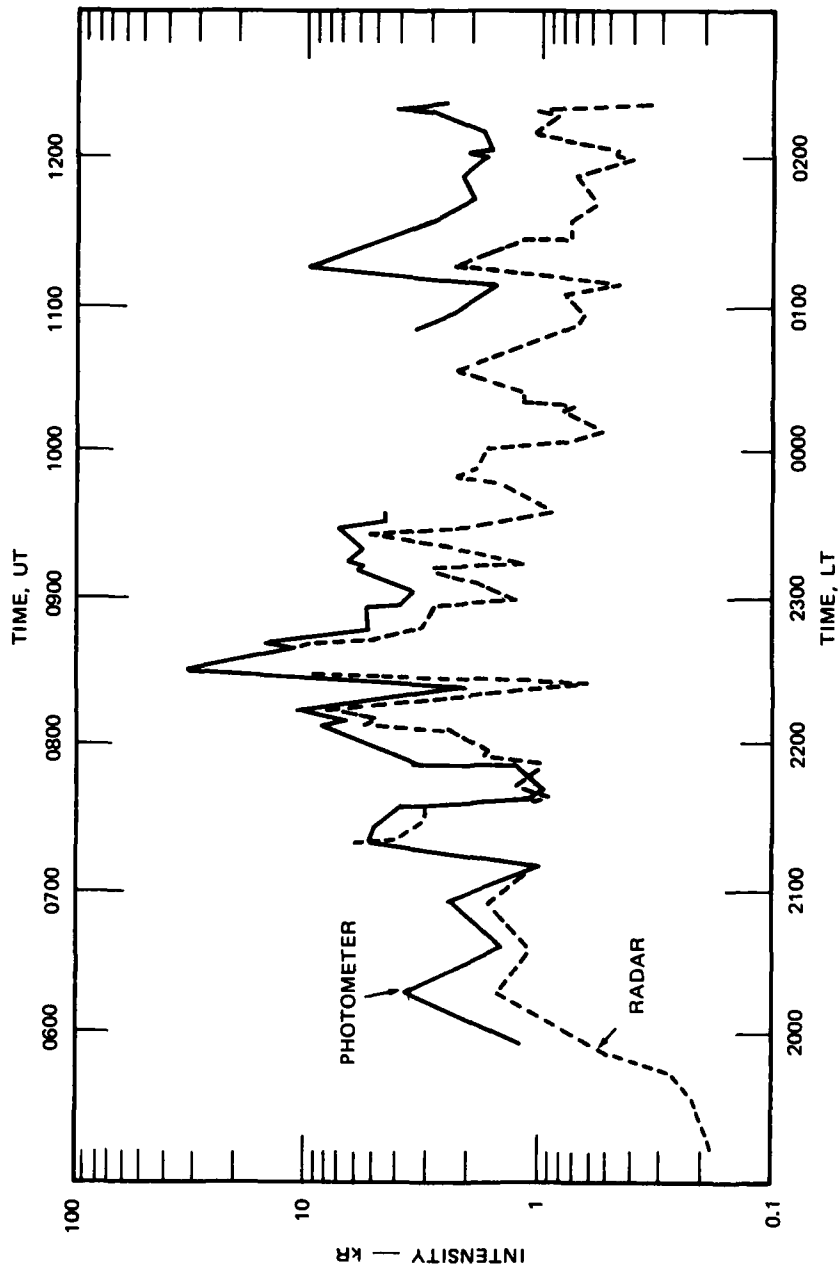


FIGURE III-16 OBSERVED AND CALCULATED 630.0-nm INTENSITY ALONG THE MAGNETIC FIELD AT CHATANIKA ON 5 MARCH 1981. The calculations include dissociative recombination and thermal excitation. Agreement occurs when these mechanisms dominate. The difference would be due to direct excitation by soft particles.

### 3. Ion Temperatures

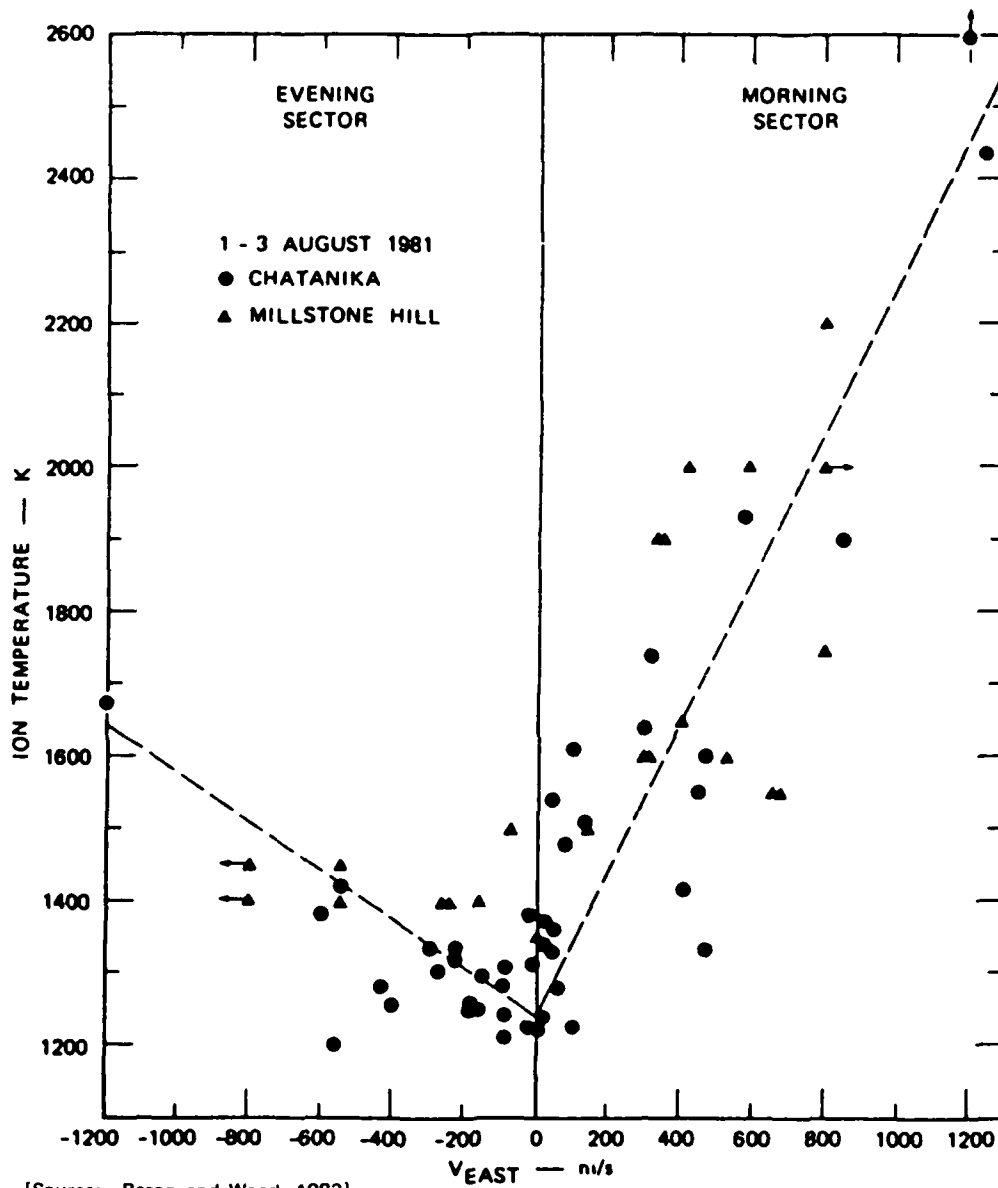
The ion temperature is another parameter that can provide insight into coupling phenomena. As was the case for the electron temperature, the time constants for heating and cooling the ions are the order of a few seconds; therefore, the ion temperature is a good indication of energy being transferred into and out of the plasma. Ions are heated above the neutral temperature by Coulomb collisions with hot electrons. This process has noticeable effects above about 300 km and takes place at all latitudes. Another source of heating predominant at high latitudes is frictional or Joule heating. It arises from collisions between ions and neutrals, most usually as the ions are driven through the neutrals by convection electric fields. The heating rate is proportional to the square of the difference between the vector-ion and vector-neutral velocities. This process has noticeable effects above 115 km. Thus enhanced ion temperatures are very useful for indicating when Joule heating is important.

#### a. Elevated Ion Temperatures in the Morning Sector

We analyzed coincident Millstone Hill and Chatanika observations of ion temperatures and electron densities. We found that, consistently, the highest observed ion temperatures were in the early morning [Baron and Wand, 1983]. This result is illustrated in Figure III-17. It shows that for a given convection velocity, the ion temperature is higher in the morning than in the evening sectors.

The explanation given by Baron and Wand [1983] is that in the evening sector, the convecting ions rapidly drag the neutrals along with them thereby reducing the velocity difference and the Joule heating. In contrast, in the morning sector the velocity difference between the ions and neutrals persists much longer, giving rise to more Joule heating.

We attributed the difference in ion drag between morning and evening to larger ion densities in the evening sector. This study was



[Source: Baron and Wand, 1983]

FIGURE III-17 PREFERENTIAL ION HEATING IN THE EARLY MORNING AT CHATANIKA AND MILLSTONE HILL. Although the range of ion velocities is similar in the morning and evening, the ion temperatures are much hotter in the morning.

pursued by Alcayde et al. [1984]. Using other MITHRAS data, they concluded that the Coriolis force is also a contributing factor. This early morning Joule heating probably affects the neutral atmosphere. The energy deposited in the neutrals could raise the temperature, and the increased temperatures give rise to pressure changes that affect the neutral wind circulation. The energy deposition can also lead to an upwelling that changes the neutral composition. These types of changes most probably produce the daytime density depletion discussed earlier. If so, they should also lead to important changes equatorward of the auroral region.

b. Comparison with Theory

The model calculations by the USU researchers [e.g., Rasmussen et al., 1986] mentioned in earlier sections have been extended to include Joule heating. The collaborative work, comparing MITHRAS data and model calculations, was started. It was expected that the results would help in our effort to analyze the complex factors that affect the ion and neutral temperatures.

c. Neutral Atmosphere

As mentioned earlier, the magnetosphere and ionosphere are closely coupled to the neutral atmosphere. Because the neutrals dominate at thermospheric altitudes, it is important to understand the behavior of the neutral parameters for providing background conditions and for identifying the largest transfers of energy and momentum. Convecting ions will drag the neutrals along, significantly changing the thermally driven wind pattern. Particle heating and Joule heating affect the neutral composition, temperature, and winds. These, in turn, affect the ion and neutral chemistry. In the following subsections, we discuss studies involving the neutral wind and temperature.

## 1. Neutral Wind

The component of the thermospheric neutral wind in the magnetic meridian is derived from radar measurements parallel to the magnetic field. The meridional wind can be derived at several altitudes in the F region, throughout the day, and during both winter and summer. The major questions concerning the thermospheric wind are still the diurnal pattern, how it is affected by solar variations and geomagnetic activity, and what are the major driving forces.

### a. Meridional Wind at Chatanika

The original MITHRAS study of the meridional wind is by Wickwar et al. [1984c]. Much of this effort went into developing the analysis procedure. Basically, the ion velocity parallel to the magnetic field arises from neutrals colliding with ions and from ion-neutral diffusion. To derive the wind from the observations involves calculating the ion-neutral diffusion, which involves the derivatives of electron density, electron temperature, and ion temperature with respect to altitude. It also involves a careful determination of the neutral atmosphere. Good agreement was found between the derived wind and the same component of the wind derived from optical observations with a Fabry-Perot interferometer.

Chatanika data from seven years were analyzed and compared to theory. The average equinox pattern was established: the wind was northward during the day at about 65 m/s and southward during the night at about 175 m/s. During periods of increased magnetic activity, the wind, on average, became more southward during the night by about 100 m/s. On individual days, the increase was as much as 400 m/s. Comparison with theory showed basic agreement, but suggested possible heating poleward of Chatanika during the morning.

### b. Nighttime Behavior

The MITHRAS observations have revealed the existence of anomalous behavior in the nighttime meridional wind. These include a secondary equatorward maximum during the night in the auroral region (Figure III-18) and an abatement at high latitudes (Figure III-19). In the top portion of Figure III-18, the wind is strongest toward the south at 1200 UT, or 0200 LT. This is a very quiet day, as indicated by a northward electric field that is always less than 10 mV/m. The wind results are typical of magnetically quiet days. The bottom portion of the figure shows a local maximum in the wind between 1000 and 1200 UT, followed by a much stronger maximum near 1400 UT. This second maximum coincides in time with the strongest southward electric field, which was 50 mV/m. This second maximum is typical of geomagnetically active days.

Figure III-19 shows the meridional wind at Sondrestrom for a 32-hr period in April 1983. At about 0200 UT (2300 LT), the wind is toward the north. Usually at this time of the night it is strongly southward, but on some days there is an abatement and on this night a reversal. Other examples of this behavior have been presented in a collaborative study with the University of Michigan [Meriwether et al., 1984].

We believe that these effects are indicative of the influence of magnetospheric convection on the neutrals. These effects are probably the result of ion drag and the shape of the convection pattern over the polar cap, for the case of Sondrestrom observations, or over the auroral zone near midnight, for the case of Chatanika observations. However, there is still a possibility that they indicate energy deposition such as will be discussed in the next subsection.

Our early research emphasized the wind determination and the large-scale meridional wind pattern [Wickwar et al., 1984c]. The anomalous behavior, just discussed, stands out in comparison with this pattern. Research has been started in order to investigate these two cases. To do so, the convection pattern, particle precipitation and Joule heating

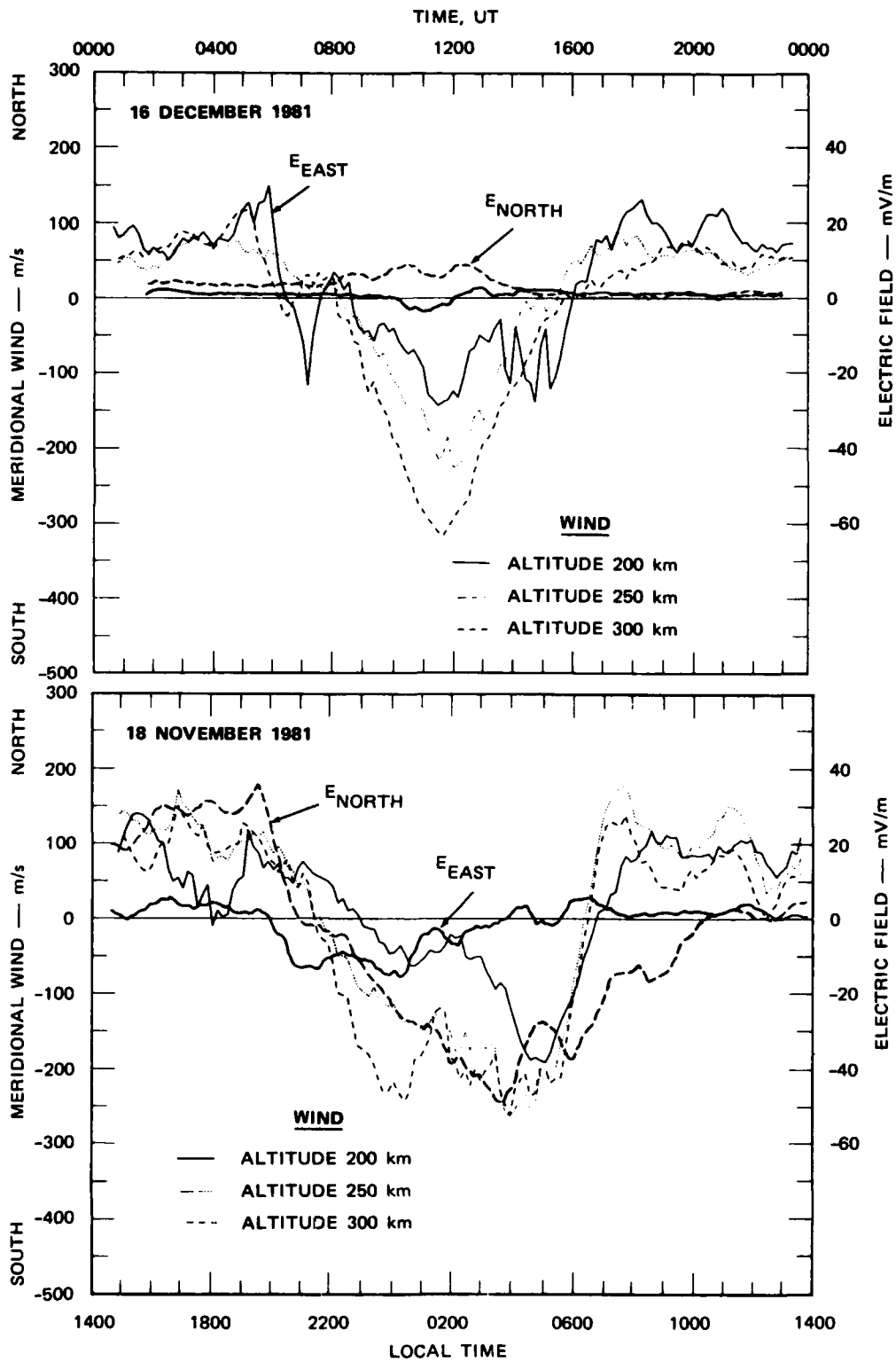


FIGURE III-18 SECOND MAXIMUM IN THE MERIDIONAL WIND NEAR MID-NIGHT UNDER DISTURBED CONDITIONS AT CHATANIKA. The top panel shows one maximum under quiet conditions. The bottom panel shows a strong second enhancement between 0200 and 0530 LT under active conditions.

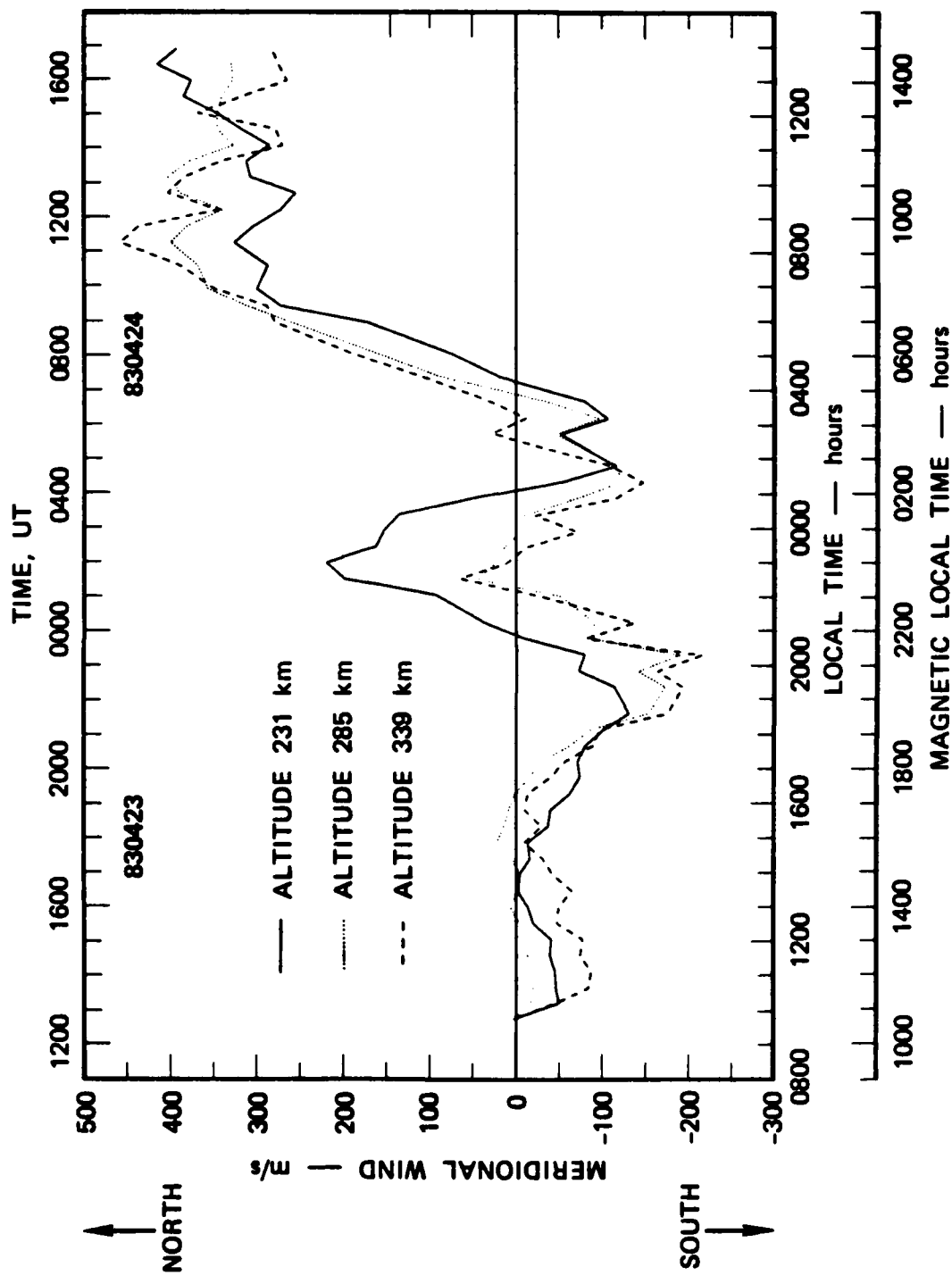


FIGURE III-19 ABATEMENT IN THE MERIDIONAL WIND NEAR MIDNIGHT AND LARGE DAY-TO-DAY VARIATION AT SONDRSTROM

have been observed over an extended latitude region on either side of the radar. The radar data have been supplemented with neutral wind data from a Fabry-Perot interferometer deep in the polar cap at Thule. This last effort is in collaboration with the University of Michigan.

c. The Role of Particle and Joule Heating

Although the importance of ion drag [Fuller-Rowell et al., 1981; Heppner and Miller, 1982; Roble et al., 1982; Hays et al., 1984; Wickwar et al., 1983] in determining the high-latitude thermospheric wind has become very clear, we have found situations at Sondrestrom that strongly suggest that energy input from both particle precipitation and Joule heating affect the neutral wind [Wickwar, 1984]. These results provide the impetus to further examine the daytime and nighttime data. As in the previous subsection, the appropriate observations come from experiments that survey a wide range of latitudes. It is then feasible to correlate the behavior of the overhead wind to the particle and Joule heating poleward and equatorward of the radar. Sufficient cases exist so that a combination of case studies and a statistical analysis would greatly increase our knowledge about these effects.

d.  $B_y$  Dependence of the Neutral Wind

We performed a statistical analysis on all the data from a two-year period for which the IMF data also existed. The results are shown in Figure III-20. This figure shows the average neutral wind at Sondrestrom for two orientations of the IMF  $B_y$  component. The differences are statistically significant.

As noted above, the wind is often greatly affected by ion drag. Because the shape of the convection pattern strongly depends on the IMF  $B_y$  component, it is not very surprising that the wind also depends on  $B_y$ .

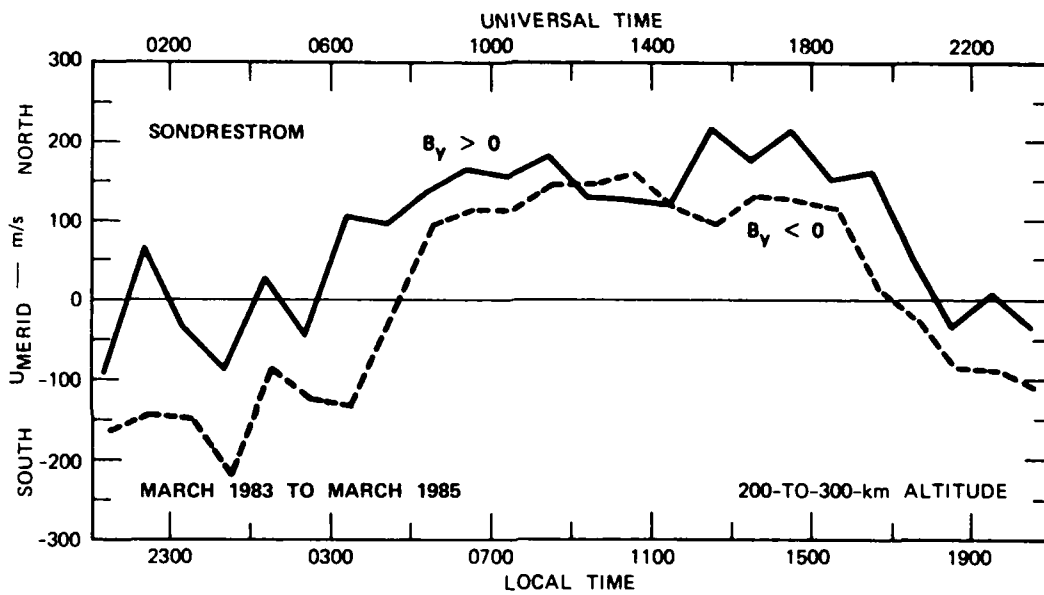


FIGURE III-20  $B_y$  DEPENDENCE OF THE MERIDIONAL WIND. The data are from Sondrestrom from the period March 1983 to March 1985.

e. Seasonal Dependence of the Neutral Wind

We performed a similar statistical analysis to look for seasonal effects. Because most of the Chatanika data were from the equinoxes, we again relied on the Sondrestrom data which included sufficient observations from the solstices to make this analysis possible. The results are shown in Figure III-21. The solid curve is for the summer; the dashed curve for the winter. Between the early morning and noon, the wind is more northward in the summer than in the winter.

This difference is consistent with what is expected from a stronger solar input in summer than in winter. However, the fact that the difference begins so early in the morning suggests that the explanation is more complex. Collaborative work, combining observation and theory, was started in order to seek an explanation for these results.

f. Altitude Gradients

The altitude dependence of the F-region wind had not been studied before. The usual working assumption was that the wind was constant with altitudes above about 200 km. This assumption is necessary in order to interpret the optical data because the emission altitude is not well known. We found that with the MITHRAS data this assumption is true under some conditions, but not others. Figure III-22 illustrates this point. It shows gradient in the midnight sector.

Wickwar et al. [1984c] had previously shown that gradients tended to appear in the radar data during the nighttime equatorward maximum. However, it is only recently that the analysis program has been improved to the point that we are sure the gradient is not an artifact of the calculations. We believe that the gradient is closely associated with ion drag during nighttime.

In going from 200- to 300-km altitude, the electron density usually increases and the neutral density always decreases. Therefore, the ratio of ions to neutrals increases greatly with altitude, with the effect that ion drag is more effective at the high end of the altitude

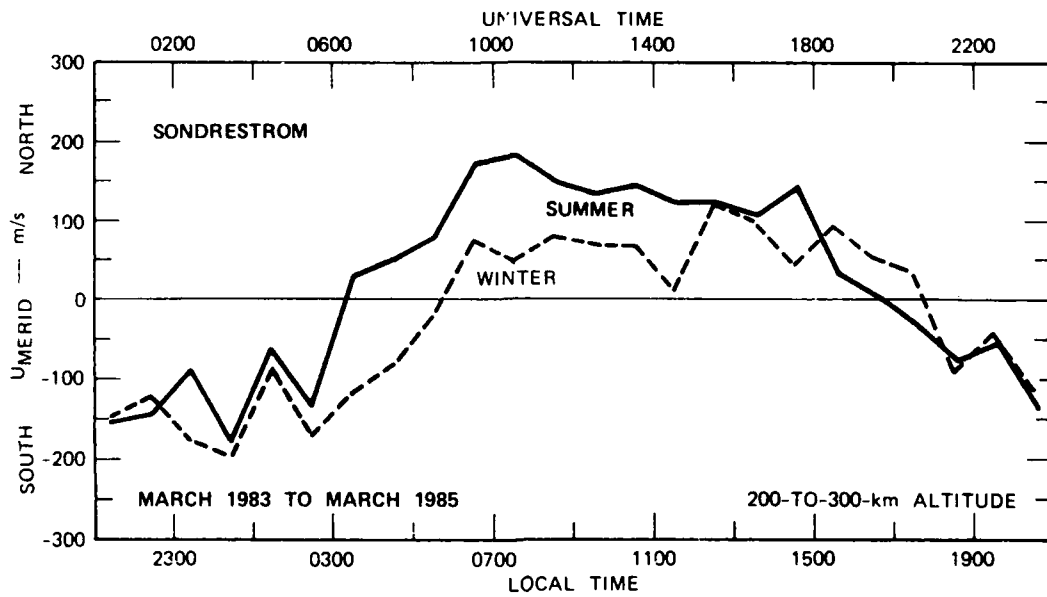


FIGURE III-21 SEASONAL DEPENDENCE OF THE MERIDIONAL WIND. The data are from Sondrestrom from the winters of 1983/84 and 1984/85 and from the summers of 1983 and 1984. Winter and summer are considered to be three months long, centered about their respective solstices.

AD-A174 883

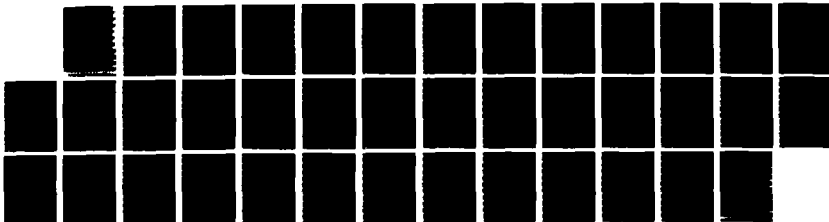
THE ANALYSIS PHASE OF NITRAS(U) SRI INTERNATIONAL  
MENLO PARK CA V B WICKMAR ET AL 23 JUN 86  
AFOSR-TR-86-2037 F49620-83-K-0005

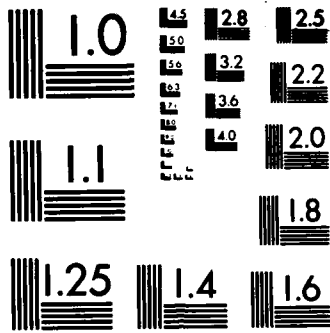
2/2

UNCLASSIFIED

F/G 4/1

NL





MICROCOPY RESOLUTION TEST CHART  
NATIONAL BUREAU OF STANDARDS-1963-A

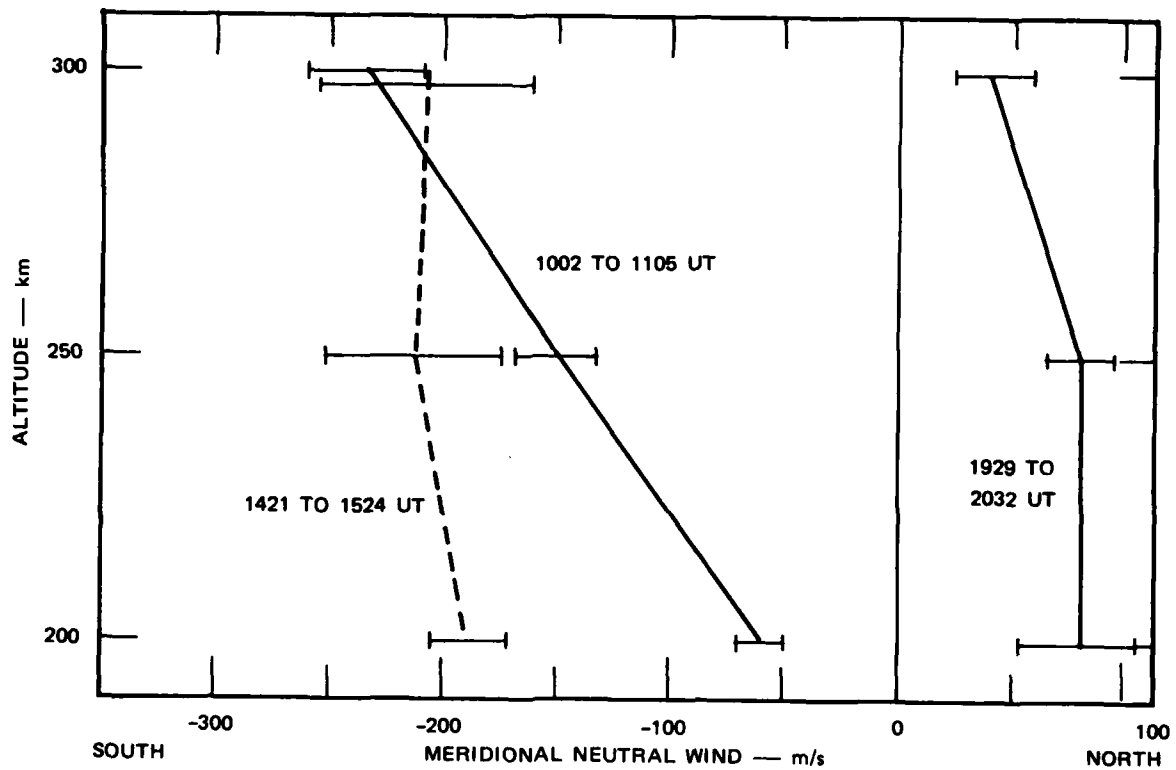


FIGURE III-22 GRADIENT IN THE MERIDIONAL NEUTRAL WIND AT CHATANIKA ON 18 NOVEMBER 1981. The curve at 1002 to 1105 UT (0002 to 0105 LT) shows the gradient; the other curves do not. The error bars are one standard deviation of the mean. They are estimated from seven 3-minute observations during a 63-minute interval.

range. The nighttime period when the gradient appears, moreover, coincides with when the peak of the F layer is at its highest altitude and when Chatanika is under the portion of the convection pattern with the strongest southward ion velocities.

g. Comparison with Theory

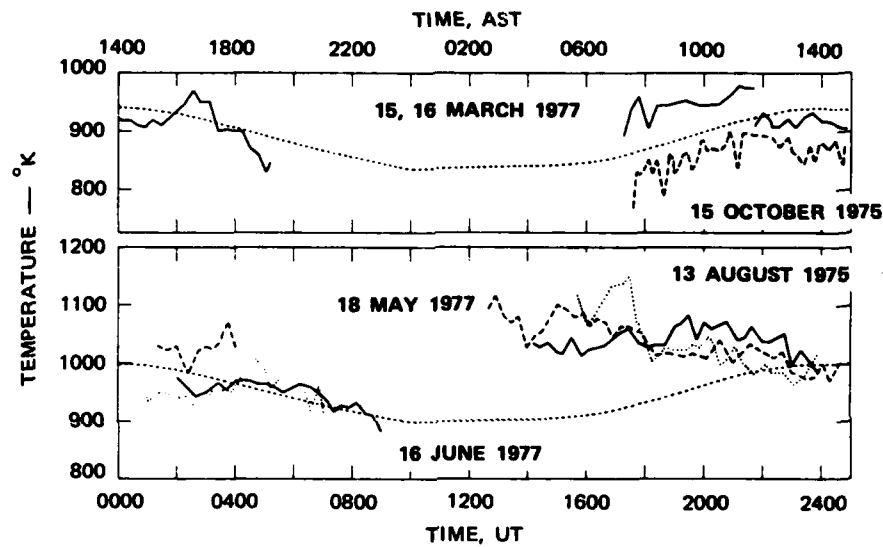
In addition to detailed examinations of the data under selected conditions, another approach has been started that involves an in-depth analysis of one or two days, which combine as many data as possible with extensive modeling. The day on which work was started was 18 November 1981. Very good coverage at high latitudes exists at Chatanika and EISCAT. Good coverage at middle latitudes also exists at St. Santin and Arecibo. At high latitudes, Millstone Hill also has convection and electron density information.

2. Neutral Temperature

The second neutral parameter of interest is the neutral temperature or its asymptotic value, the exospheric temperature. This parameter indicates changes in the neutral atmosphere. At the same time, a significant change in the neutral temperature is indicative of a very large energy input to the atmosphere. It can lead to major readjustments in the atmosphere that can affect the chemistry over wide areas and for extended periods.

a. Morning Increase

As mentioned earlier, we found that large ion temperatures often occur in the early morning. They are attributed to Joule heating. This process also deposits energy in the neutrals. The question is whether the neutrals also undergo a significant temperature increase. We have found considerable indirect evidence that they do. Several determinations of the exospheric temperature from the radar data [Wickwar et al., 1984c; Kelly et al., 1983] do suggest that significant increases occasionally occur in the morning sector. Figure III-23 from Wickwar et



[Source: Wickwar, et al., 1984c]

**FIGURE III-23 EARLY MORNING ENHANCEMENT OF EXOSPHERIC TEMPERATURE AT CHATANIKA.** The line of short dashes in both panels is from the CIRA [1972] model atmosphere. AST is Alaska Standard Time. The top panel shows temperature variation similar to that of CIRA. The bottom panel shows a large morning enhancement relative to CIRA.

a1. [1984c] shows three instances of this behavior. In the morning, the exospheric temperature was 200 K above what would have been predicted by an empirical neutral model. For comparison, we show that the temperature follows the predicted behavior on two other days.

The existence of these early-morning temperature increases are supported by other observations. A few optical measurements have revealed comparable or larger increases [Meriwether, private communication, 1984]. Anomalous increases in the equatorward meridional wind in the early morning, which have already been discussed, are consistent with significant heating. In addition, a theoretical effort to reconcile electric fields and neutral winds at Chatanika had to include such a temperature increase in the early morning [Hays et al., 1979].

Thus, it is likely that the neutral atmosphere is heated substantially in the early morning and that the mechanism is Joule heating, but the case has not yet been adequately proved. It would be important to verify this hypothesis.

The exospheric temperature is derived from the electron and ion temperatures in a manner similar to that described by Bauer et al. [1970]. The derivation is done by solving the ion energy equation when it is possible to assume that the only energy input to the ions is from Coulomb collisions with electrons. However, at high latitudes the ions are heated by collisions with neutrals--Joule heating. Working with groups at CNES and CNET, we have attempted to correct for Joule heating [Alcayde et al., 1983a]. However the correction is uncertain because of changes in ion composition. As a result, the safest procedure for determining the exospheric temperature is to consider only those times and places where the Joule heating is expected to be negligible [Wickwar and Kofman, 1984].

#### b. Behavior During Decreasing Phase of Solar Cycle

Another study involves the decrease in exospheric temperature from the time of the peak of the solar cycle to the present, i.e., starting

with the MITHRAS data. These long-term variations are important for the behavior of the neutral atmosphere and ionosphere. We have found that during the period from 1981 to 1985, the exospheric temperature has dropped by about 700 K, from 1400 K to 700 K.

During this same period, the high-latitude F layer has had roughly a factor-of-four decrease in maximum electron density and a 100-km decrease in the altitude of the layer. These changes in ionospheric behavior are closely, though not exclusively, tied to the neutral atmosphere. In addition to these general reasons for determining the exospheric temperature decrease, preliminary work suggests that the changes may not be smooth. For example, we observed a sudden decrease near the end of MITHRAS, around January 1982 [Alcayde et al., 1983b]. Whether this abrupt decrease was a perturbation or part of a monotonic decrease needs to be examined with later data.

#### IV DEVELOPMENT

As discussed in various places in the previous sections, knowledge of the solar wind and interplanetary magnetic field (IMF) is vital for understanding almost any auroral zone or polar cap phenomena. However, it has been increasingly difficult to measure and retrieve the solar wind parameters.

The only spacecraft that can regularly monitor the solar wind is currently IMP-8. In the past, the International Sun Earth Explorer, ISEE-3, provided continuous measurements of solar wind parameters, but in June 1982, its orbit was changed to the distant magnetotail and then to the Giacobini-Zinner comet. The ISEE-1 and -2 and the AMPTE-IRM orbits are such that they can monitor the solar wind for only a few weeks each year. Furthermore, ISEE-1 and -2 are expected to reenter during 1987. The WIND spacecraft, which is a part of the International Solar Terrestrial Program, will be well equipped to monitor the solar wind, but it will only be launched in the nineties. Therefore, at this time, the solar wind can only be monitored by IMP-8.

Unfortunately, NASA does not acquire IMP-8 data continuously because its telemetry is on a frequency that is not supported by the new TDRS network. Recognizing the importance of the solar wind data, telemetry is being received at Wallops Island and, very recently, at the European Space Agency Tracking station in Belgium. But, to extend the coverage, data must be acquired from the Pacific sector. For this reason, we received year-end funds to modify the SRI 150-ft antenna, so that it could acquire the IMP-8 telemetry, thereby extending the daily coverage by 3 to 4 hours.

The antenna was built by SRI in 1962 to study meteor-burst communications. In 1964 and 1965, a computer-based tracking system employing a

PDP-8 computer was added. Other improvements were also added for studying interplanetary and planetary electron densities by transmitting to instruments on Pioneer spacecraft (Pioneer 5 through 9) and Mariner 5 (Venus mission).

The antenna system is located in the foothills above Stanford University and has the following characteristics:

- Type--parabolic reflector
- Diameter--150 ft
- Design frequency--VHF through UHF
- Mount--azimuth elevation
- Gain--32 dB at 137 MHz
- Tracking--program track from punched paper tape
- Location--37.402659°N, -122.174139°E
- Altitude--145.085 m.

Work was performed on a number of elements in the antenna system. In particular, a new feed system was designed, built, and installed. Repairs were made on the old PDP-8 computer and on the tracking system. The rotary joints were repaired. The antenna system was tested. The tests showed that in spite of the intense industrial noise from Silicon Valley, the received signal-to-noise ratio is sufficient to acquire the IMP-8 telemetry.

Therefore, it has been determined that the 150-ft antenna and receiver system could be used to receive the IMP-8 telemetry. To actually use the system reliably, some further improvements would be needed, as would funding for operations.

## V CONCLUSIONS

MITHRAS has proven to be particularly valuable: not only did it greatly increase our scientific understanding of the upper atmosphere at high latitudes, but it also increased our ability as a group of researchers to address global scientific problems. A data acquisition phase was well thought out and coordinated; as a result, a valuable and sizable body of data was collected under a variety of geophysical conditions. Through the MITHRAS workshops and presentations at meetings, many researchers participated in the physical interpretation of the observations. In addition, arrangements were made for the easy exchange and transfer of the data. As a result of these efforts, other data sets have been made available and good working relationships have been established among several experimenters and theoreticians. Thus, MITHRAS became a collaborative effort among groups who work with incoherent-scatter radars, as well as with a large number of other researchers. Sufficient support has been provided since the data acquisition phase to allow for significant research activity and to enable development of new analysis techniques.

The MITHRAS project had an important role in the establishment of the incoherent-scatter data base, which is located at NCAR. It has also served as a model for a number of smaller multiradar research projects, such as GISMOS (Global Incoherent-Scatter Measurements Of Substorms) and GTMS (Global Thermospheric Mapping Study).

The MITHRAS experiment, which focused on an extensive set of incoherent-scatter data from the high-latitude region, produced a number of important scientific studies that increased our knowledge about the solar wind, magnetosphere, ionosphere, thermosphere, and the interactions among these regions:

- The best view, to date, has been obtained of the instantaneous shape of the convection pattern in the auroral region and polar cap. Instantaneous snapshots of the large-scale convection were obtained by combining Millstone Hill, Chatanika, and DE-2 electric-field measurements.
- A series of case studies established that the convection intensifies simultaneously in the morning and afternoon convection cells during a substorm.
- A case study of the convection at Chatanika, Millstone Hill, and EISCAT showed that the large-scale pattern could remain stable for a prolonged period, even though the period was one of sustained magnetic activity.
- Average patterns of plasma convection were calculated for two different orientations of the IMF By component. The patterns obtained showed that the effect of the By component is stronger and different than previously thought.
- At or near the convection reversal in the afternoon cell, i.e., at the polar cap boundary, there can be large energy inputs to the electron gas by soft particles and a downward heat flux.
- The winter nighttime F-region density strongly depends on longitude; this dependency was attributed to cross-polar cap transport of ionization and to the fact that because of the offset of the geographic and geomagnetic poles, the solar illumination of the large-scale convection pattern varies with UT.
- Using more inputs and being subject to more constraints than ever before, a theoretical model of the high-latitude ionosphere was able to successfully reproduce auroral-zone observations from two widely spaced longitudes.
- Theoretical calculations of the 6300-Å intensity from atomic oxygen showed that the hot electrons found near the afternoon convection reversal are responsible for a much larger proportion of the emission than previously considered.
- Although convection has the dominant role in determining the large-scale nighttime meridional neutral wind at F-region altitudes, local effects such as particle and Joule heating can create significant perturbations. At midnight in the polar cap a new phenomenon was observed, an abatement or sometimes even a reversal of the southward meridional wind.
- The importance of ion drag was further demonstrated in statistical analyses that showed the meridional component of the

neutral wind to be significantly correlated with the By component of the IMF. These analyses also showed that the neutral wind varies significantly with season.

- Several phenomena observed in the early morning at Chatanika--such as elevated ion and neutral temperatures, significantly perturbed meridional neutral winds, and reduced plasma densities--could be the result of very large Joule heating just poleward of the radar or in the polar cap.
- New methods were devised to determine the neutral exospheric temperature from high latitude radar data; the daily and solar-cycle variation were studied.

The MITHRAS observations were obtained specifically to take advantage of a unique radar configuration that existed for a short period in the auroral zone. The results, to date, attest to the importance of the data set as well as to the effectiveness of the research approach. Additional results are still to be obtained from studies begun later or based on the results of earlier ones.

In addition to what can be learned from this unique data set, new possibilities arise from the current configuration of the radars. Sondrestrom, EISCAT, and Millstone Hill are now located so as to provide denser sampling in a 90° segment of longitude and to cover a wider latitude region from the polar cap to just equatorward of the auroral region. This configuration offers possibilities for more detailed studies of many aspects of the interactions among the magnetosphere, ionosphere, and neutral atmosphere.

## VI REFERENCES

- Akasofu, S.-I., The solar wind-magnetosphere energy coupling and magnetospheric disturbances, Planet. Space Sci., 28, 495-501, 1980.
- Akasofu, S.-I., Auroral arcs and auroral potential structure, in Physics of Auroral Arc Formation, edited by S.-I. Akasofu and J. R. Kan, American Geophysical Union, Washington, D. C., pp. 1-14, 1981.
- Alcayde, D., P. Bauer, and J. Fontanari, Dynamical coupling of the auroral F-region ionosphere and thermosphere: Case studies, J. Atmos. Terr. Phys., 46, 625-633, 1984.
- Alcayde, D., J. Fontanari, P. Bauer, and O. de la Beaujardiere, Some properties of the auroral thermosphere inferred from initial EISCAT observations, Radio Sci., 18, 881-886, 1983a.
- Alcayde, D., P. Bauer, J. Fontanari, O. de la Beaujardiere, and C. Lathuilliere, Neutral temperature and atomic oxygen concentration in the thermosphere from auroral ionospheric incoherent-scatter observations, Aussois EISCAT Workshop, Aussois, France 1983b.
- Banks, P. M., T. Araki, C. R. Clauer, J. P. St. Maurice, and J. C. Foster, The interplanetary electric field cleft currents, and plasma convection in the polar caps, Planet. Space Sci., 32, 1551-1557, 1984.
- Baron, M. J., and R. H. Wand, F-region ion temperature enhancements resulting from Joule heating, J. Geophys. Res., 88, 4114-4118, 1983.
- Bauer, P., P. Waldteufel, and D. Alcayde, Diurnal variations of the atomic oxygen density and temperature determined from incoherent scatter measurements in the ionospheric F region, J. Geophys. Res., 75, 4825-4832, 1970.

- Burch, J. L., P. H. Reiff, J. D. Menietti, R. A. Heelis, W. B. Hanson, S. D. Shawhan, E. G. Shelley, M. Sugiura, D. R. Weimer, and J. D. Winningham, IMF By-dependent plasma flow and Birkeland currents in the dayside magnetosphere, 1. Dynamics Explorer observations, J. Geophys. Res., 90, 1577-1593, 1985.
- Caudal, G., O. de la Beaujardiere, D. Alcayde, J. Holt, and G. Lejeune, Simultaneous measurements of the electrodynamic parameters of the auroral ionosphere by the EISCAT, Chatanika, and Millstone Hill radars, Annales Geophysicae, 2, 369-376, 1984.
- CIRA 1972, Cospar International Reference Atmosphere 1972, The Committee for the COSPAR International Reference Atmosphere (CIRA) of COSPAR Working Group 4, Akademie-Verlag, Berlin, 1972.
- Clauer, C. R., P. M. Banks, A. Q. Smith, T. S. Jorgensen, E. Friis-Christensen, S. Vennerstrom, V. B. Wickwar, J. D. Kelly, and J. Doupnik, Observations of interplanetary magnetic field and of ionospheric plasma convection in the vicinity of the dayside polar cleft, Geophys. Res. Lett., 11, 891-894, 1984.
- Cogger, L. L., J. C. G. Walker, J. W. Meriwether, Jr., and R. G. Burnside, F-region airglow: are ground-based observations consistent with recent satellite results? J. Geophys. Res., 85, 3013-3020, 1979.
- Crooker, N. U., Dayside merging and cusp geometry, J. Geophys. Res., 84, 951-959, 1979.
- de la Beaujardiere, O., J. Holt, and E. Nielsen, Early MITHRAS results: The electric field response to substorms, Radio Sci., 18, 981-987, 1983.
- de la Beaujardiere, O., C. Senior, and V. B. Wickwar, MITHRAS observations of auroral-zone precipitation boundaries, URSI, January 1984a.

- de la Beaujardiere, O., M. Baron, V. B. Wickwar, C. Senior, and J. V. Evans, MITHRAS: A program of simultaneous radar observations of the high-latitude auroral zone, SRI Project 3261, final report, contract F49620-81-C-0042, Dep. of the Air Force, Bolling Air Force Base, Washington, D.C., 1982.
- de la Beaujardiere, O., V. B. Wickwar, and J. D. Kelly, Observations of polar-cap ionospheric signatures of solar/wind magnetosphere coupling, in Results of THE ARCAD 3 PROJECT and of the recent programmes in magnetospheric and ionospheric physics, Toulouse 84, 353-365, Cepadues-Editions, France, 1985c.
- de la Beaujardiere O., V. B. Wickwar, J. D. Kelly, and J. H. King, IMF- $B_y$  effect on the high-latitude nightside convection, SRI International, Radio Physics Laboratory, Menlo Park, California, Geophys. Res. Lett., 12, 461-464, 1985b.
- de la Beaujardiere, O., V. B. Wickwar, and J. H. King, Sondrestrom radar observations of the effect of the IMF  $B_y$  component on polar cap convection, Proceedings of the AGU Chapman Conference on Solar Wind-Magnetosphere Coupling, February 1985, in press, 1986.
- de la Beaujardiere O., V. B. Wickwar, G. Caudal, J. M. Holt, J. D. Craven, L. A. Frank, L. H. Brace, D. S. Evans, J. D. Winningham, and R. A. Heelis, Universal time dependence of nighttime F-region densities at high latitudes, J. Geophys. Res., 90, 4319-4332, 1985(a).
- de la Beaujardiere, O., V. B. Wickwar, M. J. Baron, J. Holt, R. M. Wand, W. L. Oliver, P. Bauer, M. Blanc, C. Senior, D. Alcayde, G. Caudal, J. Foster, E. Nielsen, and R. Heelis, MITHRAS: A brief description, Radio Sci., 19, 665-673, 1984b.
- Evans, J. V., J. M. Holt, and R. H. Wand, On the formation of daytime troughs in the F-region within the plasmasphere, Geophys. Res. Lett., 10, 405-408, 1983a.

- Evans, J. V., J. M. Holt, W. L. Oliver, and R. H. Wand, The fossil theory of nighttime high latitude F-region troughs, J. Geophys. Res., 88, 7769-7782, 1983b.
- Fontaine, D., C. Senior, and O. de la Beaujardiere, MITHRAS comparison of convection and precipitation at EISCAT and Chatanika, EOS Trans. AGU, 64, 777, 1983.
- Fontheim, E. G., L. H. Brace, J. D. Winningham, and B. A. Emery, Anomalous heating effects in the high latitude ionosphere, URSI, September 1984.
- Fontheim, E. G., R. S. B. Ong, R. G. Roble, H. G. Mayr, M. J. Baron, W. H. Hoegy, V. B. Wickwar, R. R. Vondrak, and J. A. Ionson, Effect of anomalous transport coefficients on the thermal structure of the storm time auroral ionosphere, J. Geophys. Res., 83, 4831-4836, 1978.
- Friis-Christensen, E., Y. Kamide, A. D. Richmond, and S. Matsushita, Interplanetary magnetic field control of high-latitude electric fields and currents determined from Greenland magnetometer data, J. Geophys. Res., 90, 1325-1338, 1985.
- Fuller-Rowell, T. J., and D. Rees, A three-dimensional time-dependent simulation of the global dynamical response of the the thermospheric to a geomagnetic substorm, J. Atmos. Terr. Phys., 43, 701-721, 1981.
- Grebowsky, J. M., H. A. Taylor, Jr., and J. M. Lindsay, Location and source of ionospheric high latitude troughs, Planet. Space Sci., 31, 99-105, 1983.
- Gussenhoven, M. S., D. A. Hardy, and N. Heinemann, Systematics of the equatorward diffuse auroral boundary, J. Geophys. Res., 88, 5692-5708, 1983.

- Hays, P. B., J. W. Meriwether, Jr., and R. G. Roble, Nighttime thermospheric winds at high latitudes, J. Geophys. Res., 84, 1905-1913, 1979.
- Heelis, R. A., The effects of interplanetary magnetic field orientation on dayside high latitude ionospheric convection, J. Geophys. Res., 89, 2873-2880, 1984.
- Heelis, R. A., J. C. Foster, O. de la Beaujardiere, and J. Holt, Multi-station measurements of high-latitude ionospheric convection, J. Geophys. Res., 88, 10117-10127, 1983.
- Hepner, J. P., Polar cap electric field distributions related to interplanetary magnetic field directions, J. Geophys. Res., 77, 4877-4887, 1972.
- Hepner, J. P., Empirical models of high-latitude electric fields, J. Geophys. Res., 82, 1115-1125, 1977.
- Hepner, J. P., Geophysica Norvegica, in press, 1984.
- Hepner, J. P., and M. L. Miller, Thermospheric winds at high latitudes from chemical release observations, J. Geophys. Res., 87, 1633-1647, 1982.
- Hill, V. J., D. S. Evans, and W. M. Retallak, A near real-time computer display showing the geographic location and intensity of auroral precipitation using TIROS/NOAA satellite observations, EOS Trans. AGU, 63, 1052, 1982.
- Holt, J. M., J. V. Evans, R. H. Wand, Millstone Hill studies of the trough: Boundry between the plasmopause and magnetosphere or not? Radio Sci., 18, 947-954, 1983.
- Iijima, T., and T. A. Potemra, Large-scale characteristics of field-aligned currents associated with substorms, J. Geophys. Res., 83, 599-615, 1978.

- Jacchia, L. G., Revised static models of the thermosphere and exosphere with empirical temperature profiles, Smithson. Astrophys. Obs. Rep., 332, 1971.
- Jorgensen, T. S., E. Friis-Christensen, V. B. Wickwar, J. D. Kelly, C. R. Clauer, and P. M. Banks, On the reversal from "sunward" to "antisunward" plasma convection in the dayside high latitude ionosphere, Geophys. Res. Lett., 11, 887-890, 1984.
- Kamide, Y., and A. D. Richmond, Ionospheric conductivity dependence of electric fields and currents estimated from ground magnetic observations, J. Geophys. Res., 87, 8331-8337, 1982.
- Kamide, Y., A. D. Richmond, and S. Matsushita, Estimation of ionospheric electric fields, ionospheric currents, and field-aligned currents from ground magnetic records, J. Geophys. Res., 86, 801-813, 1981.
- Kamide, Y., R. M. Robinson, S.-I. Akasofu, and T. A. Potemra, Aurora and electrojet configuration in the early morning sector, J. Geophys. Res., 89, 389-393, 1984.
- Kelly, J. D., C. J. Heinselman, and J. Petriceks, High-latitude exospheric temperature observed over a solar cycle, Radio Sci., 18, 901-905, 1983.
- Knudsen, W. C., Magnetospheric convection and the high-latitude F<sub>2</sub> ionosphere, J. Geophys. Res., 79, 1046-1055, 1974.
- Kofman, W., and V. B. Wickwar, Very high electron temperatures in the daytime F-region at Sondrestrom, Geophys. Res. Lett., 9, 919-922, 1984.
- Link, R., J. C. McConnell, and G. G. Shepherd, An analysis of the spatial distribution of dayside cleft optical emissions, J. Geophys. Res., 88, 10145-10162, 1983.
- Lyons, L. R., A simple model for polar cap convection patterns and generation of  $\theta$  auroras, J. Geophys. Res., 90, 1561-1567, 1985.

- McCormac, F. G., and R. W. Smith, The influence of the interplanetary magnetic field y component on ion and neutral motions in the polar thermosphere, Geophys. Res. Lett., 11, 935-938, 1984.
- McPherron, R. L., Magnetospheric substorms, Rev. Geophys. Space Phys., 17, 657-681, 1979.
- Meriwether, Jr., J. W., private communication, 1984.
- Meriwether, Jr., J. W., P. Shih, T. L. Killeen, V. B. Wickwar, and R. G. Roble, Nighttime thermospheric winds over Sondre Stromfjord, Greenland, Geophys. Res. Lett., 9, 932-934, 1984.
- Mozer, F. S., W. D. Gonzalez, F. Bogott, M. C. Kelley, and S. Schutz, High-latitude electric fields and the three-dimensional interaction between the interplanetary and terrestrial magnetic fields, J. Geophys. Res., 79, 56-63, 1974.
- Muldrew, D. B., F layer ionization troughs deduced from Alouette data, J. Geophys. Res., 70, 2635-2650, 1965.
- NASA Reference Publication 1120, Solar Terrestrial Physics: Present and Future, A Report Based on the Solar Terrestrial Physics Workshop, December 1982 to November 1983, edited by D. M. Butler and K. Papadopoulos, University of Maryland, College Park, Maryland, 1984.
- Potemra, T. A., T. Iijima, and N. A. Saflekos, Large-scale characteristics of Birkeland currents, in Dynamics of the Magnetosphere, 165-199, D. Reidel, Hingham, Mass., 1979.
- Potemra, T. A., L. J. Zanetti, P. F. Bythrow, A. T. Y. Lui, and T. Iijima, By-dependent convection patterns during northward interplanetary magnetic field, J. Geophys. Res., 89, 9753-9760, 1984.
- Prolss, G. W., Magnetic storm associated perturbations of the upper atmosphere: recent results obtained by satellite-borne gas analyzers, Rev. Geophys. Space Phys., 18, 183-202, 1980.

- Rasmussen, C. E., R. W. Schunk, J. J. Sojka, V. B. Wickwar, O. de la Beaujardiere, J. Foster, J. M. Holt, E. Nielsen, and D. S. Evans, Comparison of simultaneous Chatanika and Millstone Hill observations with ionospheric model predictions, J. Geophys. Res., 91, 6986-6998, 1986.
- Rawer, K., International Reference Ionosphere IRI-79 Report UAG-82, World Data Center-A (S.T.P.), Boulder, Colorado U.S.A., 1981.
- Reiff, P. H., and J. L. Burch, IMF By-dependent plasma flow and Birke-land currents in the dayside magnetosphere: 2. A global model for Northward and Southward IMF, J. Geophys. Res., 90, 1595-1609, 1985.
- Reiff, P. H., J. L. Burch, and R. A. Heelis, Dayside auroral arcs and convection, Geophys. Res. Lett., 5, 391-394, 1978.
- Robinson, R. M., R. R. Vondrak, and T. A. Potemra, Electrodynamic properties of the evening sector ionosphere within the region-2 field-aligned current sheet, J. Geophys. Res., 87, 732-741, 1982.
- Roble, R. G., and M. H. Rees, Time-dependent studies of the aurora: Effects of particle precipitation on the dynamic morphology of ionospheric and atmospheric properties, Planet. Space Sci., 25, 991-1010, 1977.
- Roble, R. G., R. E. Dickinson, and E. C. Ridley, Global circulation and temperature structure of thermosphere with high-latitude plasma convection, J. Geophys. Res., 87, 1599-1614, 1982.
- Rostoker, G., S.-I. Akasofu, J. Foster, R. A. Greenwald, Y. Kamide, K. Kawasaki, A.T.Y. Lui, R. L. McPherron, and C. T. Russell, Magnetospheric substorms--definition and signatures, J. Geophys. Res., 85, 1663-1668, 1980.
- Sato, T., and G. F. Rourke, F-region enhancements in the antarctic, J. Geophys. Res., 69, 4591-4607, 1964.

- Schild, M. A., J. W. Freeman, and A. J. Dessler, A source for field-aligned currents at auroral latitudes, J. Geophys. Res., 74, 247-256, 1969.
- Schunk, R. W., W. J. Raitt, and P. M. Banks, Effect of electric fields on the daytime high-latitude E and F regions, J. Geophys. Res., 80, 3121-3130, 1975.
- Senior, C., Courants alignes, precipitations diffuses et électrojets dans le secteur nuit de haute latitude, Proceedings of GRECO Conference, Grenoble, France, September 1982.
- Senior, C., and M. Blanc, On the control of magnetospheric convection by the spatial distribution of ionospheric conductivities, J. Geophys. Res., 89, 261-284, 1984.
- Senior, C., R. M. Robinson, and T. A. Potemra, Relationship between field-aligned currents, diffuse auroral precipitation and the westward electrojet in the early morning sector, J. Geophys. Res., 87, 10469-10477, 1982.
- Senior, C., J. R. Sharber, O. de la Beaujardiere, R. A. Heelis, D. S. Evans, J. D. Winningham, M. Sugiura, and W. R. Hoegy, E- and F-region study of the evening sector auroral oval: A Chataka/Dynamics Explorer-2/NOAA-6 comparison, submitted to J. Geophys. Res., 1986.
- Smiddy, M., M. C. Kelley, W. J. Burke, F. J. Rich, R. Sagalyn, B. Shuman, R. Hays, and S. Lai, Intense poleward directed electric fields near the ionospheric projection of the plasmapause, Geophys. Res. Lett., 4, 543-548, 1977.
- Sojka, J. J., R. W. Schunk, and W. J. Raitt, Seasonal variations of the high-latitude F region for strong convection, J. Geophys. Res., 87, 187-198, 1982.
- Spiro, R. W., R. A. Heelis, and W. B. Hanson, Ion convection and the formation of the mid-latitude F-region ionization trough, J. Geophys. Res., 83, 4255-4264, 1978.

- Vasyliunas, V. M., The interrelationship of magnetospheric processes, in Earth's Magnetospheric Processes, ed. by McCormac, 29-35, D. Reidel, Dordrecht-Holland, 1972.
- Volland, H., A model of the magnetospheric electric convection field, J. Geophys. Res., **83**, 2695-2699, 1978.
- Wickwar, V. B., Thermospheric neutral wind at  $-39^{\circ}$  azimuth during the daytime sector at Sondrestrom, Geophys. Res. Lett., **2**, 929-930, 1984.
- Wickwar, V. B., and W. Kofman, Dayside red auroras at very high latitudes: The importance of thermal excitation, Geophys. Res. Lett., **2**, 923-926, 1984.
- Wickwar, V. B., O. de la Beaujardiere, and W. Kofman, Meridional winds at Chatanika and EISCAT during Project MITHRAS, Aussois EISCAT Workshop, September 1983.
- Wickwar, V. B., O. de la Beaujardiere, and C. A. Leger, The Analysis phase of MITHRAS: Progress Report, Interim Scientific Report, contract F49620-83-K-0005, Department of the Air Force, Air Force Office of Scientific Research, Bolling Air Force Base, Washington, D.C., 1984a.
- Wickwar, V. B., L. L. Cogger, and H. C. Carlson, The 6300-A O( D) air-glow and dissociative recombination, Planet. Space Sci., **22**, 709-724, 1974.
- Wickwar, V. B., J. W. Meriwether, Jr., P. B. Hays, and A. F. Nagy, The meridional thermospheric neutral wind measured by radar and optical techniques in the auroral region, J. Geophys. Res., **89**, 10987-10998, 1984c.
- Wickwar, V. B., J. D. Kelly, O. de la Beaujardiere, C. A. Leger, F. Steenstrup, and C. H. Dawson, Sondrestrom overview, Geophys. Res. Lett., **11**, 883-886, 1984b.
- Wickwar, V. B., W. Kofman, M. Rees, R. Sica, G. Romick, G. Hernandez,

and S. Mende, Examination of a type-A red aurora with radar, optics and theoretical modeling, XXI URSI General Assembly, Florence, Italy, 1984d.

Winningham, J. D., and W. J. Heikkila, Polar cap auroral electron fluxes observed with Isis 1, J. Geophys. Res., 79, 949-957, 1974.

Winningham, J. D., F. Yasuhara, S.-I. Akasofu, and W. J. Heikkila, The latitudinal morphology of 10-eV to 10-keV electron fluxes during magnetically quiet and disturbed times in the 2100-0300 MLT sector, J. Geophys. Res., 80, 3148-3171, 1975.

Young, E. R., D. G. Torr, P. Richards, and A. F. Nagy, A computer simulation of the midlatitude plasmasphere and ionosphere, Planet. Space Sci., 28, 881-893, 1980.

Zanetti, L. J., T. A. Potemra, T. Iijima, W. Baumjohann, and P. F. Bythrow, Ionospheric and Birkeland current distributions for northward interplanetary magnetic field: Inferred polar convection, J. Geophys. Res., 89, 7453-7458, 1984.

Appendix A

MITHRAS-RADAR OBSERVATIONS

## Appendix A

MITHRAS-RADAR OBSERVATIONS  
(May 1981 through June 1982)

Day Number	Date *	Time * (start-end)			Two-Way Overlap (hr)†	Three-Way Overlap (hr)‡	ΣK <sub>p</sub>	Mode
		Chatanika	Millstone Hill	EISCAT				
133	13 May	0018-2400	2135-		2.4	-	16-	MITHRAS 2
134	14 May		-0400		-	-	25	
143	23 May	1555- -1837	1425-		8.1	-	25+	MITHRAS 1
144	24 May		-1950		13.0	-	26+	
161	10 Jun	0044- -0130	0005-		22.7	-	9	MITHRAS 3
162	11 Jun		-0400		1.5	-	13	
174	23 Jun	2050-2340	2210-		1.5	-	10-	MITHRAS 2
175	24 Jun		-		-	-	19+	
176	25 Jun		-0400		-	-	22	
178	27 Jun		0358-	0335-		19.7	-	
179	28 Jun	-0505	-1725		5.1	-	18	MITHRAS 1
185	04 Jul	0158- -0358	0210-		20.4	-	16-	MITHRAS 1
186	05 Jul		-		4.0	-	22-	
187	06 Jul		-1215		-	-	27-	
195	14 Jul	2200- -			-	-	14-	MITHRAS 2
196	15 Jul		1510-		8.8	-	7-	
197	16 Jul		-0012	-1520		0.2	-	
202	21 Jul	2152- -2359			-	-	13-	MITHRAS 3
203	22 Jul		0112-		17.1	-	28+	
204	23 Jul		-0030		-	-	34-	
213	01 Aug	0208- -0358	0550-		-	-	26-	MITHRAS 1
214	02 Aug		-2330		20.8	-	22-	
215	03 Aug		-		-	-	26-	
218	06 Aug		0720-		-	-	21+	MITHRAS 3
219	07 Aug		-0030		-	-	17+	
223	11 Aug		2005-		-	-	22+	MITHRAS 1
224	12 Aug		-		-	-	18-	
225	13 Aug		-1125		-	-	18+	
258	15 Sep		1850-		-	-	17+	MITHRAS 1 CP (-1)
259	16 Sep		-2330		14.5	-	15-	
260	17 Sep		0900- -0800		-	-	9	
265	22 Sep		1318-		-	-	20	MITHRAS 3
266	23 Sep		-		-	-	8+	
267	24 Sep		-1600		-	-	16	
272	29 Sep	0130- -0138	1949-		-	-	20+	MITHRAS 2 CP(-1)
273	30 Sep		-		1130- -0900	18.9	12.5	
274	01 Oct		-0346		3.8	1.6	24- 18	
279	06 Oct	0011- -1214			2200- -2120	-	12-	MITHRAS 3 CP(-1)
280	07 Oct		2236-		13.4	-	32	
281	08 Oct		-2400		12.2	-	30	
297	24 Oct	0031 -	0217-		-	-	22-	MITHRAS 1 CP(∅)
298	25 Oct		-		1630- -0900	23.0	5.1	
299	26 Oct		-1328		13.0	8.5	24+ 18-	
300	27 Oct		-0009		-	-	18	

Day Number	Date*	Time* (start-end)			Two-Way Overlap (hr)†	Three-Way Overlap (hr)†	ΣK <sub>p</sub>	Mode
		Chatanika	Millstone Hill	EISCAT				
300	27 Oct		2129-		-	-	18	MITHRAS 2
301	28 Oct	0004-	-		22.9	-	26	
302	29 Oct	-0200	-0415		2.0	-	20	
314	10 Nov	-	2130-		-	-	21-	MITHRAS 3 CP(0)
315	11 Nov	0000-	-	0900-1453	21.9	5.9	32-	
316	12 Nov	-0213	-0135		1.6	-	30-	
321	17 Nov		2124-		-	-	33+	MITHRAS 2 CP(0)
322	18 Nov	0017-	-	0900-	22.6	15.0	31	
323	19 Nov	-0001	-0500	-0900	5.0	-	23+	
325	21 Nov	0017-	0312-		20.5	-	23+	MITHRAS 1
326	22 Nov	-0201	-		1.9	-	19+	
327	23 Nov	-	-0926		-	-	27	
339	05 Dec	1702-	0313-		4.2	-	17+	MITHRAS 1
340	06 Dec	-1707	-0330		3.5	-	8+	
342	08 Dec	2143-	2235-	1500-	2.3	1.4	22+	MITHRAS 3 CP(-3e)
343	09 Dec	-2400	-0456	-2020	17.3	4.4	20-	
349	15 Dec	2241-	2146-	1500-	2.2	1.3	10+	MITHRAS 2 CP(-3s)
350	16 Dec	-	-	-1940	21.5	17.2	9-	
351	17 Dec	-0010	-0449		0.2	-	11	
9	09 Jan		0305-		-	-	8	MITHRAS 1
10	10 Jan	0620-	-		17.7	-	7-	
11	11 Jan	-0803	-1418		8.0	-	10+	
19	19 Jan	1800-	2116-		2.7	-	6+	MITHRAS 2 CP(-3e)
20	20 Jan	-2005	-	1500-2300	19.7	1.2	12+	
21	21 Jan		-0458				22	
26	26 Jan	1818-	2121-	1500-	5.7	2.7	13	MITHRAS 3 CP(3)
27	27 Jan	-	-	-2258	24.0	21.0	21+	
28	28 Jan	-0010	-0129		0.2	-	24	
30	30 Jan		0306-		-	-	29	MITHRAS 1 CP(3)
31	31 Jan	0608-	-	1000-2345	15.6	12.4	34-	
32	01 Feb	-1320	-1332		13.3	-	34	
40	09 Feb	1550-	1042-		8.2	-	24	MITHRAS 3
41	10 Feb	-2307	-1512		15.2	-	33+	
47	16 Feb	1805-	2031-		3.5	-	13+	MITHRAS 2
48	17 Feb	-	-		23.4	-	30+	
49	18 Feb	-0003	-0459		-	-	34+	
114	24 Apr		0441-				21	MITHRAS 1 CP(3)
115	25 Apr		-	1210-	10.0	-	37+	
116	26 Apr		-1227	-1000	10.0	-	15-	
128	08 May		0153-				10	MITHRAS 1 CP(0)
129	09 May		-2000	1018-	8.8	-	15	
130	10 May			-1003		-	11-	
138	18 May		2008-	1500-	3.9	-	26+	MITHRAS 3 CP(-2)
139	19 May		-2400	-2300	23.0	-	21	
140	20 May		-0358			-	17	
166	15 Jun		2012-				30	MITHRAS 1 CP(3)
167	16 Jun		-	1100-	13.0	-	19+	
168	17 Jun		-0358	-1100	4.0	-	13-	

\* Dates and times are UT.

† Data gaps of > 20-min duration excluded from overlap time calculation.

Appendix B

PARTICIPANTS IN MITHRAS

Appendix B

PARTICIPANTS IN MITHRAS

CEPHAG

W. Kofman  
C. Lathuillere  
G. Lejeune

Service d'Aeronomie du CNRS

P. Bauer

Kyangpook National University

B.-H. Ahn

Kyoto Sangyo University

Y. Kamide

Lockheed

S. Mende  
R. Robinson

Millstone Hill

J. Evans  
J. Foster  
J. Holt  
W. Oliver  
R. Wand  
T. Van Eyken

CNES

D. Alcayde  
J. Fontanari

CPRE

M. Blanc  
G. Caudal  
C. Senior  
D. Fontaine

Danish Meteorological Institute

E. Friis-Christensen  
T. Jorgensen

EISCAT

C. LaHoz

Max Planck, Lindau

E. Nielsen

NASA-GSFC

L. Brace  
R. Hoffman

NOAA-Boulder

D. Evans

SRI

M. Baron  
O. de la Beaujardiere  
C. Heinselman  
J. Kelly  
C. Leger  
J. Petriceks  
V. Wickwar

University of Alaska

S.-I. Akasofu  
M. Rees  
G. Romick

University of Michigan

P. Hays  
G. Hernandez  
T. Killeen  
J. Meriwether  
A. Nagy

Utah State University

C. Rasmussen  
R. Schunk  
J. Sojka  
R. Sica

NCAR

B. Emery  
A. Richmond  
R. Roble  
R. Barnes

Rice University

P. Reiff  
R. Spiro  
R. Wolfe  
G. Mantjouis

SWRI

J. Winningham  
J. Sharber

University of Illinois

J. Craven  
L. Frank

University of Texas, Dallas

R. Heelis

Appendix C

MITHRAS PUBLICATIONS, REPORTS, AND PRESENTATIONS

## Appendix C

### MITHRAS PUBLICATIONS, REPORTS, AND PRESENTATIONS

#### 1. Publications

- Alcayde, D., J. Fontanari, P. Bauer, and O. de la Beaujardiere, Some properties of the auroral thermosphere inferred from initial EISCAT observations, Radio Sci., 18, 881-886, 1983.
- Baron, M. J., and R. H. Wand, F-region ion temperature enhancements resulting from Joule heating, J. Geophys. Res., 88, 4114-4118, 1983.
- Baron, M. J., C. J. Heinselman, and J. Petriceks, Solar cycle and seasonal variations of the ionosphere observed with the Chatanika incoherent scatter radar, Radio Sci., 18, 895-900, 1983.
- Caudal, G., O. de la Beaujardiere, D. Alcayde, J. Holt, and G. Lejeune, Simultaneous measurements of the electrodynamic parameters of the auroral ionosphere by the EISCAT, Chatanika and Millstone Hill radars, Annales Geophysicae, 2, 369-376, 1984.
- de la Beaujardiere, O., J. Holt, and E. Nielsen, Early MITHRAS results: The electric field response to substorms, Radio Sci., 18, 981-987, 1983.
- de la Beaujardiere, O., V. B. Wickwar, G. Caudal, J. M. Holt, J. D. Craven, L. A. Frank, L. H. Brace, D. S. Evans, J. D. Winningham, and R. A. Heelis, Universal time dependence of nighttime F region densities at high latitudes, J. Geophys. Res., 90, 4319-4332, 1985.
- de la Beaujardiere, O., V. B. Wickwar, M. J. Baron, J. Holt, R. M. Wand, W. L. Oliver, P. Bauer, M. Blanc, C. Senior, D. Alcayde, G. Caudal, J. Foster, E. Nielsen, and R. Heelis, MITHRAS: A brief description, Radio Sci., 19, 665-673, 1984.
- de la Beaujardiere, O., V. B. Wickwar, and J. D. Kelly, Observations of polar-cap ionospheric signatures of solar wind/magnetosphere coupling, Proceedings of ARCAD Workshop, Toulouse, 84, France, 1985.
- de la Beaujardiere, O., V. B. Wickwar, J. D. Kelly, and J. H. King, IMF-By effects on the high-latitude nightside convection, Geophys. Res. Lett., 12, 461-464, 1985.
- de la Beaujardiere, O., and V. B. Wickwar, IMF control of plasma drift, ion temperature and neutral wind, Proceedings of the U.S.-Finland Auroral Workshop, October 1985.

- de la Beaujardiere, O., V. B. Wickwar, and J. H. King, Sondrestrom radar observations of the effect of the IMF By component on polar cap convection, Proceedings of the AGU Chapman Conference on Solar Wind-Magnetosphere Coupling, February 1985, in press, 1986.
- Rasmussen, C. E., R. W. Schunk, J. J. Sojka, V. B. Wickwar, O. de la Beaujardiere, J. Foster, J. M. Holt, E. Nielsen, and D. S. Evans, Comparison of simultaneous Chatanika and Millstone Hill observations with ionospheric model predictions, J. Geophys. Res., 91, 6986-6998, 1986.
- Rasmussen, C. E., J. J. Sojka, R. W. Schunk, V. B. Wickwar, O. de la Beaujardiere, J. Foster, and J. Holt, Comparison of simultaneous Chatanika and Millstone Hill temperature measurements with ionospheric model predictions, submitted to J. Geophys. Res., 1986.
- Senior, C., J. R. Sharber, O. de la Beaujardiere, R. A. Heelis, D. S. Evans, J. D. Winningham, M. Sugiura, and W. R. Hoegy, E- and F-region study of the evening sector auroral oval: A Chatanika/Dynamics Explorer-2/NOAA-6 comparison, submitted to J. Geophys. Res., 1986.
- Heelis, R. A., J. C. Foster, O. de la Beaujardiere, and J. Holt, Multistation measurements of high-latitude ionospheric convection, J. Geophys. Res., 88, 10111-10121, 1983.
- Kelly, J. D., C. J. Heinselman, and J. Petriceks, High-latitude exospheric temperature observed over a solar cycle, Radio Sci., 18, 901-905, 1983.
- Kofman, W., and V. B. Wickwar, Very high electron temperatures in the daytime F-region at Sondrestrom, Geophys. Res. Lett., 2, 919-922, 1984.
- Rino, C. L., R. C. Livingston, R. T. Tsunoda, R. M. Robinson, J. F. Vickrey, C. Senior, M. D. Cousins, J. Owen, and J. A. Klobuchar, Recent studies of the structure and morphology of auroral zone F region irregularities, Radio Sci., 18, 1167-1180, 1983.
- Senior, C., and M. Blanc, On the control of magnetospheric convection by the spatial distribution of ionospheric conductivities, J. Geophys. Res., 89, 261-284, 1984.
- Wickwar, V. B., Thermospheric neutral wind at -39° azimuth during the daytime sector at Sondrestrom, Geophys. Res. Lett., 2, 927-930, 1984.
- Wickwar, V. B., and W. Kofman, Dayside red auroras at very high latitudes: The importance of thermal excitation, Geophys. Res. Lett., 2, 923-926, 1984.
- Wickwar, V. B., J. W. Meriwether, Jr., P. B. Hays, and A. F. Nagy, The meridional thermospheric neutral wind measured by radar and optical techniques in the auroral region, J. Geophys. Res., 89, 10987-10998, 1984.

## 2. Reports and Referred Articles

Baron, M. J., and A. R. Hessing, Comment on 'A simple method for calculating the local time of corrected geomagnetic midnight,' by L. E. Monbriant, unpublished manuscript, SRI International, Menlo Park, CA, 1982.

de la Beaujardiere, O., G. Caudal, and J. Holt, MITHRAS observations of the nighttime F-region ionization, Proceedings of the U.S.-Finland Workshop on Magnetospheric/Ionospheric Phenomena in Auroral Regions, Maryland 1983.

de la Beaujardiere, O., V. B. Wickwar, J. D. Kelly, Sondrestrom-radar observations, Proceedings of the U.S.-Finland Workshop on Magnetosphere/Ionosphere Phenomena in Auroral Regions, Maryland 1983.

de la Beaujardiere, O., V. B. Wickwar, and J. D. Kelly, Observations of polar-cap ionospheric signatures of solar wind/magnetosphere coupling, Proceedings of ARCAD Workshop, Toulouse, France 1984.

de la Beaujardiere, O., M. J. Baron, C. Senior, J. Petriceks, and C. Leger, Chatanika radar observations associated with the MITHRAS program, in Origins of Plasmas and Electric Fields in the Magnetosphere, Yosemite Conference, January 1982.

de la Beaujardiere, O., M. J. Baron, V. B. Wickwar, C. Senior, and J. V. Evans, MITHRAS: A program of simultaneous radar observations of the high-latitude auroral zone, Final Scientific Report, 77 pp., SRI Project 3261, SRI International, Menlo Park, CA, 1982.

de la Beaujardiere, O., V. B. Wickwar, C. A. Leger, M. A. McCready and M. J. Baron, The software system for the Chatanika incoherent-scatter radar, Technical Report, 2nd edition, 127 pp., SRI Projects 4964 and 4995, SRI International, Menlo Park, CA, 1984.

de la Beaujardiere, O., V. B. Wickwar, and J. D. Kelly, Observations of polar-cap ionospheric signatures of solar wind/magnetosphere coupling, Proceedings of ARCAD Workshop, Toulouse, 84, France, 1985.

de la Beaujardiere, O., and V. B. Wickwar, IMF control of plasma drift, ion temperature and neutral wind, U.S.-Finland Workshop, Sondankyla, October 1985.

Leger, C. A., User's guide to AED color graphics software, Technical Memorandum, 31 pp., SRI Project 4995, SRI International, Menlo Park, CA, January 1983.

Leger, C. A., User's guide to the software system for the Sondrestrom incoherent-scatter radar, Technical Memorandum, 70 pp., SRI Projects 4995 and 4964, SRI International, Menlo Park, CA, August 1984.

Wickwar, V. B., O. de la Beaujardiere, and C. A. Leger, The analysis phase of MITHRAS, Progress Report, SRI International, Menlo Park, CA 1984.

3. Presentations

Yosemite Conference  
January 1982

de la Beaujardiere, O., M. Baron, C. Senior, J. Petriceks, and C. Leger, "Chatanika Radar Observations Associated with the MITHRAS Program."

URSI Symposium  
August 1982

Baron, M. J., "F-Region Ion Temperature Enhancements Resulting From Joule Heating."

Baron, M. J., C. J. Heinselman, and J. Petriceks, "Solar Cycle Variations of the High-Latitude Ionosphere as Observed with Incoherent Scatter Radar."

de la Beaujardiere, O., J. Holt, and E. Nielsen, "Early MITHRAS Results: The Electric-Field Response to Substorms."

Kelly, J. D., C. J. Heinselman, and J. Petriceks, "High-Latitude Exospheric Temperature Observed over a Solar Cycle."

Tsunoda, R. T., R. M. Robinson, and C. Senior, "F-Region Plasma Enhancements Along the Equatorward Boundary of the Auroral Oval."

de la Beaujardiere, O., "The MITHRAS Project."

European Geophysics Society Symposium  
August 1982

Caudal, G., D. Alcayde, O. de la Beaujardiere, and G. Lejeune, "Simultaneous Measurements of the Electrodynamical Parameters of the Auroral Ionosphere by the EISCAT and Chatanika Radars."

GRECO Conference  
September 1982

Caudal, G., D. Alcayde, O. de la Beaujardiere, and G. Lejeune, "Mesures Simultanees des Champs Electriques de l'Ionosphere Aurorale par les Radars d'EISCAT et de Chatanika."

Senior, C., "Courants Alignes, Precipitations Diffuses et Electrojets dans le Secteur Nuit de Haute Latitude."

Fall AGU Meeting  
December 1982

de la Beaujardiere, O., J. Holt, and E. Nielsen, "Early MITHRAS Results: The Electric Field Response to Substorms."

Spring AGU Meeting  
May 1983

de la Beaujardiere, O., V. Wickwar, D. Alcayde, and P. Bauer, "Measurements of the Exospheric Temperatures at Chatanika and EISCAT on 18 November 1981."

IUGG XVIII General Assembly  
August 1983

Alcayde, D., P. Bauer, O. de la Beaujardiere, J. Fontanari, and V. B. Wickwar, "High Latitude Observations of Thermospheric Temperature and Atomic Oxygen Concentration During MITHRAS Operations."

Clauer, C. R., P. M. Banks, V. B. Wickwar, J. D. Kelly, O. de la Beaujardiere, J. R. Douppnik, J. C. Foster, T. Stockflet-Jorgensen, E. Friis-Christensen, and T. Araki, "Coordinated Observations of the Polar Cusp."

de la Beaujardiere, O., V. B. Wickwar, D. Alcayde, P. Bauer, W. Oliver, T. Killeen, G. Carignan, P. Hays, and N. Spencer, "Thermospheric Parameters Measured on 18 November 1981 Using Chatanika, EISCAT, Millstone Hill, and DE-B."

Fontaine, D., M. Blanc, P. Bauer, E. Barouch, and O. de la Beaujardiere, "Equatorward Boundary of Diffuse Auroral Electron Precipitations."

de la Beaujardiere, O., V. B. Wickwar, M. J. Baron, J. Holt, R. M. Wand, W. L. Oliver, P. Bauer, M. Blanc, C. Senior, D. Alcayde, G. Caudal, J. Foster, E. Nielsen, and R. Heelis, "MITHRAS: A Brief Description."

Aussois EISCAT Workshop  
September 1983

Alcayde, D., P. Bauer, J. Fontanari, O. de la Beaujardiere, and C. Lathuilliere, "Neutral Temperature and Atomic Oxygen Concentration in the Thermosphere from Auroral Ionospheric Incoherent-Scatter Observations."

de la Beaujardiere, O., V. B. Wickwar, G. Caudal, D. Alcayde, J. Holt, R. Heelis, T. Killeen, G. Carignan, and N. Spencer, "Ionospheric and Thermospheric Parameters Measured on 18 November 1981 Using Chatanika, EISCAT, Millstone Hill, and DE-B."

Kofman, W., and V. B. Wickwar, "The Electron Energy Budget and Elevated Electron Temperatures in the High-Latitude F Region."

Wickwar, V. B., O. de la Beaujardiere, and W. Kofman, "Meridional Winds at Chatanika and EISCAT During Project MITHRAS."

U.S.-Finland Workshop on Magnetospheric/Ionospheric Phenomena  
October 1983

de la Beaujardiere, O., G. Caudal, and J. Holt, "MITHRAS Observations of the Nighttime F-Region Ionization."

de la Beaujardiere, O., V. B. Wickwar, and J. D. Kelly, "Sondrestrom Radar Observations."

Fall AGU Meeting  
December 1983

de la Beaujardiere, O., G. Caudal, and J. Holt, "MITHRAS Observations of the Nighttime F-Region Ionization."

Evans, D. S., O. de la Beaujardiere, "A Comparison Between Auroral Particle Energy Fluxes Inferred Statistically From TIROS/NOAA Observations and Directly From Chatanika Observations."

Fontaine, D., C. Senior, and O. de la Beaujardiere, "MITHRAS Comparison of Convection and Precipitation at EISCAT and Chatanika."

Kofman, W., and V. B. Wickwar, "The Electron Energy Budget and Elevated Electron Temperatures in the High-Latitude F Region."

Wickwar, V. B., O. de la Beaujardiere, and W. Kofman, "Meridional Winds at Chatanika and EISCAT During Project MITHRAS."

URSI  
January 1984

de la Beaujardiere, O., C. Senior, and V. B. Wickwar, "MITHRAS Observations of Auroral Zone Precipitation Boundaries."

Wickwar, V. B., "Radar Results From Chatanika and Sondrestrom."

Wickwar, V. B., J. D. Kelly, and O. de la Beaujardiere, "The Very High Latitude Ionosphere."

Spring AGU Meeting  
May 1984

Kofman, W., and V. B. Wickwar, "I(6300A) at Sondrestrom Deduced From Elevated Te."

Wickwar, V. B., and W. Kofman, "Greatly Elevated Te at Sondrestrom."

Chapman Conference on Magnetospheric Polar Cap  
August 1984

Meriwether, J. W., and V. B. Wickwar, "Polar Cap Thermospheric Dynamics: Optical and Radar Observations from Sondre Stromfjord, Greenland."

XXI URSI General Assembly  
September 1984

Fontheim, E. G., L. H. Brace, J. D. Winningham, and B. A. Emery, "Anomalous Heating Effects in the High-Latitude Ionosphere."

Kofman, W., and V. B. Wickwar, "F-Region Electron Energy Balance at Sondrestrom."

Wickwar, V. B., and W. Kofman, "Greatly Elevated Te at Sondrestrom."

Wickwar, V. B., W. Kofman, M. Rees, R. Sica, G. Romick, G. Hernandez, and S. Mende, "Examination of a Type-A Red Aurora with Radar, Optics and Theoretical Modeling."

GSFC Dynamics Workshop  
October 1984

Wickwar, V. B., "Magnetic-Meridian Component of the Dayside Neutral Winds at Sondrestrom Between 200- and 300-km Altitude."

DoD Topical Conference on Environmental Science  
November 1984

Wickwar, V. B., "Results and Future of High Latitude Research."

Fall AGU Meeting  
December 1984

de la Beaujardiere, O., B. Fejer, and A. Richmond, "Two Campaigns of Global Incoherent-Scatter Measurements and Observations of Substorms."

de la Beaujardiere, O., J. Holt, and D. Hardy, "Effect of the IMF Orientation on Ionospheric Polar Cap Convection."

Wickwar, V. B., "Aeronomical Effects Associated with the Convection Reversal in the Early Afternoon."

Wickwar, V. B., "High Latitude Thermospheric Dynamics--Some Challenges."

AGU Chapman Conference on Solar Wind-Magnetosphere Coupling  
February 1985

de la Beaujardiere, O., J. Holt, and D. Hardy, "Sondrestrom Radar Observation of the Effect of the IMF By Component on Polar Cap Convection."

Robinson, R. M., C. R. Clauer, O. de la Beaujardiere, and J. D. Kelly, "IMF By Control of Convection and Precipitation in the Prenoon and Postnoon Local Time Sectors."

Wickwar, V. B., "The Polar Cap Boundary Observed in the Early Afternoon with Sondrestrom Radar."

Chapman Conference, Pasadena  
February 1985

de la Beaujardiere, O., J. Holt, and D. Hardy, "Sondrestrom Radar Observation of the By Component on Polar Cap Convection."

Robinson, R. M., C. R. Clauer, O. de la Beaujardiere, and J. D. Kelly, "IMF By Control of Convection and Precipitation in the Pre-noon and Post-noon Local Time Sectors."

Spring AGU Meeting  
May 1985

Wickwar, V. B., and O. de la Beaujardiere, "The Polar Cap Boundary Observed in the Afternoon with the Sondrestrom Radar."

Romick, G. J., M. H. Rees, S. B. Mende, and V. B. Wickwar, "Comparison of Simultaneous Optical and Radar Observations from the Auroral Zone."

de la Beaujardiere, O., V. B. Wickwar, and S. Gussenhoven, "IMF-By Effect on the High-Latitude Nightside Convection."

Rasmussen, C. E., R. W. Schunk, J. J. Sojka, V. B. Wickwar, O. de la Beaujardiere, J. Foster, J. Holt, D. S. Evans, and E. Nielsen, "Comparison of Simultaneous Chatanika and Millstone Hill Observations with Ionospheric Model Predictions."

IAGA Meeting  
August 1985

de la Beaujardiere, O., D. Evans, and J. King, "IMF Control of the Nightside Polar Convection."

Kofman, W., V. B. Wickwar, G. Romick, M. H. Rees, B. A. Emery, R. G. Roble, and S. B. Mende, "Emission at 6300A Related to Magnetosphere-Ionosphere-Thermosphere Coupling."

Senior, C., O. de la Beaujardiere, and J. R. Sharber, "E- and F-Region Study of the Evening Sector Auroral Oval: A Chatanika/Dynamics Explorer-B Data Comparison."

Wickwar, V. B., "Observations Concerning the Precipitation of Energy Particles at or Near the Electric Field Reversal in the Afternoon Convection Cell."

Wickwar, V. B., O. de la Beaujardiere, and T. S. Jorgensen, "The High-Latitude Terrestrial Ionosphere."

U.S.-Finland Auroral Workshop, Sodankyla  
October 1985

de la Beaujardiere, O., and V. B. Wickwar, "IMF Control of Plasma Drift, Ion Temperature and Neutral Wind."

Fall AGU Meeting  
December 1985

Kamide, Y., A. D. Richmond, H. W. Kroehl, B. A. Hausman, O. de la Beaujardiere, J. C. Foster, and E. Nielsen, "Electric Fields and Currents Estimated from Groundbased Magnetometer and Radar Observations for GISMOS and MITHRAS."

Sharber, J. R., J. D. Winningham, C. Senior, D. S. Evans, O. de la Beaujardiere, R. Heelis, and M. Sugiura, "Study of the Evening Sector Auroral Oval with the Chatanika Radar, DE-2, and NOAA-6. I. E-Region Ionization Sources."

de la Beaujardiere, O., C. Senior, R. Heelis, J. R. Sharber, J. D. Winningham, and W. R. Hoegy, "Study of the Evening Sector Auroral Oval with the Chatanika Radar, DE-2, and NOAA-6. II. F-Region Ionization Sources."

Kofman, W., V. B. Wickwar, G. Romick, M. H. Rees, B. A. Emery, R. G. Roble, and S. B. Mende, "Emission at 6300A Related to Magnetosphere-Ionosphere-Thermosphere Coupling."

END

1-87

DTIC